

University of Louisville

ThinkIR: The University of Louisville's Institutional Repository

Electronic Theses and Dissertations

5-2023

Novel microdevices to analyze toxic volatile organic compounds.

Sujoy Halder
University of Louisville

Follow this and additional works at: <https://ir.library.louisville.edu/etd>

 Part of the [Other Chemical Engineering Commons](#)

Recommended Citation

Halder, Sujoy, "Novel microdevices to analyze toxic volatile organic compounds." (2023). *Electronic Theses and Dissertations*. Paper 4083.
<https://doi.org/10.18297/etd/4083>

This Doctoral Dissertation is brought to you for free and open access by ThinkIR: The University of Louisville's Institutional Repository. It has been accepted for inclusion in Electronic Theses and Dissertations by an authorized administrator of ThinkIR: The University of Louisville's Institutional Repository. This title appears here courtesy of the author, who has retained all other copyrights. For more information, please contact thinkir@louisville.edu.

NOVEL MICRODEVICES TO ANALYZE TOXIC VOLATILE
ORGANIC COMPOUNDS

By

Sujoy Halder

B.S. (Engineering) Shahjalal University of Science and Technology, 2012

A Dissertation

Submitted to the Faculty of the

J.B. Speed School of Engineering of the University of Louisville

in Partial Fulfillment of the Requirements

for the Degree of

Doctor of Philosophy

in Chemical Engineering

Department of Chemical Engineering

University of Louisville

Louisville, Kentucky

May 2023

Copyright 2023 by Sujoy Halder

All rights reserved

NOVEL MICRODEVICES TO ANALYZE TOXIC VOLATILE
ORGANIC COMPOUNDS

By

Sujoy Halder

B.S. (Engineering) Shahjalal University of Science and Technology, 2012

A Dissertation Approved on

April 12, 2023

by the following Dissertation Committee:

Dr. Xiao-An Fu (Dissertation Director)

Dr. Vance W. Jaeger

Dr. Michael H. Nantz

Dr. Noppadon Sathitsuksanoh

Dr. Gamini Sumanasekera

DEDICATION

This dissertation is dedicated to my parents
Janardan Halder & Aroti Rani Halder
for their endless love and invaluable learning.

ACKNOWLEDGEMENTS

I would like to express my heartfelt gratitude to my advisor Prof. Xiaoan Fu for his guidance, supervision, and encouragement during this journey. I am grateful to my advisor for giving me the opportunity and resources to work on multiple projects to acquire a diverse set of skills and experiences. His in-depth observations and suggestions guided me to explore new ideas. He offered endless patience and support that not only contributed to my research work but also helped to gain interpersonal skills.

I am very grateful to my committee members, Prof. Michael Nantz, Prof. Noppadon Sathitsuksanoh, Prof. Vance Jaeger and Prof. Gamini Sumanasekera for offering their time and valuable feedback on my research, especially in proposal defense. Special thanks to Prof. Nantz for providing continuous guidance and valuable advice on the sensor development project.

I am incredibly thankful to the University of Louisville, the University of Louisville Superfund Research Center, the department of Chemical Engineering and the National Institute of Environmental Health Sciences (NIEHS) for financial support for my research projects.

Also, I would like to acknowledge the training and support I received from the Micro/Nano Technology Center (MNTC) staff at the University of Louisville, especially

Dr. Julia Aebersold, Dr. Michael Martin and Curt McKenna. I am thankful to the department of Chemistry at the UofL for using GC-MS.

I am incredibly grateful to all my colleagues and lab members for their helpfulness, discussion, and suggestion throughout my graduate studies, including Dr. Zhenzhen Xie, Dr. Prasadanie Adhihetty, James Morris, Ellie Reed and Dr. Saurin Sutaria. Many thanks to Dr. Adhihetty for providing synthesized sensing materials and great discussion regarding gas sensor development. I am blessed to have wonderful memories and accompanies by many friends, especially Dr. Shahinur Rahaman, Dr. Anwar Hossain, Riyadh, Rafiqul, Sofiul and Dip.

I am deeply thankful to my parents for their unconditional love and for supporting me spiritually throughout my life. Last but not least, my deepest gratitude to my loving and supportive wife, Mouri Das Jui, who has been with me all these years with great love and joy.

ABSTRACT

NOVEL MICRODEVICES TO ANALYZE TOXIC VOLATILE ORGANIC COMPOUNDS

Sujoy Halder

April 12, 2023

There has been a growing interest to measure volatile organic compounds (VOCs) in a range of environmental applications. The presence of toxic VOCs in the air has been associated with serious health problems including asthma, central nervous system dysfunction, cardiovascular disease and cancer, etc. Different analytical instruments such as gas chromatography-mass spectrometry (GC-MS) and sensor systems, such as metal oxide sensors are used to analyze VOCs. However, challenges still exist in the detection of airborne VOCs because of their trace concentration and interference with complex gas mixtures.

In this dissertation, two microfabricated devices, a sensor array and a micropreconcentrator were investigated for both detection and quantitative analysis of toxic VOCs in environmental air. First, the microfabricated sensor-array has been developed for the simultaneous testing of multiple sensors. Alkali metal carboxylate-linked gold monolayer protected clusters (Au MPCs) have been investigated to selectively sense aromatic and chlorinated VOCs. Cation- π interaction towards the electron-rich aromatic region and electron-deficient cations such as Li^+ , Na^+ and K^+ was explored to develop a

sensor for aromatic compounds. Furthermore, Cs⁺-linked Au MPCs were utilized to develop a sensor for trichloroethylene because of Cs⁺ and Cl⁻ coordination. The nature of the interaction of these sensors with humidity led us to design and use a preconcentrator to trap the analyte of interest and to thermally desorb the captured compounds for producing moisture-free concentrated target VOC samples.

Next, a microfabricated micropreconcentrator (μ PC) was developed to enable the detection of trace target VOCs by the sensor array and eliminate moisture interference. Carboxen 1000 adsorbent was loaded inside the μ PC to capture benzene, toluene, ethylbenzene and xylene (BTEX) and trichloroethylene. The performance of the μ PC has been characterized and integrated with solid-phase micro-extraction (SPME) to improve signals for GC-MS analysis. Furthermore, a novel dual-compartment μ PC has been developed to capture a wide range of VOCs. This microdevice contains two different sorbents – Carboxen 1000 for trapping aromatic VOCs and silica gel coated with O-2,3,4,5,6-pentafluorobenzyl hydroxylamine (PFBHA) for capturing carbonyls via oximation. The captured compounds were eluted with dichloromethane and analyzed by GC-MS. About 90% of recoveries have been achieved for BTEX, formaldehyde, acetaldehyde and acetone.

Finally, this microdevice was used for detecting BTEX and carbonyls at different locations in Louisville, KY. The combination of this dual-compartment μ PC with our developed sensor-array could satisfy the demand for a portable system in the application of air quality monitoring and disease diagnostics from exhaled breath.

TABLE OF CONTENTS

	PAGE
ACKNOWLEDGEMENTS.....	iv
ABSTRACT.....	vi
LIST OF TABLES	xiv
LIST OF FIGURES	xvi
CHAPTER I: INTRODUCTION.....	1
1.1 Volatile organic compounds.....	1
1.2 Classification of VOCs and sources.....	2
1.3 Effects of VOCs on human health.....	3
1.4 Airborne VOCs analysis.....	5
1.4.1 Sampling methods.....	5
1.4.2 Preconcentration techniques.....	8
1.4.3 Extraction methods.....	10
1.4.4 Separation and detection technique.....	13
1.5 GCMS for VOCs detection.....	14

1.6	Chemical sensor.....	15
1.6.1	Chemiresistive sensor.....	17
1.6.2	Metal oxide-based chemiresistor.....	18
1.6.3	Conductive polymer-based chemiresistor.....	19
1.6.4	Metal nanoparticle-based chemiresistor.....	20
1.6.5	Sensor Array.....	22
1.7	Motivation of this work.....	23
1.8	Objectives of this work.....	25
1.9	Dissertation overview.....	25
CHAPTER II: DESIGN AND FABRICATION OF A MICROSENSOR ARRAY FOR SENSING VOCS		27
2.1	Introduction.....	27
2.2	Experimental.....	29
2.2.1	Microsensor array design.....	29
2.2.2	Microsensor array fabrication.....	31
2.2.3	Chemicals.....	36
2.2.4	Synthesis of commercial thiol functionalized Au MPCs.....	37
2.2.5	Sensor characterization.....	38
2.2.6	Sensor data measurement.....	40

2.3 Microsensor array characterization.....	40
2.4 Conclusion.....	49
CHAPTER III: DEVELOPMENT OF METALATED GOLD MONOLAYER- PROTECTED CLUSTERS FOR SENSING AROMATIC VOCS AND TCE.....	
3.1 Introduction.....	50
3.2 Experimental.....	53
3.2.1 Materials.....	53
3.2.2 Synthesis of metal-ion functionalized Au MPCs.....	53
3.2.3 Sensor evaluation and data acquisition.....	54
3.3 Results and discussion.....	55
3.3.1 Sensor development for aromatics VOCs.....	55
3.3.2 Sensor development for chlorinated VOCs.....	65
3.3.3 Sensor response to humidity.....	71
3.4 Conclusion.....	74
CHAPTER IV: DEVELOPMENT OF A MICROPRECONCENTRATOR FOR ANALYZING TRACE VOCS IN ENVIRONMENTAL AIR.....	
4.1 Introduction.....	75
4.2 Materials and method.....	78
4.2.1 Chemicals and materials.....	78

4.2.2 MEMS preconcentrator fabrication procedure.....	83
4.2.3 Standard sample preparation and calibration curves.....	91
4.2.4 LOD, LOQ of GC–MS with SPME sampling.....	93
4.2.5 Analytical procedure.....	94
4.2.6 GC-MS parameters.....	95
4.3 Results and discussion.....	96
4.3.1 Characterization of the preconcentrator–SPME for analysis of VOCs.....	96
4.3.2 The effect flow rates for adsorption/thermal desorption of the μ PC.....	100
4.3.3 The effect of thermal desorption temperature of the μ PC.....	103
4.3.4 Method precision.....	104
4.3.5 Application for real-world samples.....	106
4.4 Conclusion.....	108
 CHAPTER V: DEVELOPMENT OF A DUAL-COMPARTMENT MICROPRECONCENTRATOR TO DETECT AIRBORNE VOCS.....	 109
5.1 Introduction.....	109
5.2 Materials and method.....	113
5.2.1 Chemicals and materials.....	113
5.2.2 Preparation of standards and calibration curve.....	113

5.2.3 Design and fabrication of micropreconcentrator devices.....	117
5.2.4 Preparation of micropreconcentrator devices.....	118
5.2.5 Experimental setup and analysis.....	120
5.2.6 GC-MS parameter.....	121
5.3 Results and discussion.....	122
5.3.1 Characterization of device A for capturing carbonyl compounds...	122
5.3.1.1 Solvent selection for PFBHA adducts elution.....	122
5.3.1.2 Effect of Flow rate on derivatization.....	124
5.3.1.3 Effect of PFBHA coating amount on recovery.....	126
5.3.1.4 Humidity effect.....	127
5.3.1.5 Temperature effect on derivatization reaction.....	128
5.3.2 Characterization of device B for capturing BTEX.....	129
5.3.2.1 Adsorption flow rate effect.....	129
5.3.2.2 Humidity effect.....	131
5.3.3 Characterization of device C with dual compartments for capturing both BTEX and carbonyls.....	132
5.3.3.1 Calibration curves and limit of detection.....	132
5.3.3.2 Optimization of operation conditions for device C.....	135
5.3.3.3 Recovery (%) of analytes for device C.....	138

5.3.3.4 Method precision.....	139
5.3.3.5 Effect of background contamination.....	139
5.3.3.6 Application for analyzing environmental air samples.....	140
5.4 Conclusion.....	146
CHAPTER VI: CONCLUSION AND FUTURE WORK.....	147
6.1 Conclusion.....	147
6.2 Future work and recommendation.....	149
REFERENCES.....	151
CURRICULUM VITAE.....	182

LIST OF TABLES

TABLE	PAGE
Table 1.1 Classification of VOCs by WHO.....	2
Table 1.2 Human health effects due to VOCs exposure and their PEL limits for 8-hour working period.....	4
Table 1.3 Characterization of adsorbents used for adsorptive enrichment in ambient air analysis.....	9
Table 2.1 Thiols used to functionalize Au MPC chemiresistors.....	37
Table 3.1 The response and recovery times for the Li ⁺ , Na ⁺ , and K ⁺ sensors.....	61
Table 3.2 Commercially available thiols used to prepare Au MPCs chemiresistive films for benzene sensing studies.....	63
Table 3.3 Dipole moments μ (D) of analytes utilized in this experiment.....	70
Table 4.1 Summary of miniaturized preconcentrator used to detect BTEX.....	80
Table 4.2 Calibration equations, LOD and LOQ obtained for BTEX and TCE.....	93
Table 4.3 Average concentrations ($\mu\text{g}/\text{m}^3$) and standard deviations ($n = 3$) of BTEX and TCE in ambient air with 1 L samples preconcentrated by the μPC and SPME.....	107

Table 5.1 Retention time of analytes in GC-MS, calibration equation, coefficient of determination (R^2), the limit of detection (LOD), and calculated (%) recovery of these VOCs.....	133
Table 5.2 Weather conditions of the environmental air samples	141
Table 5.3 Average concentrations ($\mu\text{g}/\text{m}^3$) (N=3) of BTEX and carbonyl compounds in Rubbertown industrial areas.....	145

LIST OF FIGURES

FIGURE	PAGE
Figure 1.1: A block diagram of a typical VOC analysis that involves sample collection, extraction, separation, detection, and data acquisition.....	6
Figure 1.2: (a) Sorbent tube with multiple adsorbents (graphitized carbon black, and Carbosieve S-III) from SKC; (b) stainless steel tube packed with Tenax from Perkin Elmer.....	7
Figure 1.3: SPME steps to capture analytes of interest from the sample matrix.....	13
Figure 1.4: The diagram of a common GCMS system with all required components for a complete chemical analysis.....	15
Figure 1.5: Schematic diagram of a chemical sensor.....	16
Figure 1.6: Reversible vapor-sensor interaction as a result of sorption of analytes in the thin film of sensing material.....	17
Figure 1.7: (a) A chemiresistor sensor resistance coated with sensing material having R_0 resistance (b) sensor resistance changes to R upon interaction with analyte.....	18
Figure 1.8: Illustration of the MO_x sensor mechanism in response to acetone.....	19
Figure 1.9: Schematic representation of the film of metal monolayer-protected clusters (MPCs) sensing material deposited in between electrodes.....	21

Figure 2.1: Microsensor chip design: a) layout of each chip, b) zoomed view of IDE area.....	30
Figure 2.2: Fabricated light field photomask.....	31
Figure 2.3: Fabrication process flow diagram: a) cleaning oxidized silicon wafer, b) Photoresist coating, c) UV light exposure, d) Yes Image reversal, e) Development, f) Metal sputtering, g) Lift-off process.....	32
Figure 2.4: A diced wafer containing 52 pieces of microsensor chips.....	36
Figure 2.5: Laboratory setup for measuring chemiresistor sensor responses to VOCs.....	39
Figure 2.6: Resistance change of DDT functionalized Au MPCs with time upon exposure to synthetic air, 250 ppb, 500 ppb, 750 ppb, and 1 ppm of benzene.....	41
Figure 2.7: Resistance change of DDT functionalized Au MPCs with time upon exposure to synthetic air, 250 ppb, 500 ppb, 750 ppb, and 1 ppm of xylene.....	42
Figure 2.8: Resistance change of MUA functionalized Au MPCs with time upon exposure to synthetic air, 250 ppb, 500 ppb, 750 ppb, and 1 ppm of acetone.....	43
Figure 2.9: Resistance change of MTT functionalized Au MPCs with time upon exposure to synthetic air, 250 ppb, 500 ppb, 750 ppb, and 1 ppm of pentane.....	43
Figure 2.10: Sensor response profile for DDT functionalized Au MPCs in response to benzene, toluene, ethylbenzene, xylene, formaldehyde, acetone, ethanol, and pentane vapor at concentrations from 0.25 ppm to 1 ppm.....	44

Figure 2.11: Sensor response profile for MUA functionalized Au MPCs in response to benzene, toluene, ethylbenzene, xylene, formaldehyde, acetone, ethanol, and pentane vapor at concentrations from 0.25 ppm to 1 ppm.....	45
Figure 2.12: Sensor response profile for MBA functionalized Au MPCs in response to benzene, toluene, ethylbenzene, xylene, formaldehyde, acetone, ethanol, and pentane vapor at concentrations from 0.25 ppm to 1 ppm.....	45
Figure 2.13: Sensor response profile for MTT functionalized Au MPCs in response to benzene, toluene, ethylbenzene, xylene, formaldehyde, acetone, ethanol, and pentane vapor at concentrations from 0.25 ppm to 1 ppm.....	46
Figure 2.14: Responses of MTT, MBA, MUA, and DDT functionalized sensors to sense 1 ppm of individual benzene, toluene, ethylbenzene, xylene, formaldehyde, acetone, ethanol, and pentane.....	47
Figure 2.15: Sensor response for DDT functionalized Au MPCs in response to benzene, toluene, ethylbenzene, xylene, and a mixture of these compounds at 0.25 ppm to 1 ppm concentrations.....	48
Figure 3.1: Synthesis of metal-ion functionalized Au MPCs. Only one ligand is emphasized in MPCs 2–5. Legend: a) 50% CF ₃ CO ₂ H, CH ₂ Cl ₂ , 0 °C, 15 min; b) Et ₃ N, MeOH:CH ₂ Cl ₂ (2:1), rt, 3 h; c) methyl 4-formylbenzoate, CH ₂ Cl ₂ , rt, 17 h; d) M ⁺ OH ⁻ (LiOH, NaOH, KOH or CsOH), MeOH:CH ₂ Cl ₂ (1:9), 0 °C to rt, 17 h.....	54
Figure 3.2: Plots of A) resistances of chemiresistor 5-K ⁺ and B) responses of chemiresistor 5-K ⁺ on exposure to 100 ppb to 100 ppm of benzene at 22 °C.....	56

Figure 3.3: Resistance plot with the time of chemiresistor 5-Na ⁺ on exposure to 100 ppb of benzene at 22 °C.....	57
Figure 3.4: Sensor responses of Au MPCs 5-M ⁺ , where M ⁺ = Li ⁺ , Na ⁺ , or K ⁺ . Each point indicates the average of n = 3 measurements.....	58
Figure 3.5: Chemiresistor response to VOCs at a concentration of 5 ppm. Sensors were prepared from Au MPCs 5-M ⁺ , where M ⁺ = Na ⁺ or K ⁺	60
Figure 3.6: Responses of Au MPCs chemiresistors prepared from commercial thiols in comparison with the 5-K ⁺ chemiresistor response to 0.1 – 5 ppm benzene.....	64
Figure 3.7: Response of Au MPCs Cs ⁺ sensor to different VOCs. (Chlorinated vs aromatic vs polar vs non-polar).....	66
Figure 3.8: Response of Au MPCs Cs ⁺ sensor to chloroalkanes.....	68
Figure 3.9: Response of Au MPCs Cs ⁺ sensor to chloroalkenes.....	68
Figure 3.10: A comparison of 5-Cs ⁺ response curve for a mixture of TCE, DCM, benzene, and methanol vapor with individual compounds. In the mixture, TCE concentration varied from 1 ppb to 5 ppm but DCM, benzene and methanol amounts were fixed (100 ppb of each).....	71
Figure 3.11: Au MPCs 5-M ⁺ sensor responses to relative humidity (25–100%).....	72
Figure 3.12: A comparison of 5-Cs ⁺ sensor response profile of different amounts of water vapor with and without 1 ppm TCE.....	73

Figure 4.1: Micro gas preconcentrator (μ PC). (a) Three-dimensional view of layers. (b) Image of front faces of the μ PC containing cavity and micropillars. (c) Image of backside heater and RTD of the μ PC.....	83
Figure 4.2: (a) Fabricated dark field photomask for creating cavity and flow channel in μ PC, (b) Fabricated light field photomask for microheater fabrication on the backside of μ PC.....	84
Figure 4.3: Schematic illustration of the μ PC fabrication steps.....	86
Figure 4.4: Optical image of the cleaned wafer before anodic bonding.....	88
Figure 4.5: Calibration curves for BTEX and TCE analysis using SPME–GC-MS.....	92
Figure 4.6: Scheme of the analytical procedure from adsorption of samples to GCMS analysis.....	95
Figure 4.7: The effect of extraction time on GC-MS peak areas of 100 ppb BTEX & TCE mixture produced by SPME at room temperature.....	97
Figure 4.8: Recovery percentage of BTEX and TCE for a combination of μ PC and SPME at different initial concentrations (0.5, 1, 2, and 3 ppb) in 5 L samples.....	98
Figure 4.9: A comparison of detector signals for SPME of 1 ppb and 40 ppb BTEX TCE of 50 mL samples (without μ PC) with 1 ppb BTEX TCE of 2L concentrated by the μ PC and then thermally desorbed to 50 mL for SPME analysis.....	99
Figure 4.10: Recoveries obtained at different adsorption flow rates for 4 ppb of 2 L BTEX TCE preconcentrated into 50 mL samples.....	101

Figure 4.11: Recoveries obtained at different thermal desorption flow rates for 1 ppb of 5 L BTEX TCE preconcentrated into 50 mL samples.....	102
Figure 4.12: Recoveries obtained at different desorption temperatures for 2 ppb of 2 L BTEX and TCE preconcentrated into 50 mL samples.....	104
Figure 4.13: Comparison of GC-MS peak areas between 2 L of 1 ppb and 1 L of 2 ppb of BTEX and TCE samples using the two-stage preconcentration using μ PC and SPME for GC-MS analysis.....	105
Figure 4.14: GC-MS spectra for environmental air sample; (a) red line: SPME for 15 min extraction in the open air (b) blue dash line: SPME for 15 min extraction in 2 L air collected in a Tedlar bag (c) black line: SPME for 15 min extraction of 50 mL sample preconcentrated from 1 L air using the μ PC.....	107
Figure 5.1: (a) Calibration curves for PFBHA-deuterated-propanal, 2-butanone, butanal, 2-pentanone, hexanal with IR PFBHA-acetone-d ₆ to characterize device A; (b) Calibration curves for benzene, toluene, ethylbenzene and xylene with IR heptane-d ₁₆ to characterize device B; (c) & (d) Calibration curves for benzene, toluene, ethylbenzene, xylene, PFBHA-(formaldehyde, acetaldehyde, acetone, propanal, acrolein, 2-butanone, butanal, 2-pentanone, pentanal, hexanone and hexanal) with IR heptane-d ₁₆ to characterize device C.....	115
Figure 5.2: A GC-MS chromatogram of a standard sample containing 5 nmol of each PFBHA-deuterated-propanal, 2-butanone, butanal, 2-pentanone, hexanal and 5 nmol of PFBHA-acetone-d ₆ as an IR in a total volume of 50 μ L methanol.....	116

Figure 5.3: A GC-MS chromatogram of a standard sample containing 5 nmol of each benzene, toluene, ethylbenzene, xylene, and 5 nmol of heptane-d₁₆ as an IR in a total volume of 50 μL methanol.....116

Figure 5.4: (a) Schematic of the single-compartment microdevice, (b) Schematic of the dual-compartment microdevice, (c) Optical pictures of silica gel and carbopack X loaded single and dual-compartment microdevices.....117

Figure 5.5: Schematic diagram of the microdevice fabrication steps.....118

Figure 5.6: Schematic illustration of experimental setup to capture or derivatize VOCs..119

Figure 5.7: Comparison of recovery (%) for target deuterated carbonyls using 250 nmol of PFBHA coated on silica gel loaded (4.2 ± 0.2 mg) single-compartment microdevices extracted with 50 μL of three different solvents.....123

Figure 5.8: Recovery (%) for target deuterated carbonyls using 250 nmol PFBHA coated silica gel loaded (4.2 ± 0.2 mg) single-chamber microdevices at different flow rates (2 – 120 mL/min) extracted with 50 μL of DCM.....125

Figure 5.9: Recovery (%) for target deuterated carbonyls using different amounts (64 – 500 nmol) of PFBHA coated silica gel loaded (4.2 ± 0.2 mg) into single-chamber preconcentrator extracted with 50 μL of DCM.....126

Figure 5.10: Recovery (%) for target deuterated carbonyls at different humidity levels (25 – 100 % RH) using 250 nmol of PFBHA-coated silica gel loaded with 4.2 ± 0.2 mg single-compartment microdevices extracted with 50 μL of DCM.....128

Figure 5.11: Recovery (%) for BTEX compounds at different flow rates (20 – 80 mL/min) using single-chamber microdevices loaded with 4 ± 0.2 mg of carbopack X adsorbent...	130
Figure 5.12: Recovery (%) for BTEX compounds at different humidity levels 25 – 100% Relative humidity (RH) using single-compartment microdevices loaded with 4 ± 0.2 mg of carbopack X adsorbent.....	131
Figure 5.13: A GC-MS chromatogram of a standard sample containing 0.5 nmol of each compound (benzene, toluene, ethylbenzene, xylene, PFBHA adducts of formaldehyde, acetaldehyde, propanal, acetone, butanal, 2-butanone, pentanal, 2-pentanone, hexanal, 2-hexanone, acrolein) and 0.5 nmol of heptane- d_{16} as an IR in a total volume of 50 μ L methanol.....	134
Figure 5.14: Actual by predicted plot, lack of fit, a summary of fit, analysis of variance, effect summary, and residual by the predicted plot for (a) benzene and (b) formaldehyde	137
Figure 5.15: Prediction profiler to obtain maximum desirability.....	138
Figure 5.16: Air samples collection sites in Rubbertown area, Louisville, Kentucky....	141
Figure 5.17: A GC-MS chromatogram of 5L environmental air sample analyzed by a dual-compartment microdevice loaded with carbopack X and 250 nmole PFBHA coated silica gel.....	143

CHAPTER I

INTRODUCTION

1.1 Volatile Organic Compounds

Volatile organic compounds (VOCs) are referred to as chemicals that produce vapors easily by evaporation from certain solids or liquids at ambient temperature [1]. VOCs are ubiquitous and present in indoor and outdoor air, human exhaled breath, e-cigarette aerosol, drinking water, etc. [2-4]. U.S. Environmental Protection Agency (EPA) defines VOCs as any carbon compounds, excluding carbon monoxide, carbon dioxide, carbonic acid, metallic carbides, or carbonates and ammonium carbonate, which participate in atmospheric photochemical reactions except those designated by EPA as having negligible photochemical reactivity [5]. The volatility of an organic compound is related to its boiling point. The European Union defines a VOC to be any organic compound with a boiling point ≤ 250 °C measured at a standard atmospheric pressure of 101.3 kPa [6]. World Health Organization (WHO) also describes VOCs as all organic substances made up of predominantly carbon and hydrogen with boiling temperatures below 250 – 260°C, excluding pesticides [7]. Generally, VOCs are recognized as a class of hydrocarbons with a vapor pressure greater than 0.1 mmHg at 25 °C.

1.2 Classification of VOCs and Sources

VOCs are classified based on molecular structure or functional group. These include aliphatic hydrocarbons, aromatic hydrocarbons, alcohols, ethers, esters, carbonyls, etc. WHO categorizes indoor VOCs into three groups listed in table 1.1 [5].

Table 1.1: Classification of VOCs by WHO [5].

Description	Boiling Point (°C)	Example of Compounds
Very volatile organic compounds (VVOC)	<0 to 50 – 100	Propane, butane, methyl chloride
Volatile organic compounds (VOC)	50 – 100 to 240 – 260	Formaldehyde, toluene, acetone, ethanol, 2-propanol, hexanal
Semi-volatile organic compounds (SVOC)	240 – 260 to 380 – 400	Pesticides (DDT, chlordane), plasticizers (phthalates), fire retardants (PCBs)

VOCs in indoor air are coming from personal products, household products, building materials, body spray, cleaning agents, cooking oil, vapor intrusion from outdoor, etc. [8]. In outdoor air, VOCs are released into the ambient air from both biogenic (mainly vegetation) and anthropogenic sources (e.g. car exhaust, petroleum fuels, biomass burning, industrial solvents, landfills, and sewage treatment plants) [9].

1.3 Effects of VOCs on human health

The health effects depend on the concentration and composition of the VOCs, and the frequency and length of exposure [10]. Most VOCs are not intensely toxic but long-term exposure may lead to chronic health effects. Some VOCs are harmful to human health or cause harm to the environment too. The most common effects for humans include skin and eye irritation, headaches, loss of taste, nausea, damage to the liver, kidneys, and central nervous system, cardiovascular diseases, and some potential to cause cancer [11, 12]. Occupational Safety and Health Administration (OSHA) regulates the occupational exposure limits (OELs) of VOCs. They set Permissible Exposure Limits (PELs), Threshold Limit Values (TLVs), and Recommended Exposure Limits (RELs), respectively, to protect the workers from the unpleasant health effects because of VOC exposure [13]. These exposure limits vary from low ppb to high ppm levels based on the toxicity of these compounds. Table 1.2 presents the health effects and PELs for 8-hour work shift of some toxic VOCs [14-18].

Because of these adverse effects on human health, it is crucial to monitor these compounds present in indoor and outdoor air. Also, VOCs are not only present in the air, but also in the water, human blood, sweat, urine, and exhaled breath. Researchers found VOCs in the urine that could be successfully used as the biomarker for lung cancer diagnosis [19]. Also, diabetics patients produce a higher amount of acetone in exhaled breath than healthy persons [20]. Researchers are using a non-invasive method of breath analysis to diagnose the early stage of lung cancer [21]. Thus, the analysis of VOCs in gaseous or liquid media facilitates assessments of air pollution, water contamination, monitoring of exposures to toxic chemicals, and disease diagnosis.

Table 1.2: Human health effects due to VOC exposure and their PEL limits for an 8-hour working period.

VOC	Health effects	PEL
Benzene	Cancer, rapid or irregular heartbeat, leukemia, unconsciousness	1 ppm
Toluene	Lethality, morbidity, liver and kidney damage, central nervous system dysfunction, narcosis, sore throat, dizziness, headache, birth defect	200 ppm
Ethylbenzene	Skin, eye irritation, chest constriction, cardiovascular diseases	100 ppm
Xylene	Eye and respiratory irritation, nerve problem, cardiovascular diseases, kidney diseases	100 ppm
Styrene	dopaminergic, nerve conduction, neurobehavioral changes as well as ototoxicity and color vision impairment	100 ppm
Formaldehyde	Eyes, nose, throat irritation, skin rashes, shortness of breath, wheezing, changes in lung function	0.75 ppm
Acetaldehyde	Eyes, skin, respiratory tract irritation, erythema, coughing, pulmonary edema, necrosis	200 ppm

1.4 Airborne VOCs analysis

Traditionally, collection of VOCs from the gaseous sample has entailed purge-and-trap or headspace sampling followed by separation in chromatographic column and analysis with a detector such as a flame ionization detector (FID), photoionization detector (PID) or a mass spectrometer (MS) [22]. The quantitative determination of VOCs usually involves the following major steps: sample collection, preconcentration and/or derivatization of VOCs, extraction of concentrated VOCs, separation, and detection in the detector, which is illustrated in Figure 1.1. The total volatile organic compound (TVOC) is usually used to explore indoor and outdoor air quality [23]. The TVOC determination method usually skips the separation process and directly measures the VOCs mixture together by a PID or FID. It cannot differentiate the identity and quantity of each VOC present in the environmental air. Also, the measurement is not accurate enough because TVOC measurement is based on single calibration compound data to represent the whole VOC complex [24]. So, individual VOC monitoring is essential to protect people from toxic VOC exposure. The details of each step from VOC sampling to quantitative measurements are presented below.

1.4.1 Sampling methods

The first step of measuring airborne VOCs is the collection of the environmental air sample. There are several prevalent sampling methods have been used.

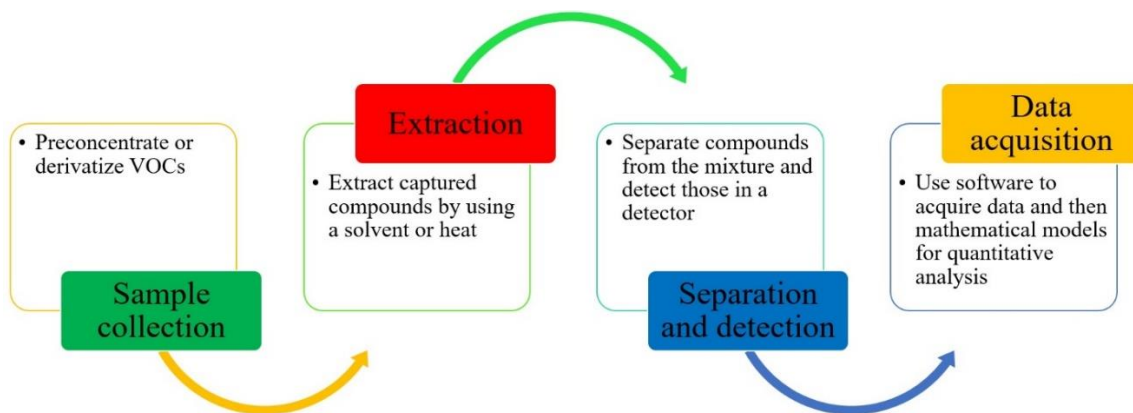


Figure 1.1: A block diagram of a typical VOC analysis that involves sample collection, extraction, separation, detection, and data acquisition.

Active sampling:

Active sampling is performed by drawing a certain volume of the air using a pump through an adsorbent tube with a constant, generally low air flow rate. In some cases, sampling can be done for a longer period to collect a large volume of the air sample [5].

Grab sampling:

Grab sampling is carried out for a very short period (10 – 30 seconds) generally using evacuated stainless steel canisters. However, evacuated canisters can also be used for time-integrated sampling over minutes to days using a suitable flow-restrictive inlet [5].

Passive sampling:

Passive sampling consists of adsorbents packed in a tube where VOCs are captured on adsorbents diffusively. The cross-section of the tube and the distance between the opening of the tube and the adsorbent surface determines the sampling rate of the passive sampler [25]. The use of this sampling technique avoids the need to visit a sampling site multiple times to collect repetitive air samples [26]. VOCs concentrate on the collecting medium over time until they reach equilibrium with the surrounding medium. The use of passive sampling provides time-averaged concentrations of VOCs over the deployment period [27]. Figure 1.2 shows the commercial sorbent tubes for passive sampling [28].



Figure 1.2: (a) Sorbent tube with multiple adsorbents (graphitized carbon black, and Carbosieve S-III) from SKC; (b) stainless steel tube packed with Tenax from Perkin Elmer (copied from Ref. [28]).

1.4.2 Preconcentration techniques

Instruments with detectors such as MS or FID are often used for measuring VOCs. However, the detection limits of these instruments are typically in the parts per million range [29]. There are more sophisticated instruments in practice that measure chemical-specific VOCs in the air sample. The primary step of detecting individual VOCs requires preconcentration of the target VOCs.

Preconcentration on solid sorbents:

Enrichment of VOCs onto solid sorbents, either by active or passive sampling is a well-established sample preparation technique for measurements of VOCs in the air. Different types of materials including porous carbon, zeolite, carbon nanotube, Tenax, metal-organic framework (MOF), and polymer have been used to trap VOCs [30-32]. Generally, the same adsorbent can be used for passive and active sampling for capturing VOCs. The strength of interactions between the adsorbent and the analyte influences both the sorption and desorption of the analytes from the trapping medium. An ideal candidate for preconcentrating VOCs should also have a large breakthrough volume for the analytes of interest, complete desorption of them at moderate temperatures, or use a suitable solvent. However, no single available sorbent meets all of these criteria and therefore it was recommended the use of multiple sorbents to detect a wider range of VOCs [30].

The main types of solid adsorbents used in air monitoring are porous polymers, graphitized carbon blacks, carbon molecular sieves, and activated charcoal [30]. Table 1.3 shows the properties of adsorbent materials to capture different VOCs [30, 33].

Table 1.3: Characterization of adsorbents used for adsorptive enrichment in ambient air analysis.

Sorbent	Strength	Volatility range	Surface area (m ² /g)	Maximum desorption temperature (°C)	Target analyte
Tenax TA	Weak	Bp 100 – 400°C	~35	350	Aromatics, non-polar compounds (bp > 100°C), and less volatile polar compounds (bp > 150°C)
Tenax GR	Weak	Bp 100 – 450°C	~35	350	Alkyl benzenes, PAHs, PCBs, and as above for Tenax TA
Chromosorb 106	Medium	Bp 50 – 200°C	~750	250	Wide range of VOCs including volatile oxygenated compounds
Porapak N	Medium	Bp 50 – 150°C	~300	190	Specific for volatile nitriles: acrylonitriles, acetonitrile, and propionitrile. Also good for pyridine, volatile alcohols from ethanol, and MEK (methyl-ethyl-ketone).
Carbopack X	Medium	n-C _{5/6} to n-C ₈	~240	400	Hydrocarbon, BTEX
Carbosieve SIII	Very strong	Bp (-30) – 150°C Ethane to n-C ₅	~800	400	Very volatile compounds such as C ₂ , C ₃ and C ₄ hydrocarbons
Carboxen 1000	Very strong	C ₂ –C ₅	>1200	400	Very volatile hydrocarbons
Active charcoal	Very strong	Bp (-80) – 50°C	>1000	400	Very volatile compounds, such as C ₂ , C ₃ , and C ₄ hydrocarbons

Bp: Boiling point

VOCs derivatization:

Derivatization is carried out to convert a chemical compound to another product of a similar chemical structure which enhances detectability in the detector or improves the chromatographic performance of the target analytes [34]. Some of the VOCs are too volatile, showing less stability. So it is difficult to identify those using direct sampling and analysis. For this reason, reacting with a suitable reagent to form a stable derivative would promote better sensitivity for compound analysis [35]. For instance, aldehydes reacted with 2,4-dinitrophenylhydrazine (DNPH) followed by liquid extraction and liquid chromatography for separation have been commonly used for the analysis of these compounds [34, 36]. EPA TO-11A method determines formaldehyde in ambient air using DNPH coated silica gel cartridge, and the adduct is analyzed by using high-performance liquid chromatography (HPLC) with ultraviolet (UV) detection [37]. Another prevalent derivatizing reagent is o-(2,3,4,5,6-pentafluorobenzyl)-hydroxylamine hydrochloride (PFBHA) which forms stable oximes and amenable for GC-MS or GC electron-capture detector (ECD) analysis [38]. The reaction is swift, and the PFBHA derivatives are formed quickly at ambient temperature [39]. EPA 556 method utilizes PFBHA to determine carbonyls in drinking water using GC-ECD [40].

1.4.3 Extraction methods

After pre-concentration or derivatization of VOCs, these concentrated or derivatized products need to be collected for further analysis. There are many extraction

techniques presently in practice such as chemical and thermal desorption, solvent extraction, solid phase micro-extraction, etc. [5].

Chemical desorption:

After pre-concentration of VOCs on the solid sorbent, especially activated charcoal, chemical desorption is performed using some organic solvent. Carbon disulfide (CS₂) is widely used for this purpose [41]. BTEX compounds were captured by activated charcoal and subsequently desorbed by this solvent for further analysis [41].

Thermal desorption:

An effective method of extraction from solid sorbent is thermal desorption. In this non-destructive method, the solid sorbent exposed to target analytes is heated at a high temperature typically in the range of 150°C to 350°C depending upon the characteristics of the solid sorbent [5, 42]. The desorbed VOCs from the sorbent surface are collected in a smaller volume for further analysis. Alternatively, the desorbed sample can be sent to a detector for detection and analysis [28].

Solvent extraction:

In this method, the trapped or derivatized VOCs are collected using an appropriate liquid solvent. Sometimes derivatizing reagents can be added after extraction to convert the analytes into products for more suitable subsequent separation and/or detection [34].

This method is of particular use for the analysis of carbonyl compounds in the air with DNPH, forming hydrazones that can be analyzed via HPLC and MS or UV detector [5, 34].

Solid phase micro-extraction technique

Solid phase microextraction (SPME) is one of the broadly used extraction techniques to detect VOCs from gaseous and liquid mediums [43]. SPME typically consists of a silica fiber coated with sorbent coating, for example, polydimethylsiloxane, divinyl benzene, carboxen, polyacrylate [44]. The fiber is inserted headspace or directly into the liquid medium to extract the VOCs. The fiber is left to become in equilibrium with the surrounding medium for a period, usually, from minutes to hours [45]. Then the fiber is thermally desorbed into the GC instrument injection port at a higher temperature for subsequent analysis. SPME is widely applied in airborne VOCs measurement because of its short extraction time, and solvent-free operation [46]. However, SPME has some shortcomings including low sensitivity for incompatible compounds, sample loss, and limited choice of fiber coatings [47, 48]. Figure 1.3 represents the SPME steps to capture VOCs [49].

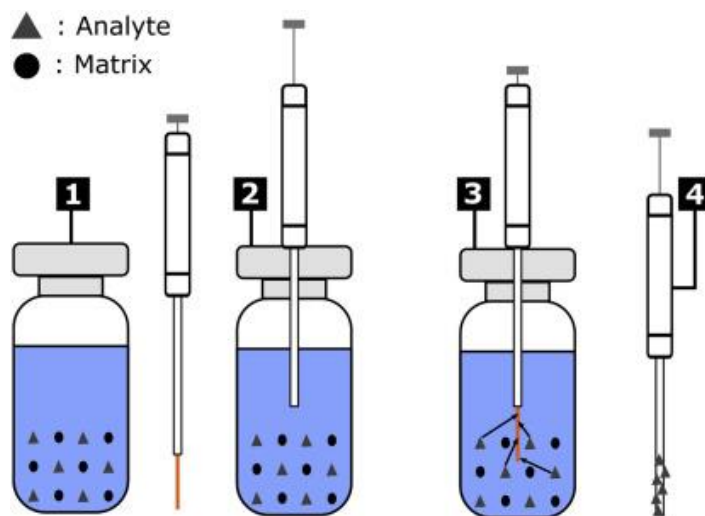


Figure 1.3: SPME steps to capture analytes of interest from the sample matrix (copied from Ref. [49]).

1.4.4 Separation and detection technique

Many advanced analytical techniques are used to analyze environmental VOCs after sampling and extraction. Gas chromatography (GC) is the most widely used separation technique to separate target compounds inside a column [50]. Generally, a column contains a stationary phase adsorbed onto the surface of an inert solid packing. The column temperature is regulated to achieve better separation and resolution of analytes [5]. Analytes are separated based on different physical properties such as polarity, molecular weight, and structure [28]. Then the separated compounds enter the detector. There are several commonly used detectors, such as FID, thermal conductivity detector (TCD), ECD, and PID. All detectors have specific target compounds, but the most accurate and versatile detector is the mass spectrometry detector (MSD) [51]. This detector is superior to other

detectors because it can also identify unknown compounds using a mass spectral library [52].

1.5 Gas chromatography-mass spectrometry (GC-MS) for VOCs detection

GC-MS technology provides a reliable and sensitive method for VOC analysis and produces highly reproducible results [53]. Figure 1.4 shows a schematic diagram of GC-MS [28]. A typical GC-MS system comprises of analytical component, external carrier gas, detection, and data acquisition system [28]. The sample is first introduced into the GC injection port by an injector or auto-sampler. The sample is vaporized and immediately passed into the column with a carrier gas (such as nitrogen, or helium). In the column, the compounds in the mixture are separated based on the difference in the chemical properties between different molecules and their relative affinity to the stationary phase of the column [54, 55]. MS breaks each molecule into ionized fragments and detects the fragments by their mass-to-charge ratio. Molecules injected into mass spectrometry are subjected to trap, ionize, accelerate, deflect, and detect ionized molecules [28]. However, the GC-MS technique has some limitations. This instrument is expensive and requires skills to operate effectively [56]. A good calibration is necessary for the quantitative analysis of VOCs. Also, sample pre-concentration steps are required before injecting the sample into the GC column for detecting trace airborne VOCs, which can lead to analyte loss and contamination issues [57]. Therefore, real-time measurements are not possible.

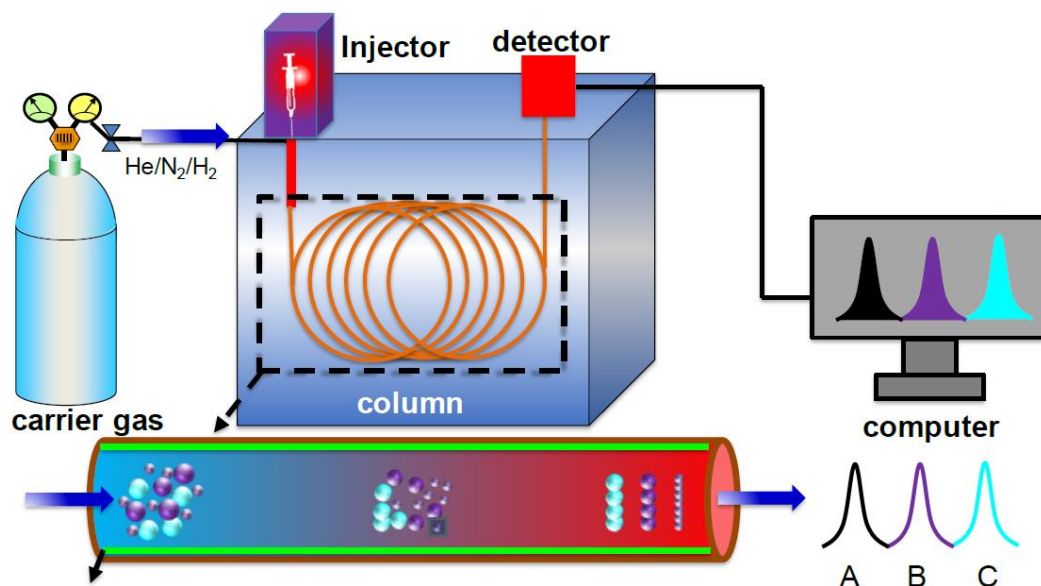


Figure 1.4: The diagram of a common GC-MS system with all required components for a complete chemical analysis (copied from Ref. [28]).

1.6 Chemical sensor

Besides the traditional VOC detection methods, the application of chemical sensors to identify VOC is more promising for sensitive and selective analysis. A chemical sensor is a small device that detects and measures the chemical property of a compound and provides the information by converting chemical information into an electrical signal [58]. A chemical sensor is composed of a sensing material and a transducer [59]. The sensing material interacts with the target molecules in the sample matrix and the transducer converts the chemical data into a measurable signal. The chemically selective sensing material is coated on the surface of the physical transducer. Once the analyte is selectively absorbed into the coating layer or film, the property of the material changes [60]. These changes can be transformed into a measurable electronic signal by some form of

transduction. Based on the principle of transduction, chemical sensors are divided into four fundamental groups: thermal sensor, mass sensor, chemiresistor sensor, and optical sensor [61-63]. Figure 1.5 shows a schematic diagram of a chemical sensor [61].

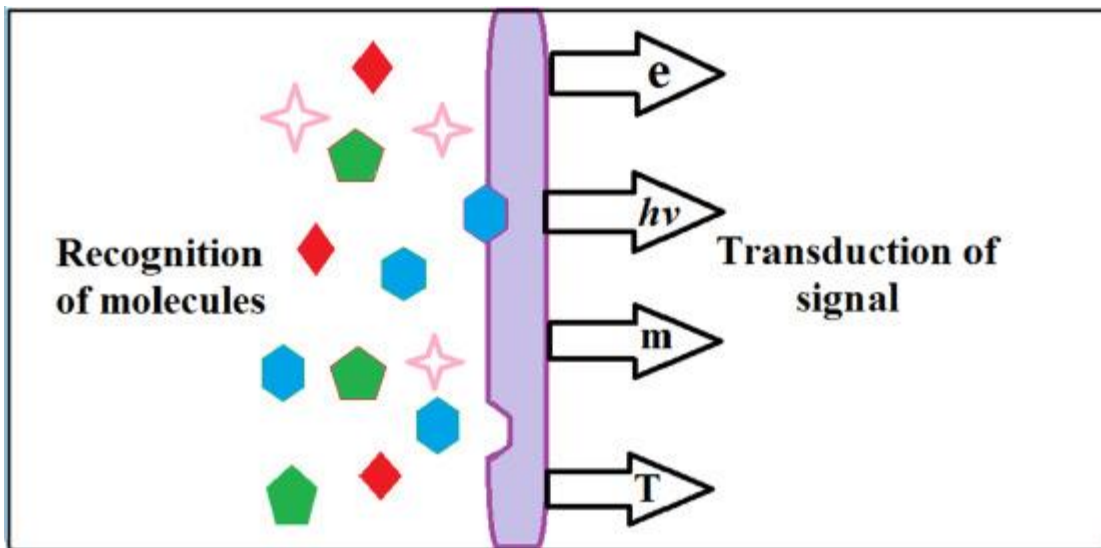


Figure 1.5: Schematic diagram of a chemical sensor (copied from Ref. [61]).

The deviation of measurable properties such as mass, temperature, resistance, and light absorbance is occurred because of the sorption of an analyte onto the surface of the sensing material (adsorption), or into the bulk of a deposited thin film (absorption). Thus, the sensor response contains a sorption step, involving phase transfer equilibria and kinetics, and a transduction step, leading to an electronic signal [64-66]. The absorption of VOCs from the gas phase into a thin film on a sensing material is shown schematically in Figure 1.6. In most sensor applications, the interaction between the analyte and the sensing thin film is reversible. Among these four chemical sensors, the chemiresistive sensor is

extensively used because of its convenient operation and availability of a wide range of sensing materials to detect VOCs.

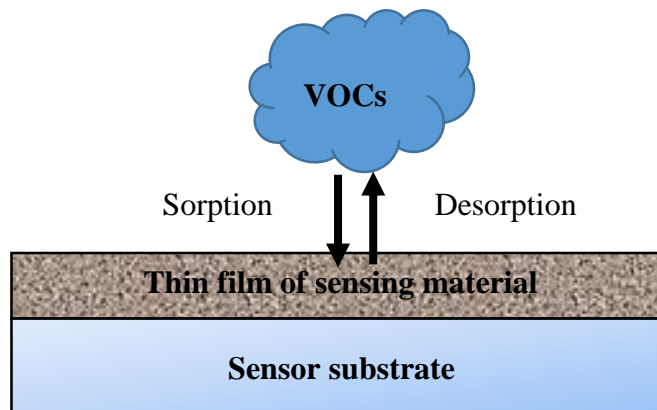


Figure 1.6: Reversible vapor-sensor interaction as a result of sorption of analytes in the thin film of sensing material.

1.6.1 Chemiresistive sensor

Chemiresistor is one type of electrochemical sensor that responds to an analyte by measuring the change of resistance or conductivity of sensing material. The chemiresistor sensor consists of a chemically sensitive conductive film deposited onto the electrode [67]. A schematic of a chemiresistor is shown in Figure 1.7. When a potential is applied across the thin film of sensing materials, there is a measurable current or resistance (R_0) across the film that changes to R upon interaction with an analyte. Chemeresistors can be divided according to the materials used for sensing the analyte of interest such as metal oxide, carbon nanotube, graphene, conductive polymer, and metal nanoparticle [68-70].

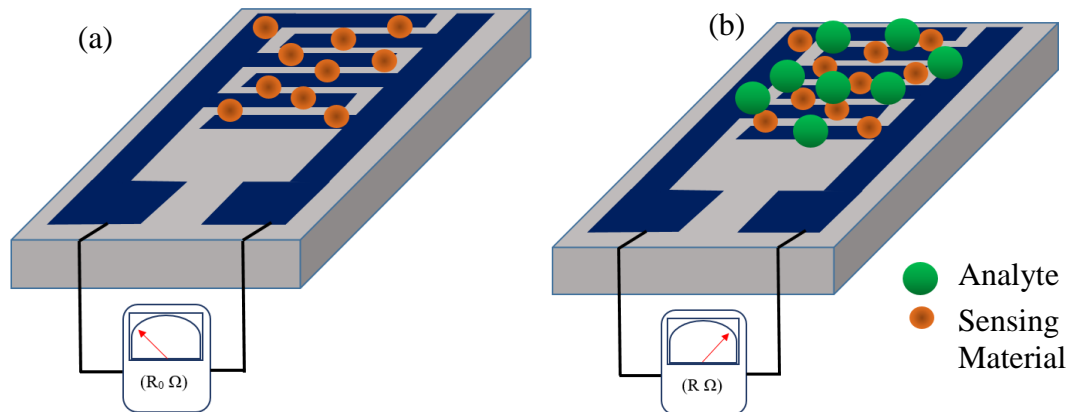


Figure 1.7: (a) A chemiresistor sensor resistance coated with sensing material having R_0 resistance (b) sensor resistance changes to R upon interaction with analyte.

1.6.2 Metal oxide-based chemiresistor

Metal oxide (MO_x) based chemiresistive sensors have been widely studied for VOC analysis and used in a variety of applications [71]. These sensors are mostly used for reducing and oxidizing gases. These sensors can interact with the target VOCs whereby the metal oxide undergoes reduction and oxidation reaction, leading to the exchange of electrons, thereby changing the resistance of the sensor and yielding an electrical signal [72, 73]. Zinc oxide (ZnO), iron oxide (Fe_2O_3), titanium dioxide (TiO_2), nickel oxide (NiO), tin dioxide (SnO_2), and others have been reported as electrochemical sensors [73-75]. Sometimes, metal oxides are incorporated with other nanomaterials such as graphene to increase sensitivity [75]. Zhang et al. used graphene/ WO_3 in acetone analysis where metal oxide is affected by temperature and forms ionized oxygen species such as O_2^- , O^- on the surface of metal oxide [76]. The formation of this species is predominant for the performance of the sensor that occurs on the surface of the electrode, as shown in Figure

1.8 [73, 76]. MOx sensors provide several advantages, such as low cost, portability, measurement simplicity, ease of fabrication, and lower limit of detection [71-76]. However, one of the disadvantages of MOx sensors is that they do not operate at room temperature as the high temperature is required to overcome the activation barriers [73].

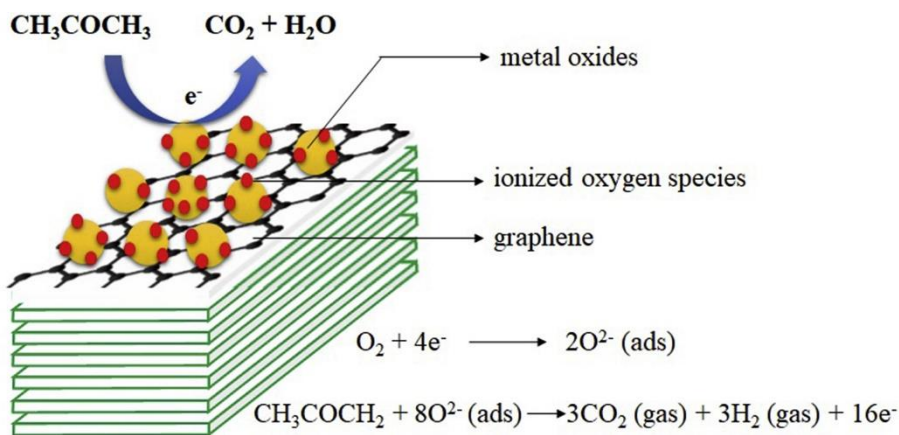


Figure 1.8: Illustration of the MOx sensor mechanism in response to acetone (copied from Ref. [73]).

1.6.3 Conductive polymer-based chemiresistor

Conductive polymer materials of nanometer sizes have emerged as promising candidates for electrochemical sensor applications [77, 78]. Polyaniline (PANI), polypyrrole (PPy), and poly(3,4-ethylene dioxythiophene) (PEDOT) are mostly studied conductive polymers as sensing materials [79-81]. Conductive polymers have several benefits such as simple synthesis, structural diversity and flexibility, lightweight, and inexpensiveness [80]. Surface functionalization of these nanomaterials can lead to a significant improvement of properties relevant to their sensor applications. Covalent and non-covalent interactions have been commonly used to functionalize these nanomaterials

[82]. For covalent approaches, conducting-polymer nanomaterials can be altered by grafting functional groups on the polymer backbone or by applying functionalized monomers during polymerization. On the other hand, the non-covalent approaches can be achieved during synthesis and the electrostatic adsorption of guest molecules on the nanomaterial surface [82, 83].

1.6.4 Metal nanoparticle-based chemiresistor

Metal nanoparticles are an extraordinary candidate for gas sensing applications because of their size, shape, morphology, chemical purity, and dispersity [84]. Metal nanoparticles are dispersed in between electrodes and help to increase the surface area to volume ratio, and favor the adsorption of the gases. Various metals such as Au, Pt, Pd, Ag, and alloys of these metals have been reported for sensing gases [85, 86]. However, Au nanoparticles with selective functional groups are the most familiar chemically modified metal nanoparticles used in sensing applications [85]. When the analyte interacts with tailored organic functional groups, it alters the distance between the conductive metal nanoparticles, or in some cases leading to a charge transfer between the organic functional groups and the nanoparticles [87].

The interaction between the sensing material and the analyte occurs because of covalent bonding, hydrogen bonding, or molecular recognition [88, 89]. An Analyte diffuses into the films at a proportion described by its partition coefficient and this identifies the sensitivity and selectivity of the sensing material. The conductivity of the

films of Au nanoparticles has been reported as an activated core-to-core electron hopping mechanism by the following equation:

$$\sigma_{EL} = \sigma_0 \exp[-\beta_d \delta_{edge}] \exp\left[-\frac{E_A}{RT}\right] \dots \dots \dots (1.1)$$

σ_{EL} = electronic conductivity ($\Omega^{-1} \text{ cm}^{-1}$)

σ_0 = pre-exponential constant

δ_{edge} = edge-to-edge distance

β_d = electron tunneling coefficient (\AA^{-1})

E_A = activation energy (kJ mol^{-1})

R = gas constant

T = temperature (K)

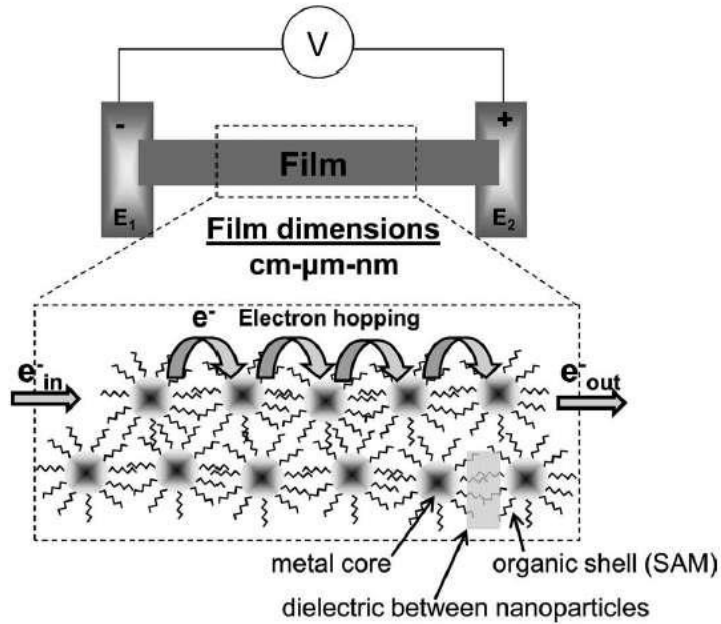


Figure 1.9: Schematic representation of the film of metal monolayer-protected clusters (MPCs) sensing material deposited in between electrodes (copied from Ref. [85]).

The electron hopping mechanism that occurs through the self-assembled monolayer (SAM) of gold nanoparticles is shown in Figure 1.9 [85]. The first part in Equation 1.1 shows that σ_{EL} is exponentially proportional to the nanoparticle edge-to-edge distance (δ_{edge}) and the tunneling coefficient (β_d). The value of δ_{edge} relates to the length or number of carbons in the alkyl chain of the SAM. β_d is referred to as an attenuation factor that depends on the structure and molecular configuration of the SAM. Also, the second part in Equation 1.1 shows that conductivity is exponentially related to the temperature and the energy of activation [85].

In general, when the film of metal nanoparticles interacts with an analyte, the analyte diffuses into the film and causes to increase in the core-to-core distance through film swelling. Thus, it changes the electronic conductivity of the film. Also, the dielectric properties of the nanoparticle significantly affect the electron tunneling and the activation energy, which tends to a change in the conductivity of the film. At a fixed temperature of sensing experiments, the aforementioned variables influence the overall film conductivity. Sometimes, it is hard to determine the dominant factor.

1.6.5 Sensor array

The biggest challenge of the chemical sensor is the presence of interference. All chemical sensors suffer from a lack of selectivity which hinders getting detailed information on the matrix composition of the sample [90]. Although extensive efforts have been made to improve the selectivity of chemical sensors, the development of a single sensor to distinguish different vapors is difficult. However, a sensor array with several

sensor materials with different selectivity and sensitivity can be used to sense a wide variety of vapors. Gas sensor array employs pattern recognition of combined responses of cross-reactive sensing materials [91].

Sensor arrays have been used commercially and for real-world applications. Shan et. al. utilized a sensor array device made with gold nanoparticles functionalized with different organic ligands to detect COVID-19 from exhaled breath [92]. WOLF eNose is a commercial sensor array device for the detection of VOCs, and it has been associated with the detection of urinary tract infections [93].

1.7 Motivation of this work

Despite scientists' dedication to improving different analytical techniques to detect various VOCs, there are only a few inexpensive portable commercial devices available on the market for analyzing a wide range of VOCs present in the air. The real challenges are as follows:

1. Chemical sensors suffer from poor selectivity for a particular compound because a sensor material shows interaction with a certain group of compounds.
2. Another challenge for the chemical sensor is the presence of interference as the environmental air contains a mixture of different VOCs. The sensor response would be significantly different for a mixture of compounds from a particular compound.
3. Most standalone chemical sensors and detectors are not sensitive or accurate for quantitative analysis of airborne VOCs at trace levels due to their detection limits.

4. Conventional detectors used for VOC analysis are expensive, bulky, consume a lot of electric power, not suitable for field analysis.
5. There are GC-MS and LC-MS-based analytical techniques to detect a group of compounds such as BTEX and carbonyl compounds, but there is no single sampling technique to identify a wide range of VOCs. Detection of BTEX and carbonyls separately is cumbersome and time-consuming.

Since a single sensor is not good to analyze target VOCs in the air because of interference with other traces VOCs, a sensor array or an electronic nose containing multiple sensing materials could overcome this problem. These sensor materials interact selectively with a group of compounds that help to sense a wide variety of VOCs. In recent years, microelectromechanical system (MEMS) technology has been widely used to produce microdevices that have lower fabrication costs, thermal mass, portability, and less power consumption. Also, using gold-thiolate monolayer-protected clusters (Au MPCs) as a sensing material provides advantages over other materials such as room-temperature operation, improving sensitivity and selectivity by changing the composition of the thiolate monolayer.

Microfabricated devices can be used as a micropreconcentrator (μ PC) or microreactor to capture various compounds by using different sorbents, reagents, etc. for sampling VOCs. Based on current challenges to detect airborne VOCs efficiently, we proposed to develop a micro-sensor array and a new micropreconcentrator to fulfill the goal of analyzing a wide range of VOCs.

1.8 Objectives of this work

The overall objective of this work is to develop a sensor array and a micropreconcentrator to detect airborne toxic VOCs. Four specific objectives are described below:

1. Design and fabricate a microfabricated sensor array for detecting VOCs.
2. Develop thiol-functionalized Au MPCs for sensing aromatic and chlorinated VOCs.
3. Develop a micropreconcentrator for increasing sensitivity and integration with SPME for GC-MS analysis.
4. Develop a novel dual-compartment micropreconcentrator to detect BTEX and carbonyls together by GC-MS with a single run and utilize it to measure the concentrations of these VOCs in the environmental air.

1.9 Dissertation overview

This dissertation presents three projects concerned with determining VOCs using micro-sensor arrays and micropreconcentrators. These projects involve the design, fabrication, and characterization of silicon-based microdevices. The application of this work includes VOC exposure assessment, air pollution monitoring, and disease diagnosis.

There are six chapters in this dissertation. The first chapter describes the background of this study including VOCs, their types and health effect, VOCs sampling, and analysis. The detection mechanism of VOCs by GCMS and chemical sensors is described here. The motivation and objectives of this work are also stated in this chapter.

Chapter 2 presents the design and fabrication of a micro-sensor array on a Si substrate. The commercial thiol functionalized Au MPCs are used to characterize the sensor array. The sensor measurement setup and the response calculation are explained. Chapter 3 introduces new molecular recognition motifs to improve the sensitivity and selectivity of sensors to detect BTEX and TCE. The response profile of different alkali metal ion-carboxylate functionalized Au MPCs for several non-aromatic, aromatic and chlorinated VOCs are explained in this chapter. The sensing material interaction with humidity suggests developing a preconcentrator to produce moisture-free concentrated samples for the sensor.

In chapter 4, the development of a micropreconcentrator device to capture BTEX compounds is presented. The relation of analyte recovery with important variables including adsorption and desorption flow rate, desorption temperature are demonstrated. Chapter 5 explores the development of a novel dual-compartment micropreconcentrator to detect BTEX and carbonyls together in a single run. The optimized reaction conditions for carbonyl derivatization are presented. Finally, the airborne VOCs are analyzed from different locations in the Louisville area using this microdevice. Chapter 6 provides the overall conclusion of this dissertation and recommendation for future research works.

CHAPTER II

DESIGN AND FABRICATION OF A MICROSENSOR ARRAY FOR SENSING VOCS

2.1 Introduction

Chemical sensors are utilized to detect hazardous VOCs because of their high sensitivity, lower cost, less power consumption, portable size, and great potential to combine into a sensor array for multi-component analysis [58, 63]. Chemical sensors can be classified based on transduction methods, such as piezoelectric [94], colorimetric [95], fluorescence [96], and chemiresistors [97]. Chemiresistor is a widely used chemical sensor where the resistance is measured across the film of sensing material upon interaction with the target analyte [85]. Carbon nanotubes [98], metal oxide nanowires and composites [99, 100], nanoparticles [101, 102], semiconductors [103], and polymer nanofibers [104] have been studied for chemiresistor applications to detect different VOCs. Metal nanoparticles functionalized with ligands are a well-suited candidate for room-temperature sensing operation and can be modified to sense various analytes incorporating organic functional groups [85].

Nowadays, thiol-functionalized gold nanoparticles are well-studied because they can be easily functionalized with various thiol groups. It improves the sensitivity and selectivity for the specific detection of different target analytes by changing the composition and surface chemistry of the thiolate monolayer [105]. Moreover, chemical stability, higher surface area to volume ratio, size controllability, and surface tunability of these nanoparticles provide an ideal platform for sensor applications [106]. The functional groups on the surface of the gold nanoparticles can interact with target compounds, causing a change in the electrical resistance of the thin film due to the adsorption or desorption of the target compound, which can be measured using a simple circuit [107]. Ibanez et al. prepared hexane thiolate-coated gold monolayer-protected clusters (C_6 Au MPCs) and used a thin film of these nanoparticles to sense toluene vapors [108]. Evans et al. synthesized Au MPCs protected with thiol $S-C_6H_4-X$, where $X = -OH, -COOH, -NH_2,$ and $-CH_3$, for sensing methanol, ethanol, 2-propanol, hexane, pentane, toluene, chloroform, and acetic acid [109, 110].

However, these chemiresistor sensors have common challenges that include low sensitivity, poor selectivity, and interference from mixtures of VOCs. Since the environmental air contains various VOCs with different concentration levels and humidity, it is hard to obtain all information on toxic VOCs using a single chemiresistor. A sensor array containing multiple sensors responsive to different compounds is a promising tool for environmental air monitoring [90, 111]. The basic components of a sensor array are sensing materials, transducers, pattern recognition, and device [102]. Han et al. developed a sensor array to detect and differentiate VOCs and nitro-aromatic compounds using thin film assemblies of alkanethiol-capped Au MPCs. These nanoparticles were formed by

molecularly mediated assembly using linkers of different chain lengths and functional groups [102].

Miniaturization of devices is carried out to lower fabrication costs, minimal usage of sensing material, faster response, and easy integration with microelectronics [112, 113]. Micro-electromechanical system (MEMS) technology is used to fabricate microdevices. In this chapter, we describe the design and fabrication of a silicon-based microsensor array. To characterize the microdevice, several commercial thiols functionalized Au MPCs were synthesized. Thin films of the commercial thiols functionalized Au MPCs were applied on interdigitated electrodes and resistance across the film was measured to calculate the response.

2.2 Experimental

2.2.1 Microsensor array design

The microsensor array was designed using L-edit software. The dimension of the sensor chip is 1 cm x 1 cm. Figure 2.1 shows the layout of a complete chip design. The chip features four circularly shaped (diameter 2 mm) sensing areas of interdigitated electrodes (IDE) (line width 20 μm and spacing 10 μm) with contact pads. The area of the contact pad is 6 mm². The gap between each contact pad is 1 mm. The distance from the contact pad to the IDE is 0.6 mm, which is connected by a 100 μm wide metal line. Each circular IDE edge-to-edge distance is 0.6 mm.

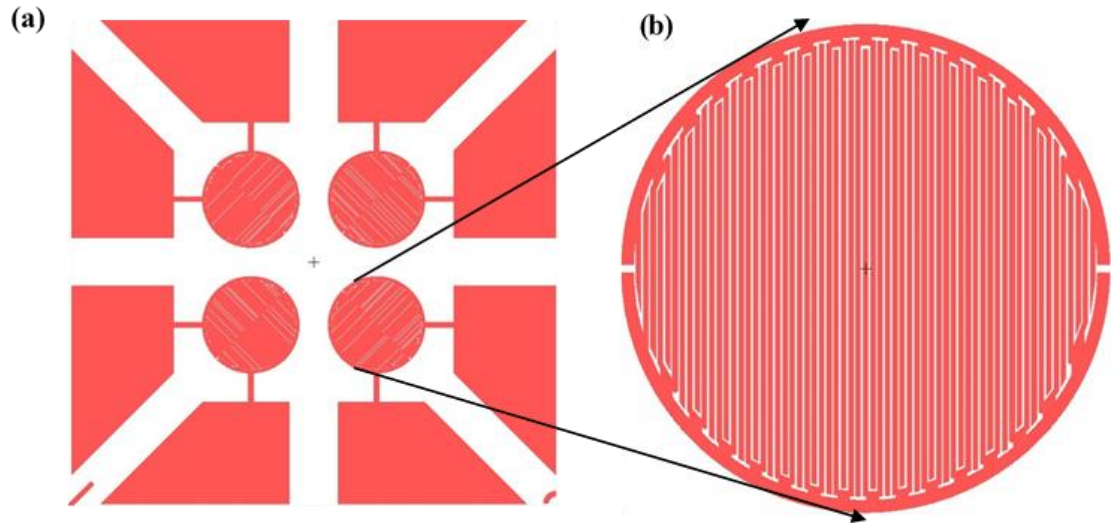


Figure 2.1: Microsensor chip design: a) layout of each chip, b) zoomed view of IDE area.

A similar chip design was placed in an arrangement to fit onto a standard 4-inch silicon wafer. A total of 52 pieces of the chip were obtained from this arrangement. The wafer design was sent to the Micro/Nano Technology Center (MNTC) at the University of Louisville to create a light field photomask. A Heidelberg DWL 66FS UV laser patterning system was used for the generation of the photomask. Figure 2.2 represents the fabricated photomask. The microfabrication steps to prepare this sensor substrate was carried out in the cleanroom facility.

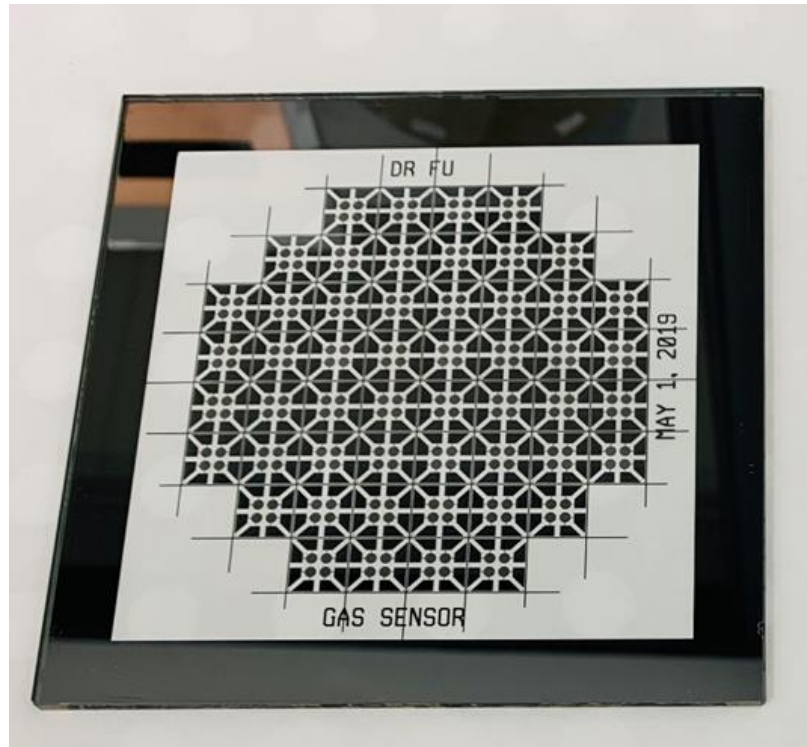


Figure 2.2: Fabricated light field photomask.

2.2.2 Microsensor array fabrication

The microsensor array was fabricated on a single-side polished (diameter 4") oxidized 500 μm thick 1-10 $\text{ohm}\cdot\text{cm}$ resistive n-type silicon wafer. Silicon dioxide, on top of the wafer, acts as electrical insulation. Shipley 1813 photoresist was used for patterning and it also worked as a sacrificial layer that was eliminated by dissolving the wafer in acetone. Pt/Cr metals were deposited for IDE and contact pads. The detailed fabrication steps shown in Figure 2.3 are described in the following paragraphs.

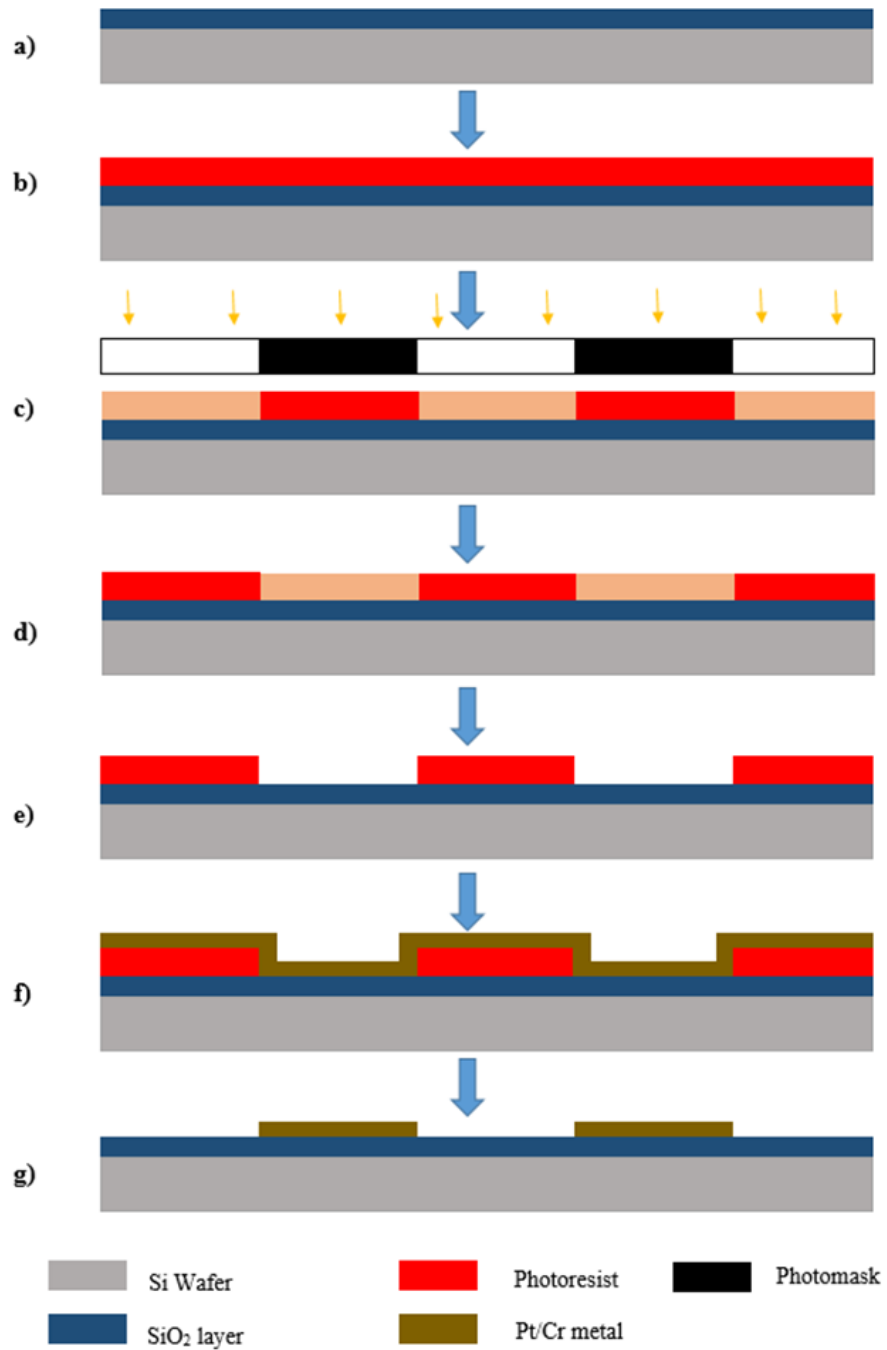


Figure 2.3: Fabrication process flow diagram: a) cleaning oxidized silicon wafer, b) Photoresist coating, c) UV light exposure, d) Yes Image reversal, e) Development, f) Metal sputtering, g) Lift-off process.

Photolithography:

Photolithography is a technique to create patterns on a thin film or substrate using light. Ultraviolet (UV) light is used to bring a design from a photomask to a light-sensitive polymer photoresist [114]. Photoresists are classified into two groups: positive photoresists and negative photoresists. The UV light causes a positive photoresist to decompose and be washed away by a developer solution where UV light is exposed. A negative photoresist has the opposite property, which becomes insoluble to the developer solution after exposing to light [115].

In this step, the wafer was first cleaned with acetone, methanol, deionized (DI) water, and nitrogen to get rid of any trace contaminations on the surface of the wafer such as dust, organic, ionic, and metallic compounds (Figure 2.3a). A positive photoresist Shipley 1813 was coated on the cleaned silicon wafer at a spin speed of 500 rpm for 1 second and a rotation speed of 4000 rpm for 30 seconds. The rotation caused the photoresist to be spread uniformly across the surface of the wafer with the excess being spun off. The thickness of the photoresist was around 1.3 μm (Figure 2.3b).

Preparation of the photoresist is completed by soft bake, where the wafer was gently heated at a moderate temperature to evaporate the solvent and partially solidify the photoresist. The soft bake reduces the prevailing solvent content on the substrate to promote photoresist adhesion. The wafer was soft-baked at 115°C temperature for two minutes. The wafer was then patterned by contact exposure method using Karl Suss Mask Aligner MA6/BA6. UV source was exposed on the wafer for 12 seconds at 12 W/cm^2 through a clear field photomask (Figure 2.4c).

YES Image Reversal:

This process reverses the action of a positive resist so negative images are often formed with the identical resolution and processing that a positive resist allows. In addition, image reversal helps to obtain higher resolution and improved lift-off profiles by permitting variations of the slope of the photoresist sidewall. The key advantages of using image reversal on positive resists rather than using negative photoresists or an opposite mask are higher resolution, re-entrant sidewalls, and smoother sidewall edges to ease sputter materials without bridging [116].

Ammonia was employed during this process. There are three steps in the image reversal process: image exposure dose, ammonia exposure, and flood exposure. In ammonia exposure, the main factor is the temperature of the exposure. In this experiment, 90 °C was maintained in the YES image reversal oven (Figure 2.3d). When the substrate has been exposed to ammonia, the remaining photoactive compounds should be exposed to UV and that was done by flood exposure. As the long bake was performed during the ammonia step, the flood exposure should be 2-3 times higher than the normal imaging exposure. Flood exposure was done for 25 seconds using Karl Suss Mask Aligner MA6/BA6. After flood exposure, the photoresists of the initial UV light unexposed area became soluble in the developer solvent.

Development:

The wafer was developed in Microposit MF319 solution for 90 seconds followed by rinsing under a DI water bath and drying with N₂ (Figure 2.3e). The wafer was observed

under an optical microscope to check the patterns. Then the wafer was hard-baked for 2 minutes using the hotplate at 115 °C.

Sputtering:

Before running metal sputtering, the wafer surface was treated with O₂ plasma to remove any organics, which promotes better adhesion of metal to the substrate surface. March RIE CS1701 was used for this cleaning step and O₂ gas flowed for 15 seconds. The wafer was then sputtered with Chromium (Cr) and platinum (Pt) metals using a Kurt J. Lesker PVD 75 (Figure 2.3f). To promote the Pt adhesion to the SiO₂ layer, a thin layer of Cr was deposited before sputtering the Pt. Cr and Pt were sputtered for 2 and 6 minutes respectively in 300 W DC power, which results in a total of 185 nm thick metal layer.

Lift-off:

The wafer was placed in an ultrasonic bath with acetone to complete the lift-off process. Frequent monitoring was carried out to check the complete removal of metals from undesired areas. IDEs and contact pads became visible after 10 minutes (Figure 2.3g). The wafer was placed in a DI water bath followed by drying in a spin dryer. The wafer was checked under a microscope to ensure completeness. Then metal layer thickness was measured by using the Dektak profilometer. Finally, the wafer was diced into a 1 cm x 1 cm microsensor chip (Figure 2.4).

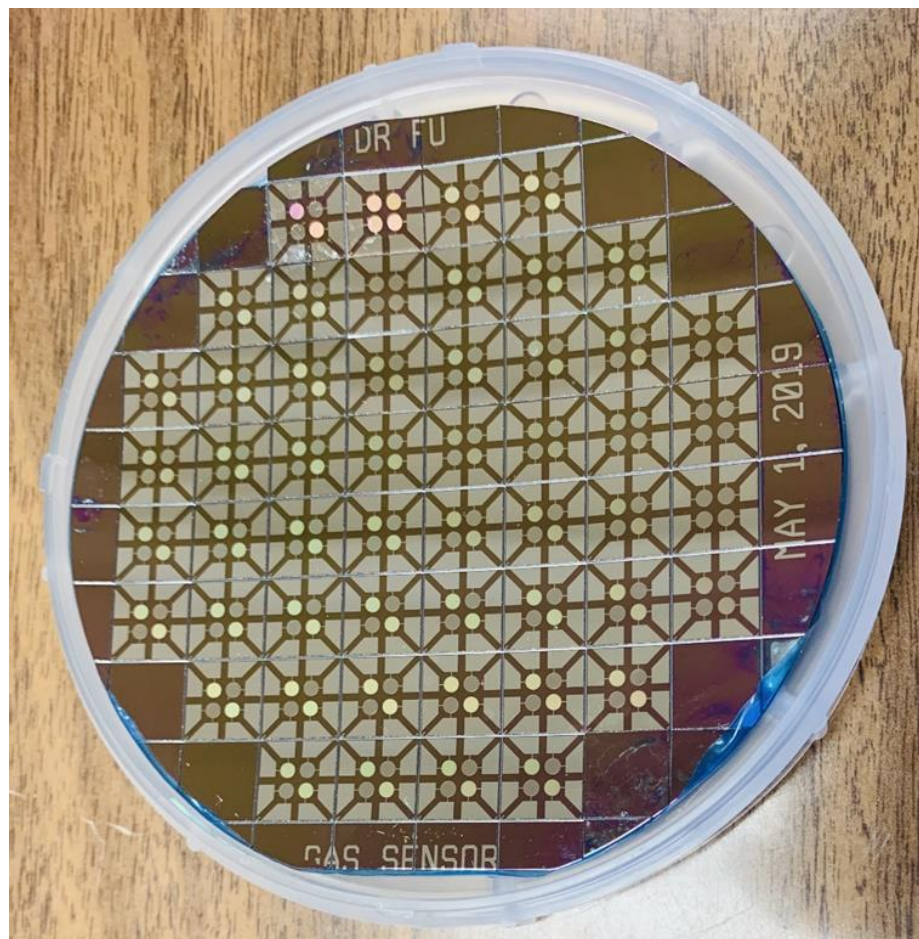


Figure 2.4: A diced wafer containing 52 pieces of microsensor chips.

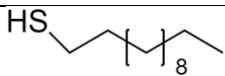

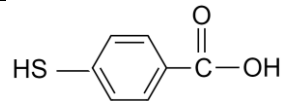
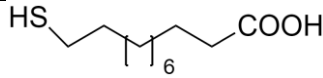
2.2.3 Chemicals

Hydrogen tetrachloroaurate (III) ($\text{HAuCl}_4 \cdot 3\text{H}_2\text{O}$), tetraoctylammonium bromide (TOAB), sodium borohydride (NaBH_4), 1-dodecanethiol (DDT), 4-methoxy- α -toluenethiol (MTT), 4-mercaptobenzoic acid (MBA), and 11-mercaptoundecanoic acid (MUA) were obtained from Sigma Aldrich. Solvents such as ethanol, acetonitrile, and dichloromethane were obtained from Sigma Aldrich. Synthetic air was purchased from Welders Supply Co. of Louisville. Milli-Q® ultrapure water was used for synthesis.

2.2.4 Synthesis of commercial thiol functionalized Au MPCs:

Thiol-functionalized gold nanoparticles were synthesized by a modified two-phase method [117]. Aqueous Gold (III) chloride (0.05 g of $\text{HAuCl}_4 \cdot 3\text{H}_2\text{O}$ was dissolved in 4 ml ultrapure water) was transferred to a toluene solution containing phase transfer reagent TOAB (dissolving 0.08 g of TOAB in 20 ml Toluene). The solution was stirred vigorously until the organic phase was isolated; then the 1:1 molar ratio of thiol: $\text{HAuCl}_4 \cdot 3\text{H}_2\text{O}$ was added to the solution. An aqueous solution of NaBH_4 (0.056 g of NaBH_4 dissolved in 4 mL ultrapure water) was added dropwise to the solution. A rapid color change occurred after adding NaBH_4 solution that indicated the formation of nanoparticles. The reaction occurred by vigorous stirring at room temperature for at least 3 hours and produced a dark brown-colored solution of the thiol-capped Au MPCs. The solvent was removed from the solution by a rotary evaporator and followed by multiple washing using acetonitrile. Au MPCs were dried at room temperature overnight to make a solid form. Four different Au MPCs were synthesized using different functional motifs presented in table 2.1.

Table 2.1: Thiols used to functionalize Au MPC chemiresistors.

Thiol	Symbol	Structure
1-dodecanethiol	DDT	
4-methoxy- α -toluenethiol	MTT	
4-mercaptobenzoic acid	MBA	
11-mercaptoundecanoic acid	MUA	

2.2.5 Sensor characterization:

The microsensor chip was wire-bonded on a 24 Pin dual in-line pin (DIP) Round Solder IC Socket by 200 μm diameter Al wire. Four different thiol-functionalized Au MPCs were dispersed in toluene in different vials by sonication for 5 min and then drop-casted onto the four different IDE areas of the microchip by dropwise addition. The chip was kept in an oven at 40 °C overnight to ensure the removal of solvent from the film. The solvent was evaporated to afford a flat, roughly circular film of nanoparticles.

The microsensor chip carrier was placed in a 4-way standard cross stainless-steel test chamber (C-0275, Kurt J. Lesker Company) fitted with inlet and outlet tubing. Sensing film resistances were monitored and recorded by a multi-channel multimeter (Keithley DAQ 6510) and a single-channel multimeter (Keithley 2400). In a typical experiment of a particular gas sample, sensor response was measured over 5 min under a vacuum of 28 inches Hg to remove VOCs adsorbed on the Au MPCs sensor film, followed by gas sample exposure at atmospheric pressure, and then again for 5 min under vacuum of 28 inches Hg. The cycles were repeated at least three times to check reproducibility. Each sensor material was exposed to 250 ppb, 500 ppb, 750 ppb, and 1 ppm of benzene, toluene, ethylbenzene, xylene (mixture of m, p, and o – isomers), formaldehyde, acetone, ethanol, and pentane gaseous samples.

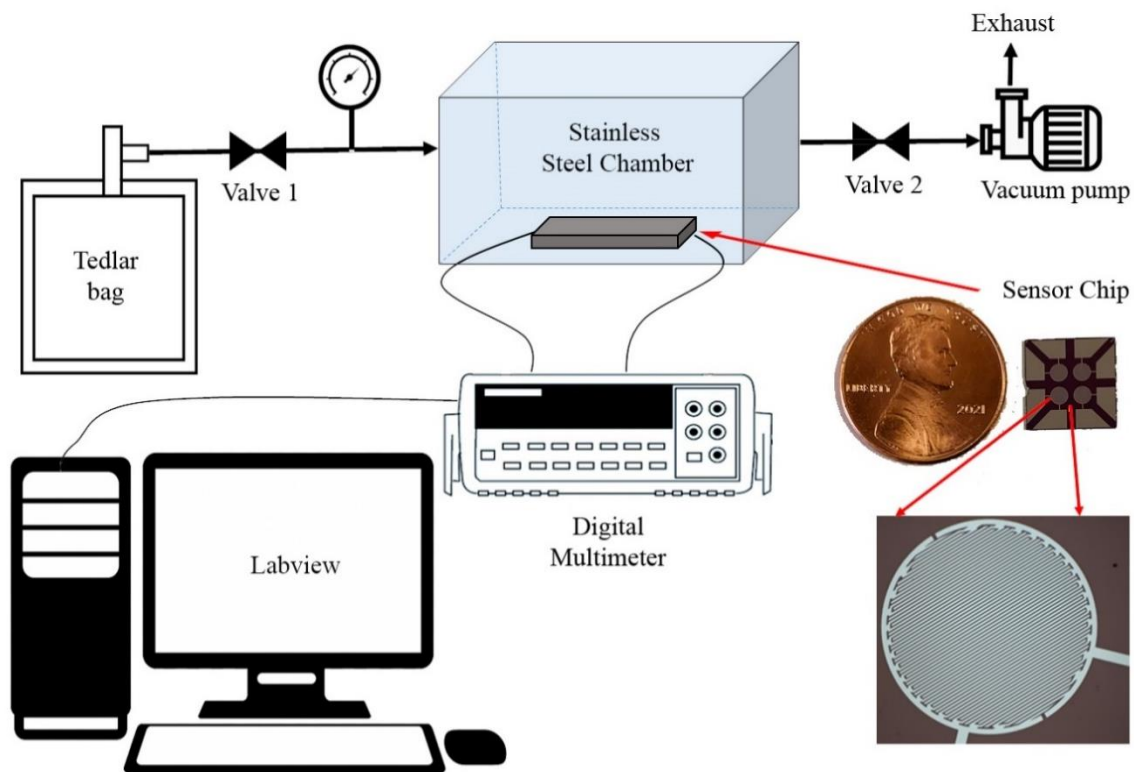


Figure 2.5: Laboratory setup for measuring chemiresistor sensor responses to VOCs.

All the gaseous analyte samples were prepared using Tedlar bags. A 1000 ppm concentration of benzene vapor was produced by injecting 3.7 μL of benzene into a Tedlar bag containing 1 L of dry air. Similarly, 1000 ppm of toluene, ethylbenzene, xylene, formaldehyde, acetone, ethanol, and pentane were made by injecting corresponding amounts of the solvents. Then, 100 mL of the above gas samples were removed from the Tedlar bag using an air-tight syringe and injected into a new Tedlar bag containing 900 mL of dry air, resulting in a concentration of 100 ppm. The 10 ppm samples were prepared similarly and the 1 ppm, 750 ppb, 500 ppb, and 250 ppb of analyte samples were then produced by dilution processes using the 10 ppm sample. A small KNF diaphragm vacuum pump was used to evacuate the test chamber followed by an introduction of the analyte

directly from the sample bag attached to the test chamber. All the experiments were performed under ambient conditions (at 22 °C). Figure 2.5 represents the experimental setup for VOC measurement.

2.2.6 Sensor data measurement:

The sensor response is defined by the following equation:

$$\text{Response} = R_{\text{gas}}/R_0 - 1 \dots \dots \dots (2.1)$$

where R_0 and R_{gas} are the maximum resistances of the sensor in synthetic air and the presence of the analyte, respectively. The response time is the time to get maximum resistance change due to analyte exposure. Recovery time is defined as the time taken by the sensor under vacuum to achieve 90% of the initial resistance.

2.3 Microsensor array characterization

In this section, the general response characteristics for the sensor array with various thiol-functionalized Au MPCs tested to different vapors are described. Four different Au MPCs were added onto the IDE areas of a sensor chip and tested for simultaneous measurement using the aforementioned analytes. These sensing materials vary from each other in terms of their chemical and physical properties, including morphology, hydrophobicity, and chain length. Because of these dissimilarities, the film conductivity is unlike each other. The variability in the conductivities is due to the result of combined

factors, including core edge-to-edge distance, electron tunneling coefficient, and activation energy of electron transfer [85].

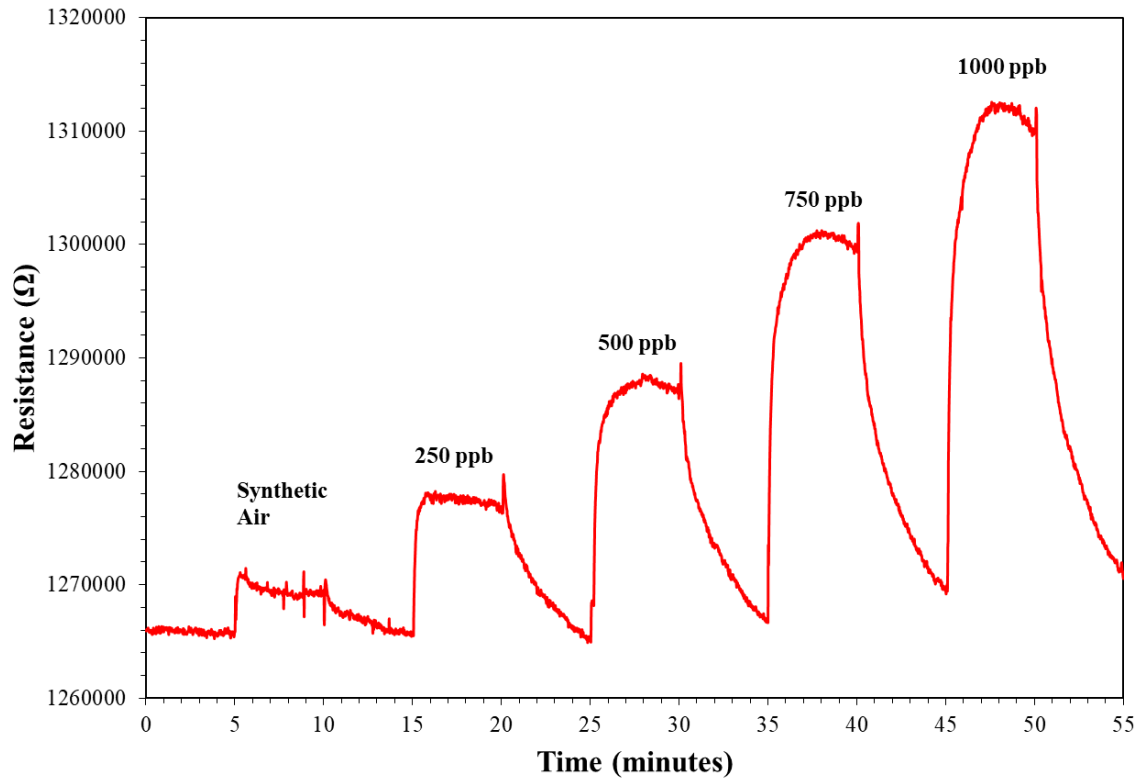


Figure 2.6: Resistance change of DDT functionalized Au MPCs with time upon exposure to synthetic air, 250 ppb, 500 ppb, 750 ppb, and 1 ppm of benzene.

Figure 2.6 illustrates the resistance plot of DDT-functionalized Au MPCs at different concentrations of benzene. The resistance of the sensing film increased when benzene was introduced into the testing chamber and returned to baseline upon chamber evacuation. The elevation of resistance indicates the film swelling effect that increases the edge-to-edge distance upon diffusion of the analyte into the film [85]. Joseph et al.

observed the same positive response or resistance increase upon exposure to toluene for 1,12-dodecanedithiol functionalized gold nanoparticles [118]. Resistance increased for these four sensors in response to tested analytes similar to as reported results [102, 119]. Figure 2.7, 2.8 and 2.9 shows the resistance plot of DDT, MUA and MTT-functionalized Au MPCs in response to xylene, acetone and pentane, respectively.

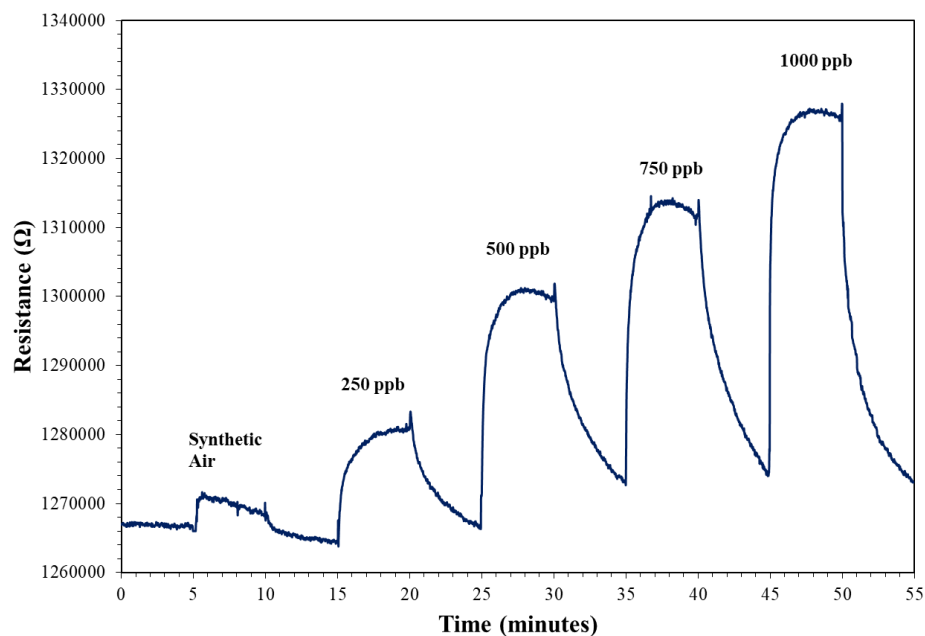


Figure 2.7: Resistance change of DDT functionalized Au MPCs with time upon exposure to synthetic air, 250 ppb, 500 ppb, 750 ppb, and 1 ppm of xylene.

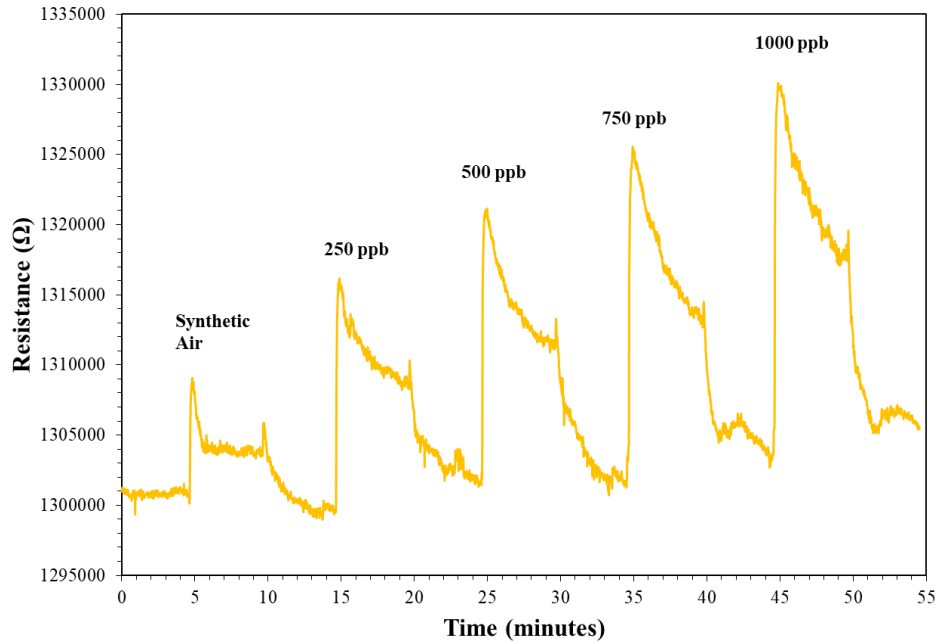


Figure 2.8: Resistance change of MUA functionalized Au MPCs with time upon exposure to synthetic air, 250 ppb, 500 ppb, 750 ppb, and 1 ppm of acetone.

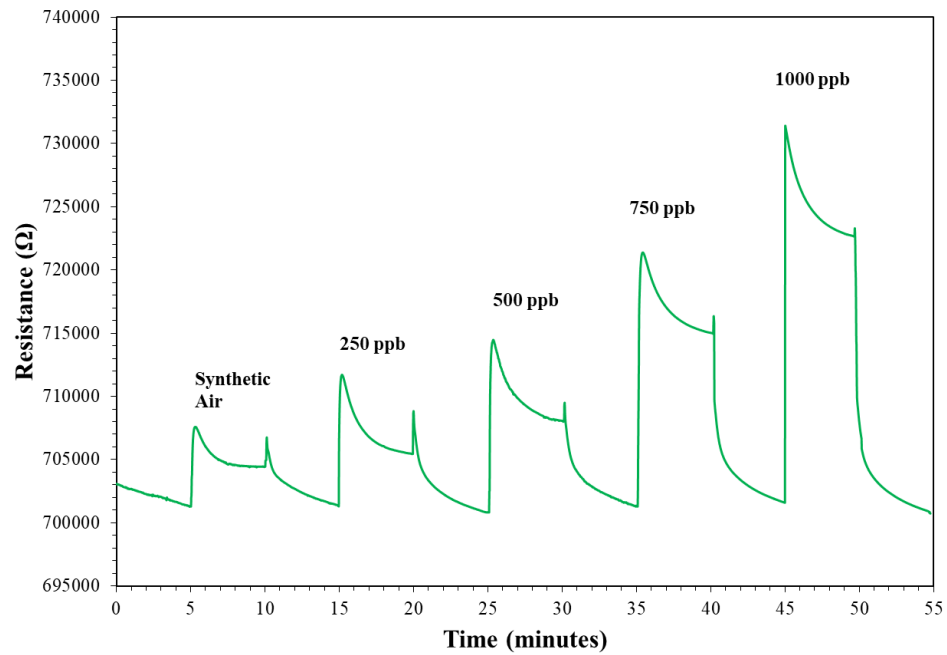


Figure 2.9: Resistance change of MTT functionalized Au MPCs with time upon exposure to synthetic air, 250 ppb, 500 ppb, 750 ppb, and 1 ppm of pentane.

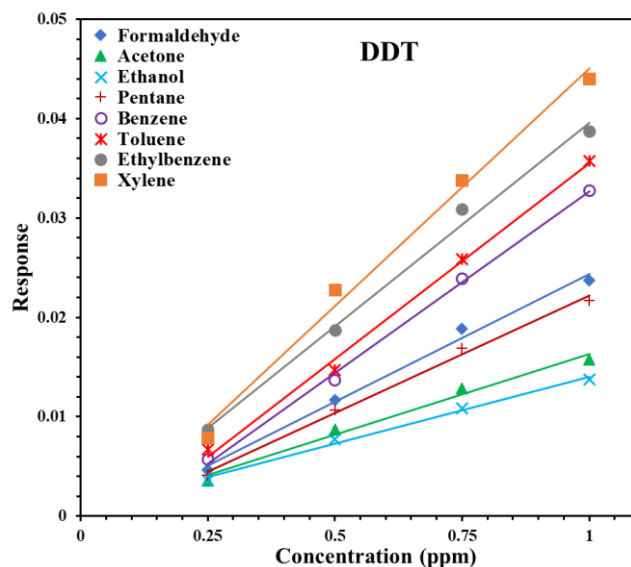


Figure 2.10: Sensor response profile for DDT functionalized Au MPCs in response to benzene, toluene, ethylbenzene, xylene, formaldehyde, acetone, ethanol, and pentane vapor at concentrations from 0.25 ppm to 1 ppm.

Equation 2.1 is used to calculate the response. The responses of DDT-functionalized Au MPCs to tested analytes are shown in Figure 2.10. This sensor shows linear responses to different concentrations of analytes, though the response profile varies for different compounds. The VOCs present in environmental air are at sub-ppb level, so we tested the responses at low concentrations of analytes. From the response profile, the DDT sensor showed higher interaction for xylene and lower response to ethanol. Figure 2.11 to 2.13 shows the response plots of MUA, MBA, and MTT functionalized Au MPCs tested on these eight analytes.

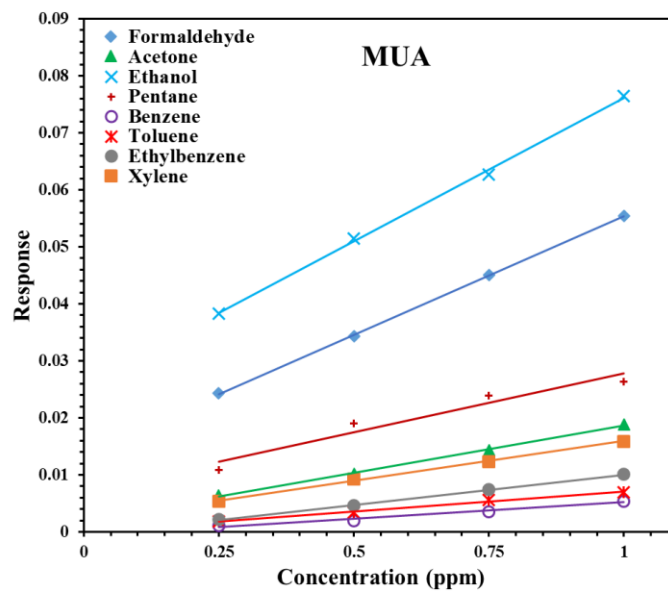


Figure 2.11: Sensor response profile for MUA functionalized Au MPCs in response to benzene, toluene, ethylbenzene, xylene, formaldehyde, acetone, ethanol, and pentane vapor at concentrations from 0.25 ppm to 1 ppm.

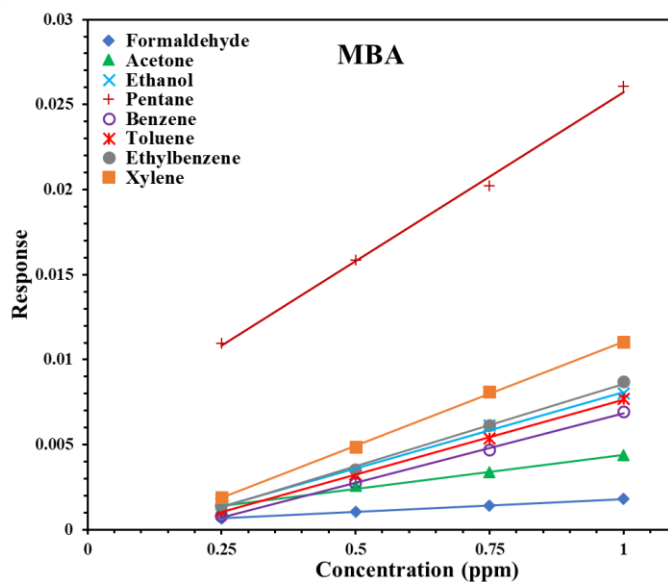


Figure 2.12: Sensor response profile for MBA functionalized Au MPCs in response to benzene, toluene, ethylbenzene, xylene, formaldehyde, acetone, ethanol, and pentane vapor at concentrations from 0.25 ppm to 1 ppm.

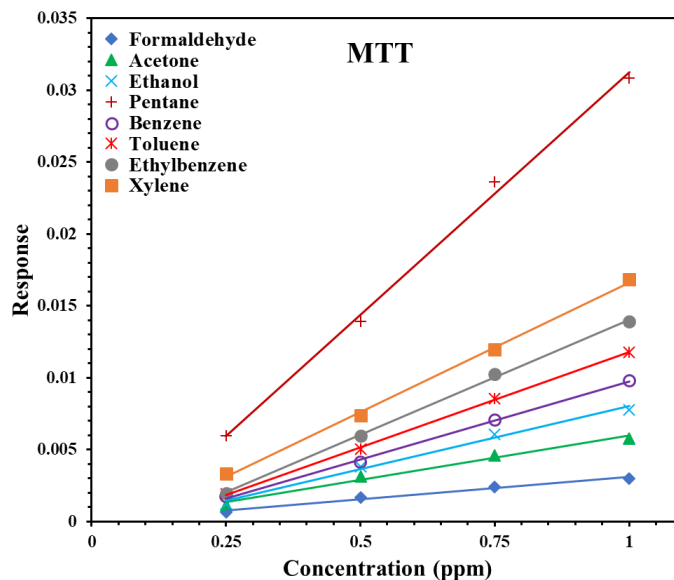


Figure 2.13: Sensor response profile for MTT functionalized Au MPCs in response to benzene, toluene, ethylbenzene, xylene, formaldehyde, acetone, ethanol, and pentane vapor at concentrations from 0.25 ppm to 1 ppm.

To differentiate the sensitivity for different VOCs, here we plot the responses of four sensors to individual compounds (1 ppm of benzene, toluene, ethylbenzene, xylene, formaldehyde, acetone, ethanol, and pentane) in Figure 2.14. At a first glance, all sensors are responsive to every analyte and individual thiols induce different selectivity. DDT sensor shows higher interaction towards BTEX compounds than other sensors as it contains a straight alkane carbon chain in the thiol ligand. MUA sensor provides a higher response for formaldehyde, acetone, and ethanol because $-\text{COOH}$ functional group in this thiol can contribute hydrogen bonding toward these analytes. MTT sensor shows a higher response to pentane.

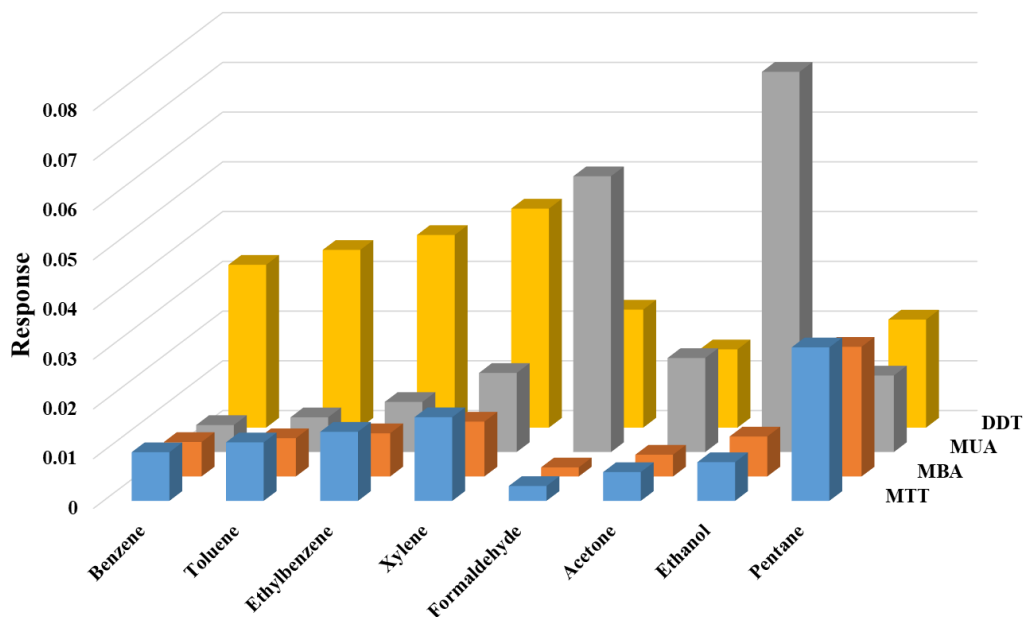


Figure 2.14: Responses of MTT, MBA, MUA, and DDT functionalized sensors to sense 1 ppm of individual benzene, toluene, ethylbenzene, xylene, formaldehyde, acetone, ethanol, and pentane.

For a real-world application, the gas sensor array is exposed to a mixture of compounds at different concentrations present in the environmental air. So, we tested this sensor array containing DDT, MUA, MBA and MTT-functionalized Au MPCs to a mixture of benzene, toluene, ethylbenzene and xylene (BTEX) at four concentration levels (each compound concentration 0.25, 0.5, 0.75 and 1 ppm). In Figure 2.15, a comparison of DDT sensor responses for the BTEX mixture and individual compounds is presented. It is observed that the DDT sensor response for the BTEX mixture was higher than the combined response of individual compounds. This could be the result of a synergistic effect because the presence of multiple gases can lead to a synergistic effect that enhances the sensitivity of the gas sensor [120]. Also, when a gas mixture comes in contact with the

sensing material of a gas sensor, it results in an increased surface area available for the adsorption of gas molecules which might lead to a higher response of the gas sensor to the gas mixture as compared to a single compound [121].

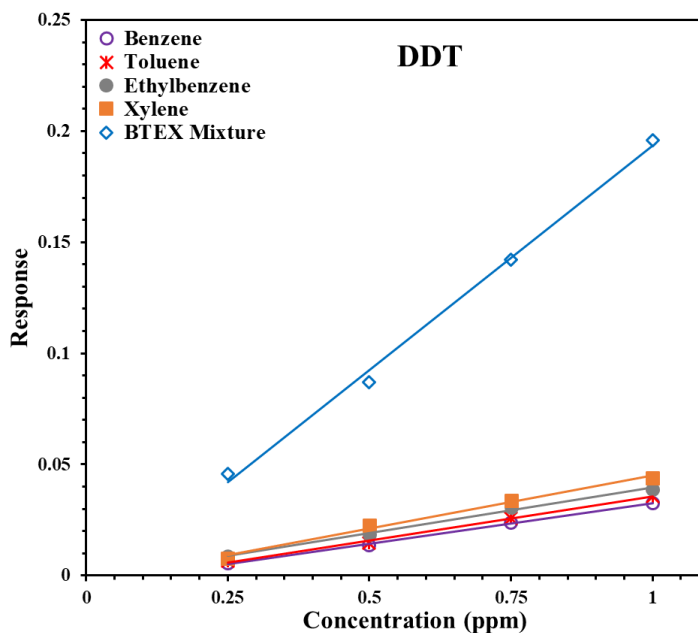


Figure 2.15: Sensor response for DDT functionalized Au MPCs in response to benzene, toluene, ethylbenzene, xylene, and a mixture of these compounds at 0.25 ppm to 1 ppm concentrations.

Overall, sensor films containing different chain lengths and functional groups show variable sensitivities and selectivity and the response values are lower at these low concentrations. These results guide us to improve selectivity for target analytes and to obtain higher responses at lower concentrations.

2.4 Conclusion

In conclusion, we demonstrated the characterization and functionality of a microsensor chip that affords four different sensor materials as a sensor array and performs simultaneous testing of analytes. The commercial thiol functionalized nanostructured materials displayed linear responses to the analyte concentrations from 250 ppb to 1 ppm. Sensor films with different chain lengths and functional groups showed variable responses and sensitivities to VOCs. However, the overall selectivity of these sensors is low, which requires the development of other ligands to improve the sensor selectivity.

CHAPTER III

DEVELOPMENT OF METALATED GOLD MONOLAYER- PROTECTED CLUSTERS FOR SENSING AROMATIC VOCS AND TCE

3.1 Introduction

The detection of toxic VOCs in the environmental air using a portable sensor is an important research area because these sensors can be used for real-time analysis [122, 123]. BTEX (benzene, toluene, ethylbenzene, and xylenes) is a group of aromatic VOCs that are considered harmful and are often measured as abundant in polluted air [124]. According to the World Health Organization (WHO), exposure to BTEX can cause short and long-term adverse health effects to the central nervous system, lungs, and liver as well as cause diseases including leukemia and cancer [12, 125]. Also, Trichloroethylene (TCE) harms the central nervous system, liver, kidney, immune and reproductive systems [126]. Therefore, it is important to rapidly detect these hazardous gases from indoor and outdoor facilities to prevent exposure to high levels of these toxic compounds.

The use of nanomaterials in sensor development to detect VOCs at trace levels has been widely reported [127, 128]. Metal oxides, graphene, carbon nanotubes, conductive polymer, and thiolated Au MPCs have been studied for detecting VOCs in the environment

[98-102, 129]. However, these gas sensors face challenges for real-world applications because of low sensitivity, poor selectivity, and cross-sensitivity with humidity and air matrix [106]. Over the past two decades, gold monolayer-protected clusters (Au MPCs), where the metal nanoparticle core is surrounded by a self-assembled monolayer of organic ligand, generally thiolate-based, have been studied for VOC sensing [130]. Thiol-functionalized Au MPCs have unique properties such as high chemical stability, ease of synthesis, distinctive optical properties, large surface-to-volume ratio, and a higher level of conductivity which promote these as a better candidate for gas sensing applications [131-133]. The electronic properties can be tuned by modifying the composition, morphology, size, and surface chemistry of Au MPCs. A few chemiresistor sensors have been reported for sensing BTEX and TCE using thiolate-coated Au MPCs. Wohltjen et al. synthesized octanethiolate-coated Au MPCs and tested sensor responses to toluene, TCE, 1-propanol, and water vapors [134]. They observed the increase in resistance of Au MPCs upon interacting with toluene and TCE vapors, although the change of resistance was different for each analyte. The film of Au MPCs swelled because of the diffusion of gaseous molecules into the film and caused a decrease in electron hopping. Kim et al. explored benzene and methyl ester-functionalized thiolate-coated Au MPCs for sensing benzene and toluene vapors [135]. Joseph et al. used hexadecanedithiol functionalized Au MPCs to study the response of toluene, TCE, 1-propanal, and water vapors at 5000 ppm concentration [136]. They found a higher response for TCE than toluene using this sensor. The concentration levels for these experiments were in the ppm range and the selectivity and cross-sensitivity were not monitored. Thus, these sensors limit the application for

environmental VOC analysis and inspire to development of a new sensor to selectively detect aromatic VOCs and TCE.

Several research groups have explored the effect of polar- π and π - π interactions for sensing aromatic VOCs, but the use of cation- π interactions has not been reported yet [102, 137, 138]. Cation – π interaction is considered a strong attraction that can be explored to make a notable contribution to molecular recognition phenomena [139, 140]. This interaction is an electrostatic attraction between a quadrupole moment of the electron-rich aromatic region and electron-deficient cation. Several characteristics including the nature of the cation and π system, solvation, and geometry of interaction influence the strength of this interaction [139, 141-143]. Our approach is to develop a new chemiresistor that exploits the use of cation- π interactions using Au MPCs to achieve higher sensitivity and selectivity for sensing BTEX [106]. Au MPCs are derived from a short-chain thiolate ligand fitted with aminoxy functionality for the ready introduction of carboxylate salts. Lithium, sodium, and potassium carboxylate-linked Au MPCs were examined for their ability to sense BTEX vapors as well as in comparative studies to probe the role of the cation- π interaction.

Furthermore, cesium carboxylate-linked Au MPCs were tested for TCE sensing as several X-ray crystallography studies show Cs metal ion coordination to vinyl-chlorides as well as to other saturated chloro-substituted compounds [137, 139]. Cs⁺-saturated smectite clay absorbs more TCE than the clays exchanged using the other metal cations [144]. This study suggests that there is an interaction between the Cs ion and Cl atoms of organochlorine compounds. Therefore, it could show differences in binding energy and the

bond strength of the coordination based on how the Cs⁺ is presented. Thus, we aimed to explore the sensing application of cesium carboxylate-linked Au MPCs for TCE detection.

3.2 Experimental

3.2.1 Materials

All chemical reagents were purchased either from Millipore Sigma, VWR International, or Fisher Scientific International and used as received. All solvents and analytes were freshly distilled before use. Synthetic air (<4 ppm of moisture) was purchased from Welders Supply Company, Louisville, KY, USA. Tedlar bags, acquired from Supelco (Bellefonte, PA, USA) were used to prepare the analyte samples.

3.2.2 Synthesis of metal-ion functionalized Au MPCs

Dr. Adhihetty (from Dr. Nantz's research group at the University of Louisville) synthesized and characterized all thiols and metal ion-functionalized Au MPCs described in this chapter. The experiments to test the sensor response for these synthesized Au MPCs were performed in our experimental setup (shown in Figure 2.5). The synthesized aminoxy Au MPCs were characterized using ¹H NMR, ¹³C NMR, FT-IR, TEM, and UV-visible spectroscopy and reported elsewhere [106, 145]. Figure 3.1 shows the synthesis steps of metal-ion functionalized Au MPCs. Aminoxy-functionalized Au MPCs 2 were prepared by the reaction of thiol 1 under two-phase Brust-Shiffrin conditions [106]. Aminoxy Au MPCs 3 can serve as a platform for incorporating a wide variety of surface functionality by reaction with aldehydes, a convenient synthetic approach to be highly useful when seeking to tailor Au MPCs. To introduce surface carboxylic ester functionality, Au MPCs 3 were reacted with methyl 4-formylbenzoate. Ester hydrolyses

using alkali metal hydroxide salts afforded the target metal ion-carboxylate linked Au MPCs 5- M^+ , where the M^+ studied included Li^+ , Na^+ , K^+ , and Cs^+ .

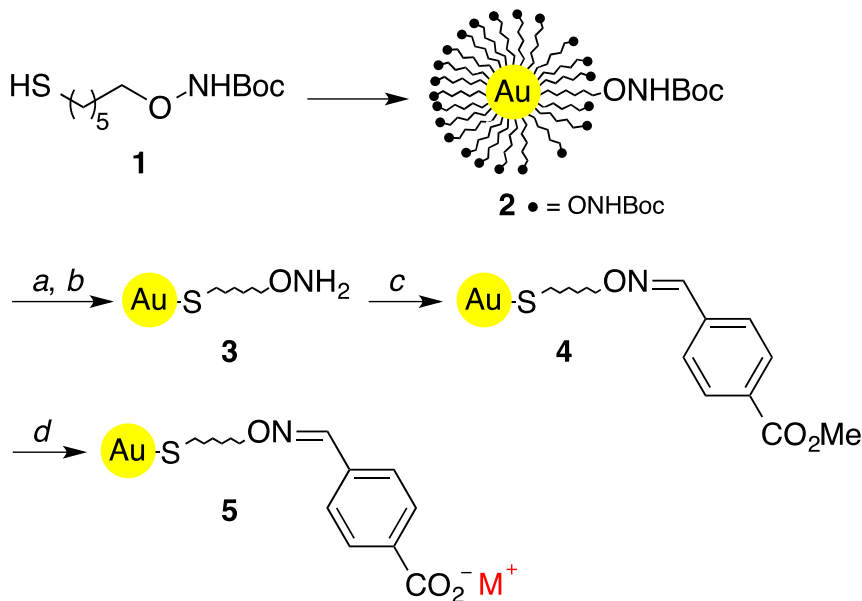


Figure 3.1: Synthesis of metal-ion functionalized Au MPCs. Only one ligand is emphasized in MPCs 2–5. Legend: a) 50% CF_3CO_2H , CH_2Cl_2 , 0 °C, 15 min; b) Et_3N , $MeOH:CH_2Cl_2$ (2:1), rt, 3 h; c) methyl 4-formylbenzoate, CH_2Cl_2 , rt, 17 h; d) $M^+ OH^-$ ($LiOH$, $NaOH$, KOH or $CsOH$), $MeOH:CH_2Cl_2$ (1:9), 0 °C to rt, 17 h.

3.2.3 Sensor evaluation and data acquisition

Li , Na , K , and Cs metal ion-carboxylate linked Au MPCs were deposited on IDEs by the drop-cast method. The sensor response was measured over 5 min under a vacuum of 28 inches Hg to remove VOCs from the testing chamber and adsorbed on the Au MPCs sensor film, followed by gas sample exposure at atmospheric pressure, and then again for 5 min under a vacuum of 28 inches Hg. The cycles were repeated at least three times to check reproducibility. The film resistances were measured and recorded by a single-channel multimeter (Keithley 2400). Benzene, toluene, ethylbenzene, xylene,

nitrobenzene, cyclohexane, ethanol, acetone, trichloroethylene, perchloroethylene, 1,2-dichloroethane, chloroform, DCM, 1,2-dichlorobenzene, cyclohexene, 1,1-dichloroethylene, trans-1,2-dichloroethylene, cis-1,2-dichloroethylene, and 1,1-dichloroethane were used as the vapor analytes. All the analytes were purified by molecular sieves before analysis. The target concentrations were prepared the same as described in chapter II (section 2.2.5).

The sensor response is calculated by the following equation:

$$\text{Response} = R_0/R_{\text{gas}} - 1 \dots \dots \dots (3.1)$$

where R_0 and R_{gas} are the resistances of the sensor in synthetic air and the presence of the analyte, respectively. The response time is the time to get maximum resistance change upon analyte exposure. The recovery times are defined as the time taken by the sensor under vacuum to achieve 90% of the initial resistance.

3.3 Results and discussion

3.3.1 Sensor development for aromatics VOCs

Figure 3.2A presents the resistance changes of the chemiresistor 5-K⁺ for sensing benzene at the concentration range of 100 ppb to 100 ppm. With an increasing concentration of benzene, the resistance deviation from the baseline increased. The resistance changes were rapid and reversible. From the resistance profile, it is found that the resistance of this sensor decreases in the presence of benzene, which can be the result of analyte diffusion into the organic matrix surrounding the metal cores or due to analyte surface binding, as with postulated cation- π interactions. Using equation 3.1 for response

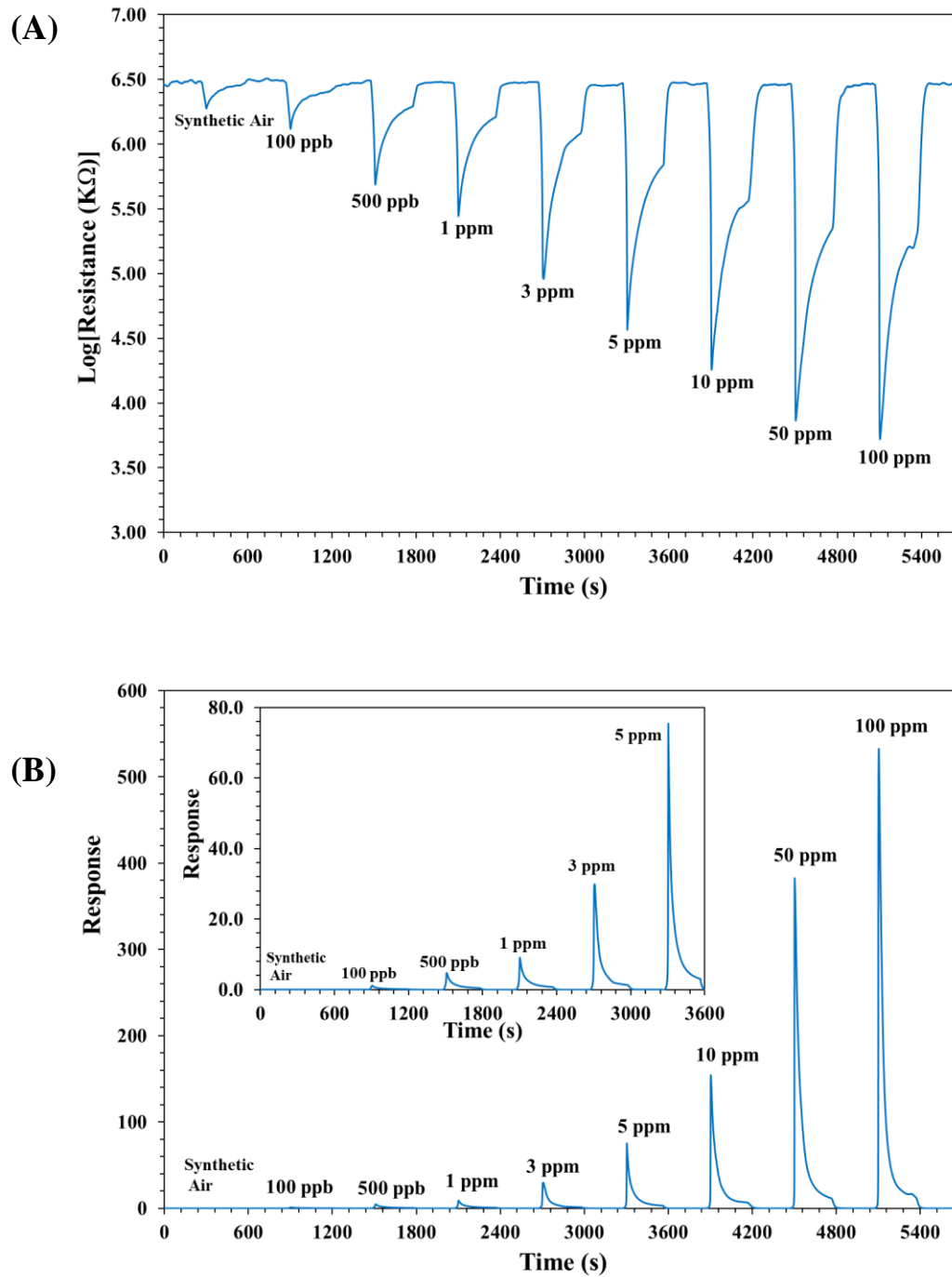


Figure 3.2: Plots of A) resistances of chemiresistor 5-K⁺ and B) responses of chemiresistor 5-K⁺ on exposure to 100 ppb to 100 ppm of benzene at 22 °C.

calculation, the response for benzene increased with higher concentrations (Figure 3.2B). The increase of resistance from the minimum point indicates an equilibrium process of analyte diffusion and interaction with ligands on the surface of the gold nanoparticles. The increases in resistance from the minimum points are similar for all tested benzene concentrations. The increase of resistance from the minimum point took about 10 min to reach a plateau resistance (Figure 3.3).

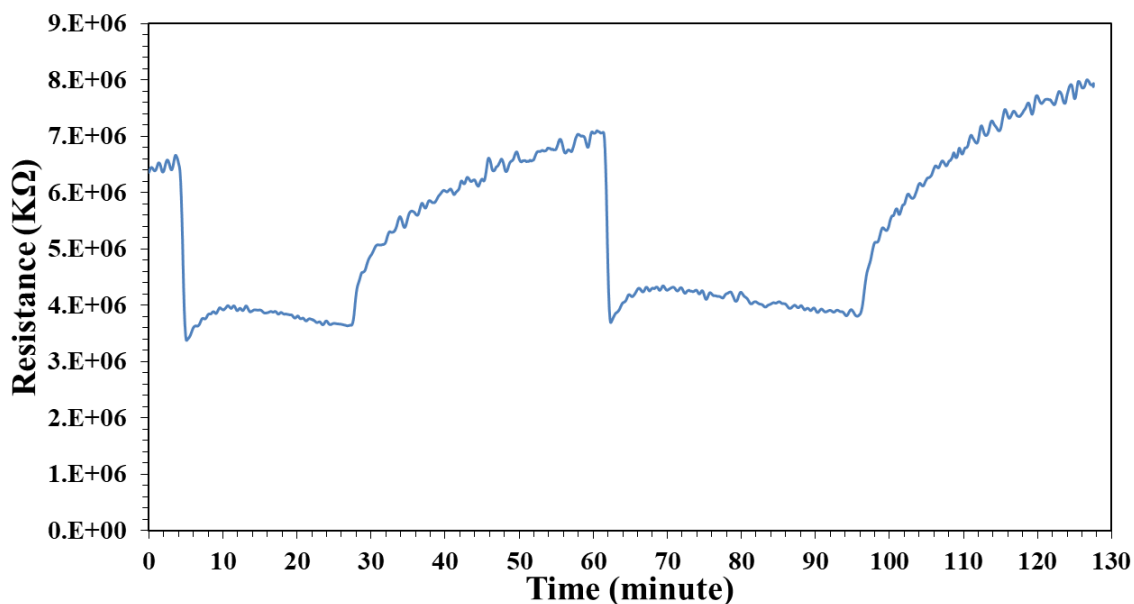


Figure 3.3: Resistance plot with the time of chemiresistor 5-Na⁺ on exposure to 100 ppb of benzene at 22 °C.

To further examine the dominant factor of cation- π interactions between thiol and aromatic compounds, sensor responses to other aromatic and non-aromatic compounds were measured. Figure 3.4 shows the responses of Li⁺, Na⁺, and K⁺-functionalized sensors on exposure to a panel of aromatic VOCs as well as nitrobenzene, cyclohexane, ethanol, and acetone. The Au MPCs 5-M⁺ show a linear relationship between the response and

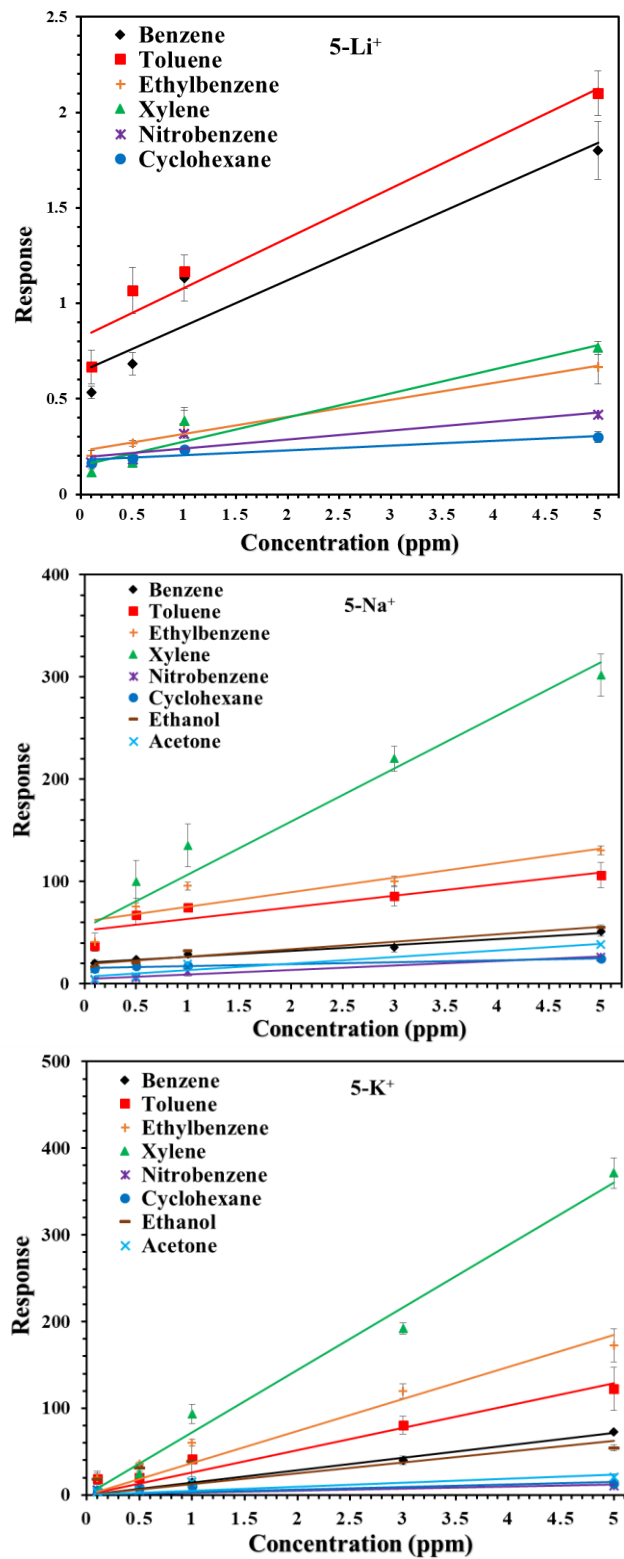


Figure 3.4: Sensor responses of Au MPCs 5-M⁺, where M⁺ = Li⁺, Na⁺, or K⁺. Each point indicates the average of n = 3 measurements.

analyte concentration in the range of 100 ppb to 5 ppm. The slope of the linear regression curve is a direct measurement of sensitivity. The sensors show higher sensitivity for analytes containing a π system (benzene, toluene, ethylbenzene, and xylene), a result that is consistent with a sensing mechanism elicited by cation- π interactions. Further support for the involvement of cation- π interactions is noted by the higher sensitivity toward the aromatic VOCs containing alkyl substitution.

Alkyl substituents increase π -electron density in the ring via induction, which in turn can be expected to promote a greater association of the π system with an electron-deficient metal ion, a relationship that has been previously reported [146]. Indeed, the alkyl-substituted analytes toluene, ethylbenzene, and xylene (commercial mixture of isomers) elicited greater sensor responses than benzene. Furthermore, the highest responses observed for the Na^+ and K^+ bound sensors were for xylene, the most electron-rich aromatic VOC examined. The Li^+ bound sensor was overall less sensitive than the Na^+ and K^+ bound sensors since lithium is more tightly bound by carboxylate anion than either sodium or potassium, thus decreasing its electrostatic potential for engaging in cation- π interactions.

Of particular interest for the analytes examined are the relatively flat slopes obtained for cyclohexane, ethanol, and acetone. Cyclohexane and ethanol cannot engage in cation- π interactions, and cation- π interactions of nonaromatic π -systems, such as in acetone, are little known and limited to the complex of ethylene-ammonium cation, acetylene-calcium cation, and intramolecular complexation of carbonyl π -systems [147, 148]. Cation- π interactions often must compete with polar M^+ -hydrophilic interactions, but with the present sensors, the polar substrates did not elicit significant responses, suggesting the dominant response for the synthesized chemiresistors corresponds to cation- π

interactions and not to hydrophilic interactions or analyte permittivity into the hydrophobic monolayer core.

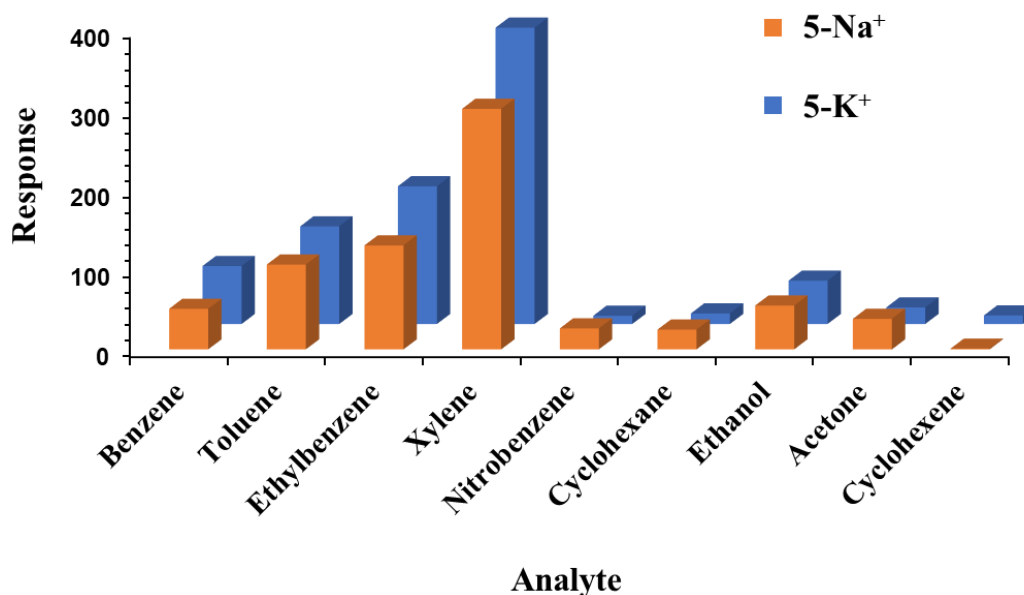


Figure 3.5: Chemiresistor response to VOCs at a concentration of 5 ppm. Sensors were prepared from Au MPCs 5-M⁺, where M⁺ = Na⁺ or K⁺.

Although nitrobenzene contains an aromatic π -system, the response curves of the three chemiresistors examined to nitrobenzene also are flat. The lack of response of the Na⁺ and K⁺-functionalized chemiresistors to nitrobenzene at a concentration of 5 ppm is shown in Figure 3.5, which compares sensor responses to the BTEX VOCs and cyclohexane, ethanol, and acetone at the same concentration to represent the sensitivity of the sensors toward electron-rich aromatic VOCs. A reasonable interpretation of this result is that the nitro group diminishes the π -electron density of the aromatic ring via a resonance

withdrawing effect to substantially reduce the ability for metal ion coordination via cation- π interactions. Also, both the Na^+ and K^+ -functionalized chemiresistors show a low response to cyclohexene, in which the alkene- π bond does not coordinate alkali metals as well the π -systems of aromatic substrates.

The response times for Li^+ , Na^+ and K^+ sensors were around 10s, 8s, and 8s, respectively. The recovery times for the Li^+ , Na^+ and K^+ sensors were 60 s for most of the analytes. Table 3.1 shows the response and recovery times for all tested VOCs. The limit of detection (LOD) was calculated from the response curve for these tested analytes using linear regression according to the formula: $\text{LOD} = 3.3 (\text{Sy}/\text{S})$ [Sy = the standard deviation of the response and S = the slope of the response curve]. The calculated LOD ranges from 0.1 to 3 ppb for these compounds.

Table 3.1: The response and recovery times for the Li^+ , Na^+ , and K^+ sensors.

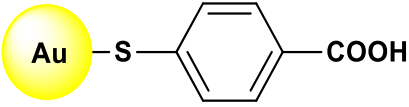
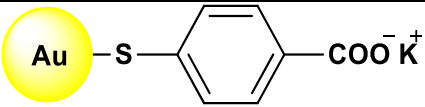
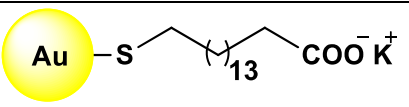
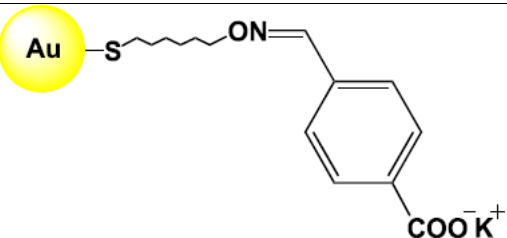
Analyte	Sensor response time (s)			Sensor recovery time (s)		
	Li^+	Na^+	K^+	Li^+	Na^+	K^+
Benzene	10	8	7	60	60	60
Toluene	10	8	7	60	60	60
Ethylbenzene	10	8	8	60	60	60
Xylene	10	7	7	60	60	60
Nitrobenzene	10	7	7	60	50	40
Cyclohexane	10	7	7	60	40	50
Ethanol		8	7		60	60
Acetone		7	7		60	60

To further validate that sensor resistance changes are due specifically to cation- π interactions of carboxylate-linked metal cations, we examined sensor responses to both the structurally analogous methyl ester functionalized Au MPCs 4 and to potassium hydroxide-treated Au MPCs. No significant changes in resistance were observed by introducing BTEX at different concentrations to Au MPCs 4, which do not contain bound alkali metal ions. To eliminate the possibility that the ester hydrolysis procedure in which 4 is treated with metal hydroxide can deposit metal ions onto Au MPCs other than as a metal ion-carboxylate, dodecane thiolate-coated Au MPCs were reacted with 0.1 M KOH in the same manner as in the synthesis of Au MPCs 5-K⁺. The response of the resultant KOH-treated Au MPCs to benzene then was examined. We did not observe any notable response to benzene at all concentrations examined. These results underscore that the attachment of metal ions to the Au MPCs monolayer in the form of metal carboxylates is crucial for sensor recognition of aromatic VOCs.

To examine if the cation- π sensing mechanism can be extrapolated to carboxylate salts of other thiol-acids, Au MPCs-based sensors using commercially available thiols were prepared for comparison with the 5-K⁺ sensor. The initial resistances and structures of these sensing materials are given in Table 3.2. The 5-K⁺ chemiresistor showed the highest initial resistance compared to the other films examined. Figure 3.6 shows sensor responses to benzene at a concentration range from 100 ppb to 5 ppm. The sensor prepared from 4-mercaptobenzoic acid (4-MBA) responds a little to benzene vapor at high concentrations. However, the same sensor fitted with K⁺ ions (4-MBA-K⁺) did respond to benzene vapor, albeit not at the level of the 5-K⁺ sensor. The Au MPCs chemiresistor prepared from 16-mercaptohexadecanoate potassium salt (16-MHDA-K⁺) also responded to the benzene

vapor concentrations examined, but at much lower response values than the 4-MBA-K⁺ sensor. The data show that metal ion incorporation via carboxylate salt formation elicits

Table 3.2: Commercially available thiols used to prepare Au MPCs chemiresistive films for benzene sensing studies.

Coated thiol	Au MPCs chemiresistive film	Initial film resistance
4-mercaptobenzoic acid (4-MBA)		17 x 10 ⁶ Ω
4-mercaptobenzoate, potassium salt (4-MBA-K ⁺)		15 x 10 ⁶ Ω
16-mercaptohexadecanoate, potassium salt (16-MHDA-K ⁺)		0.8 x 10 ⁶ Ω
5-K ⁺		5.0 x 10 ⁹ Ω

responses to benzene, with the hydrophobic nature of the organic matrix of the sensor influencing the degree of the response. The oxime ether linkage (-ON=C-) in the 5-K⁺ sensor forms a conjugated π system with the aromatic ring. This arrangement, especially given the para-substitution of the oxime ether to the carboxylate salt, can be expected to electronically influence the carboxylate substituent and the extent of K⁺ coordination.

While more studies are needed to fully understand the role of ligand structure and substitution on metal ion-based interactions with aromatic VOCs, it is clear that these K^+ functionalized Au MPCs sensors exhibit a higher response to benzene than the responses of previously studied thiolate-coated Au MPCs sensors mentioned in the introduction.

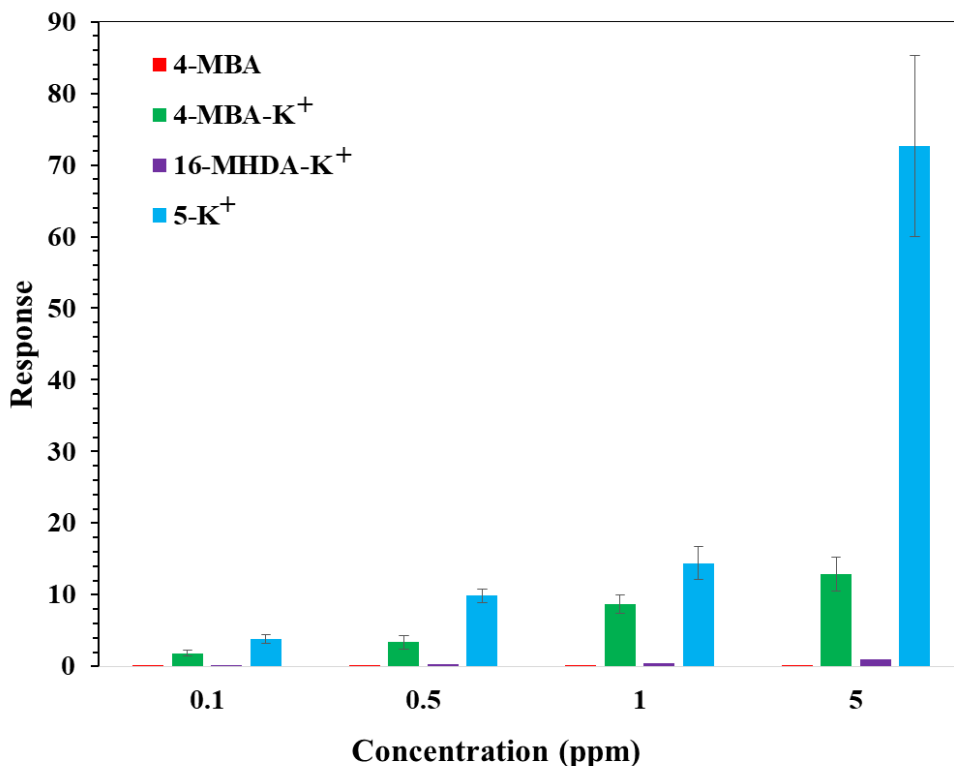


Figure 3.6: Responses of Au MPCs chemiresistors prepared from commercial thiols in comparison with the 5- K^+ chemiresistor response to 0.1 – 5 ppm benzene.

In regards to the long-term stability of metal ion-functionalized chemiresistors, we studied the responses of sensor 5- Na^+ toward exposure to 1 ppm benzene at different times. The response of this sensor was measured on the day it was prepared, after 30 days, and after 180 days. The response value was reduced by 30% after one month and 63% after six

months. We also tested 5-Na⁺ and 5-K⁺ gold nanoparticles that had been stored in the refrigerator for more than one year. The corresponding chemiresistors prepared from these nanoparticles had similar levels of responses as chemiresistors prepared from freshly synthesized thiol-functionalized gold nanoparticles. This result indicates that new sensors can be prepared by removing the previous sensing film from the IDEs and adding a new layer of the same sensing material.

3.3.2 Sensor development for chlorinated VOCs

In this study, the influence of morphology, hydrophilic-hydrophobic character, and ionic strength of the metalated Au MPCs for TCE vapor sensing was examined. First, the 5-Cs⁺ sensor was tested for different analytes including chlorinated, aromatic, polar, and non-polar compounds. Figure 3.7 shows the 5-Cs⁺ sensor response for these analytes at 0.1 ppm, 0.5 ppm, 1.0 ppm, 2.5 ppm, and 5.0 ppm vapor concentrations. We observed a similar response profile of other cation-functionalized Au MPCs. 5-Cs⁺ sensor interaction towards benzene is mainly due to the cation- π interaction and the response is higher than cyclohexene, which has a lower π -electron density than benzene. Among the chlorinated analytes, the highest response was observed for TCE at high vapor concentrations than DCM. TCE contains three high electronegative chlorine atoms and those atoms pull σ and π electrons toward themselves and create a high electron density around the Cl atoms. Due to the presence of high electronegative chlorine atoms (chloro substituents are an electron-withdrawing group), TCE has a low π electron density relative to benzene and cyclohexene which makes it less suitable for cation- π interaction. So, it is rational to expect that TCE

does not interact with the cesium cation at the surface of the Au MPCs through the π electron density of alkene functionality. However, TCE interacts with the sensor film, presumably through cesium-chlorine coordination. The strength of cesium cation–chlorine coordination in TCE and DCM is higher than the cation- π interaction in benzene. Furthermore, the 5-Cs⁺ sensor responded to gaseous methanol (polar) which might be due to the methanol oxygen coordination to the cesium cation which is known [149, 150].

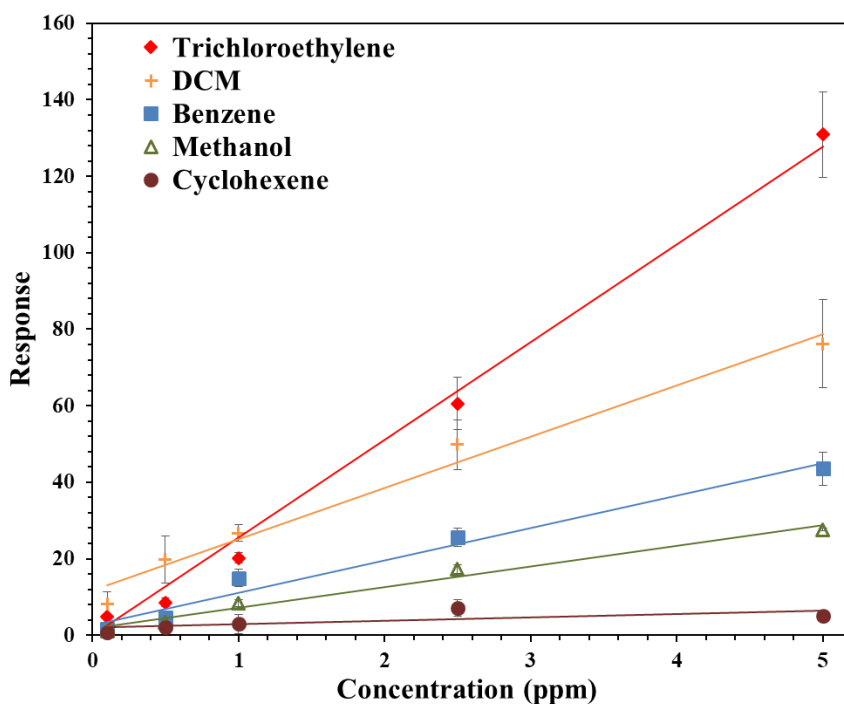


Figure 3.7: Response of Au MPCs Cs⁺ sensor to different VOCs. (Chlorinated vs aromatic vs polar vs non-polar).

To further investigate the interaction of the 5-Cs⁺ sensor towards chlorinated analytes, different analytes of chlorinated alkanes were exposed to the sensing film. Figure 3.8 represents the comparison of sensor responses for chlorinated alkane vapors with TCE vapors. Interestingly, TCE still exhibits a higher response for this sensor. TCE and 1,2-dichloroethane feature vicinal dichloride whereas chloroform, DCM, and 1,1-dichloroethane contain geminal chlorides. So, it can be suggested that analytes with vicinal chloro units might have the affinity to develop a metallocycle via coordination of dichloro unit to cesium cation as proposed by Smith *et al.* [151] and this formation is stronger for TCE due to the high electron density distributed around the chlorine atoms. Also, the cesium attracts more favorably with chlorine due to its Lewis acid–base nature. It has been observed that the electronegativity is more in DCM than in chloroform. The larger the difference in electronegativity, the higher the dipole moment and that could be the reason for the higher response for DCM than chloroform. Although, a lower response was obtained for 1,1-dichloroethane which has a higher dipole moment than DCM and chloroform. It could be a reason for the geminal structure of the analyte or steric hindrance to interact.

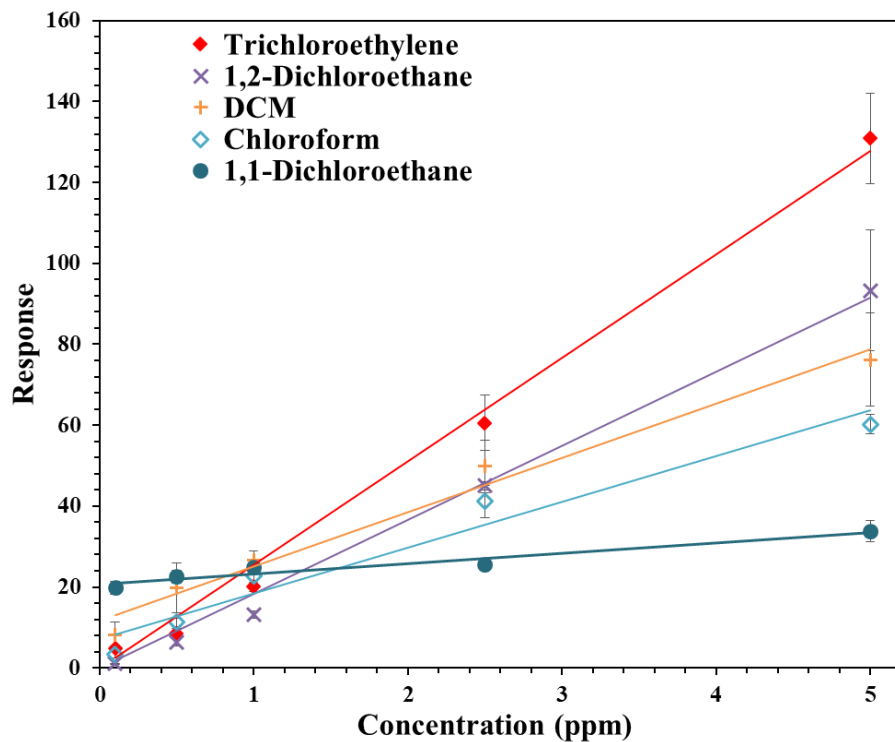


Figure 3.8: Response of Au MPCs 5-Cs⁺ sensor to chloroalkanes.

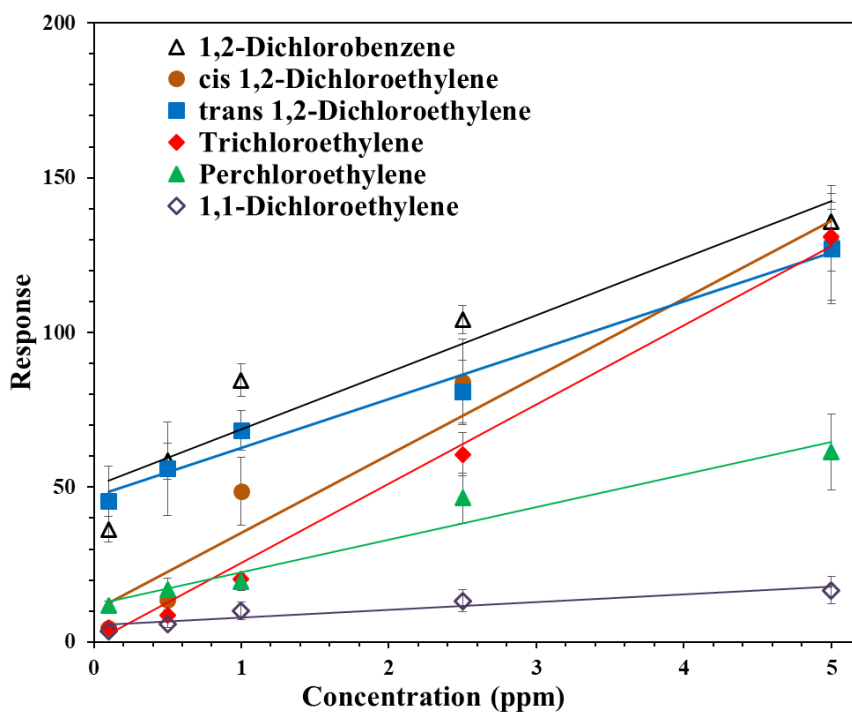


Figure 3.9: Response of Au MPCs 5-Cs⁺ sensor to chloroalkenes.

To understand this specific coordination interaction for TCE and other chlorinated compounds, a list of chlorinated alkenes was tested (Figure 3.9). The 5-Cs⁺ sensor shows higher responses for the vicinal 1,2-dichloro unit containing alkenes than geminal 1,1-dichloroethylene. This observation suggests that the previously explained metallocycle formation via vinyl 1,2-dichloro unit coordination to cesium cation is prominent and can be harnessed as a recognition element for TCE sensing. The net molecular dipole moment is an important factor to enhance cesium-chlorine coordination. Among analytes from Figure 3.9, 1,2-dichlorobenzene features vicinal dichloride with the highest net dipole moment. Cation- π interaction is also possible between the cesium cation and π electron. Due to the combination of all the factors, the 5-Cs⁺ sensor exhibits the highest sensor response for 1,2-dichlorobenzene. Also, a higher response was observed for *cis* 1,2-dichloroethylene than TCE due to the high electron density around the chlorine atoms. *cis*-1,2-dichloroethylene, *trans*-1,2-dichloroethylene, and 1,1-dichloroethylene are isomers, but they differ significantly in dipole moments. The net dipole moments of all tested analytes are presented in table 3.3 [145]. The sensor response was lower for perchloroethylene (PCE) than TCE and this might be due to the lower electron density around the chlorine atoms in PCE than TCE. This observation suggests that the analyte with low electron density around the chlorine atom promotes less Cs-Cl interaction and produces a lower sensor response. Furthermore, 1,1-dichloroethylene containing geminal dichlorides produced a lower response. This observation supports the previous explanation of sensor responses for analytes with vicinal and geminal chlorines.

Table 3.3: Dipole moments μ (D) of analytes utilized in this experiment.

Analyte	Net dipole moment μ / D
1,2-Dichlorobenzene	2.54
1,1-Dichloroethane	2.35
cis-1,2-dichloroethylene	1.9
1,2-Dichloroethane	1.86
Methanol	1.70
Dichloromethane (DCM)	1.55
1,1-dichloroethylene	1.3
Chloroform	1.02
Trichloroethylene (TCE)	0.88
Cyclohexene	0.33
Benzene	0
trans-1,2-dichloroethylene	0
Perchloroethylene (PCE)	0

To explore the interferences of 5-Cs⁺ sensor with other VOCs, a gaseous mixture of TCE, DCM, benzene and methanol was prepared in Tedlar bags containing 1L synthetic air where TCE amounts varied (100 ppb, 500 ppb, 1 ppm, 2.5 ppm and 5 ppm) but DCM, benzene and methanol amounts were fixed (100 ppb of each compound) in five Tedlar bags. Figure 3.10 shows a comparison of 5-Cs⁺ sensor responses for the mixture with individual compounds. It is observed that the response was higher for the mixture and maintained a parallel distance at higher concentrations (1 ppm – 5 ppm) with the response curve for TCE vapor. In the mixture, the interaction with DCM, benzene and methanol vapors might increase the response for the mixture more than individual TCE. This

phenomenon could be helpful to distinguish TCE with high concentration from other VOCs that present at trace levels.

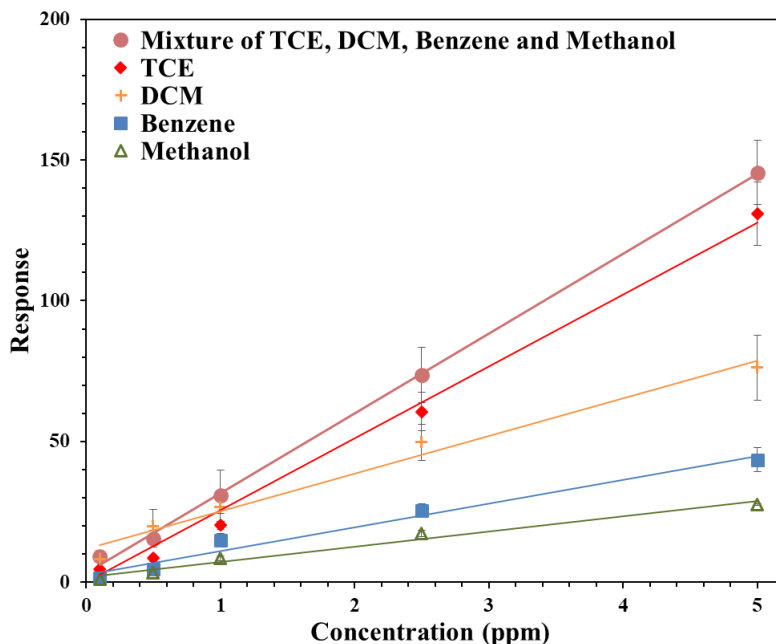


Figure 3.10: A comparison of 5-Cs⁺ response curve for a mixture of TCE, DCM, benzene, and methanol vapor with individual compounds. In the mixture, TCE concentration varied from 1 ppb to 5 ppm but DCM, benzene and methanol amounts were fixed (100 ppb of each).

3.3.3 Sensor response to humidity

Apart from cation- π interactions, these sensor materials also show strong interaction with water. To examine the effects of hydration, the responses of the sensors to water spiked into synthetic air were studied. In this study, predetermined amounts of water were injected into 1 L Tedlar bags containing synthetic air to achieve the desired relative humidity (RH). Theoretically, 1% RH is equivalent to 312 ppm water at 25 °C. For

instance, 29 μL of water was injected into a 1 L Tedlar bag to make 25% RH and heated until the water was evaporated. The same procedure was carried out to prepare 50%, 75%, and 100% RH. Figure 3.11 shows the responses of Li^+ , Na^+ , K^+ , and Cs^+ functionalized Au MPCs sensors to relative humidity (25–100%) at 22 °C. The interaction of Au MPCs 5- M^+ to water moisture shows the order $\text{K}^+ > \text{Na}^+ > \text{Cs}^+ > \text{Li}^+$. The large responses of Na^+ and K^+ functionalized Au MPCs to humidity cause significant interference in measuring BTEX in the environmental air.

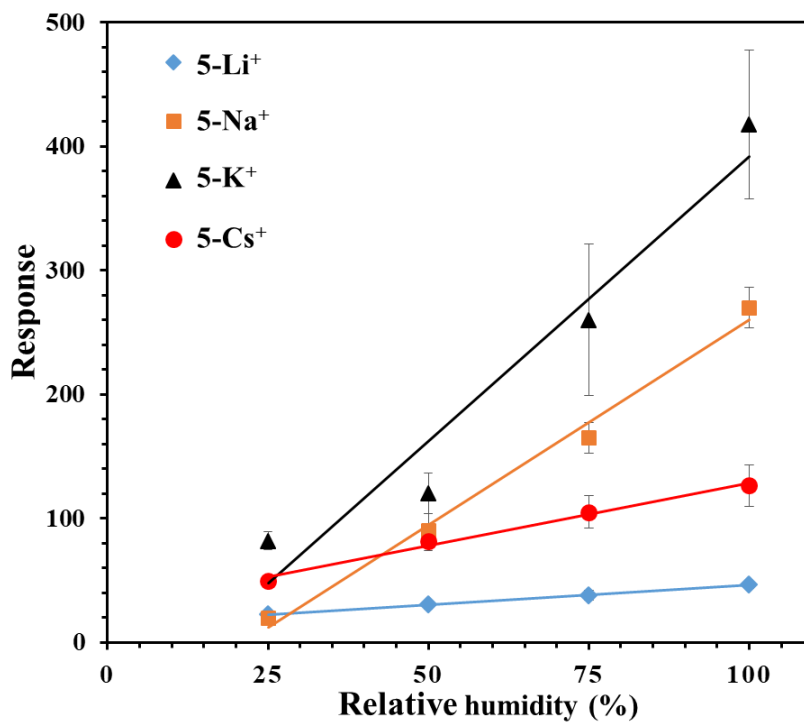


Figure 3.11: Au MPCs 5- M^+ sensor responses to relative humidity (25–100%).

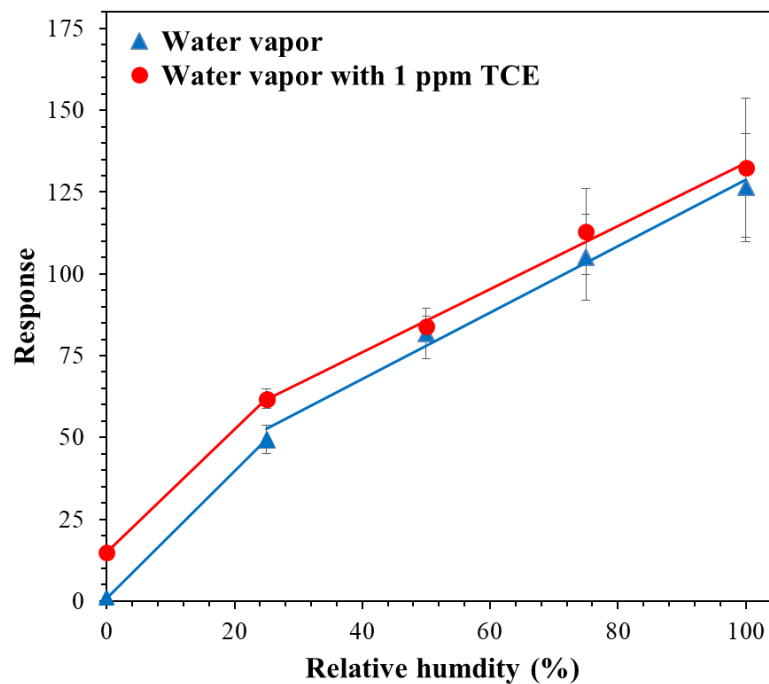


Figure 3.12: A comparison of 5-Cs⁺ sensor response profile of different amounts of water vapor with and without 1 ppm TCE.

Figure 3.12 presents the response of 5-Cs⁺ sensor to water vapor with and without 1 ppm TCE. The difference between the responses at each humidity point indicates the response for 1 ppm TCE. This difference is close to the response value of 1 ppm TCE. One way to eliminate the effect of humidity is to use a sorbent tube to absorb water from environmental air samples. Another approach is to use a preconcentrator with selective sorbents to capture and concentrate BTEX target analytes and then to use synthetic air for the elution of the preconcentrator. The preconcentration process will not only eliminate humidity but also concentrate target compounds for more accurate analysis. Further study using these sensors for the detection of BTEX in environmental air after a preconcentration

process is needed. The development of a micropreconcentrator is described in the next chapter.

3.4 Conclusion

The sensor response depends on the morphology of the sensing materials and non-covalent interactions with the vapor analytes such as cation- π interactions, halogen bonding, metal ion coordination, Van der Waals, and hydrogen bonding. We reported here that linking alkali metal ions to the surface of Au MPCs-based chemiresistors results in sensors with demonstrated sensitivity and selectivity toward aromatic and chlorinated VOCs. The trends in the observed response data for the Li, Na, and K ion chemiresistors toward aromatic and non-aromatic VOCs, both in terms of metal ion composition and aromatic ring π -electron density, support cation- π interactions as a dominant mechanism among many possible interactions to develop a selective sensor for detecting aromatic VOCs. Furthermore, cesium ion chemiresistor responses toward chloro hydrocarbons are greatly affected by the morphology, hydrophilic-hydrophobic nature, and the dielectric constant of the sensing film. The net molecular dipole moment and the presence of a vicinal dichloro unit in the analyte can form a stable metallocycle that influences the selectivity and sensitivity of the Au MPC Cs⁺ chemiresistor for TCE detection. Further studies are required to examine the robustness of the stable metallocycle complex formation with cesium cation. However, the present results point toward metalated Au MPCs as a promising sensing material to explore for selectively sensing aromatic VOCs and TCE.

CHAPTER IV

DEVELOPMENT OF A MICROPRECONCENTRATOR FOR ANALYZING TRACE VOCs IN ENVIRONMENTAL AIR

4.1 Introduction

The analysis of toxic volatile organic compounds (VOCs) in environmental air is important because toxic VOCs induce adverse effects on human health including cancers and cardiovascular diseases [11, 152]. Among the wide spectra of VOC pollutants, significant attention has been given to benzene, toluene, ethylbenzene, and xylene (BTEX) and trichloroethylene (TCE) not only because of their toxicity and/or carcinogenic nature for chronic exposure but also for their involvement in atmospheric photochemical reactions [12, 153, 154]. BTEX exposure has been responsible for numerous health conditions, such as skin and eye irritation, headache, neurological dysfunctions, and cardiovascular disease [125, 152, 155]. The sources of BTEX in environmental air include industrial emissions, automobile exhaust, petroleum products, and solvent usage [156-159]. Indoor BTEX sources are mostly cleaning products, paints, adhesives, cooking oil fumes, and vapor intrusion [153, 160]. The US Occupational Safety and Health Administration (OSHA) set a short-term exposure limit of 5 ppm of BTEX over 15 min as a Permissible Exposure Limit (PEL) [161]. Trichloroethylene (TCE) harms the central nervous system, liver,

kidney, immune and reproductive systems [126]. Chronic exposure to toxic BTEX at concentrations below their PEL causes cardiovascular disease and cancers [11, 12, 152, 153]. Thus, there is still a need to develop convenient, rapid, and accurate analytical methods for periodically monitoring toxic VOCs in both indoor and outdoor air and to alert people and prevent their exposure to high levels of these VOCs.

Gas chromatography-mass spectrometry (GC-MS) is the golden standard tool for the analysis of trace VOCs in environmental air, but this approach requires a long preconcentration time and large volumes of air samples [162]. The GC-MS method requires a special instrument for the preconcentration and thermal desorption of VOCs. Simultaneous on-site quantification of VOCs in both indoor and outdoor air demands a highly sensitive instrument for lower concentration VOCs [163]. Several types of sensors including electromechanical sensors, metal oxide sensors, electronic nose, and gold nanoparticle-based sensor arrays, have been developed for detecting target VOCs in the air [164]. Some of these techniques provide high sensitivity and lower detection limits toward target compounds, less power consumption, accurate and repeatable results; however, these sensors suffer significant interference by other VOCs in the air matrix [152]. Hence, the development of inexpensive, real-time, portable analytical methods with sensitivity, repeatability, and accuracy is a substantial challenge.

Solid phase microextraction (SPME) is a prominent sampling technique that uses coated fiber to extract analytes from different kinds of media such as liquid or gas phases. The quantity of analyte extracted by the SPME fiber depends on the type of fiber and is proportional to the analyte concentration [44, 165-167]. The solventless SPME technique provides a linear response over an extensive range of analyte concentrations. SPME has

been widely used for the determination of VOCs in environmental air [44, 162, 165, 166]; however, the analysis of sub-ppb levels of VOCs in the air by SPME in conjunction with GC-MS is challenging because the limit of detection (LOD) of the instrument is approached at these levels [46, 167-171].

Many miniaturized preconcentration and detection systems have been developed for the portable analysis of toxic VOCs in environmental air which are summarized in Table 4.1. These include small-diameter tube and needle extraction, SPME, and microfabricated preconcentrators. Most of the reported preconcentrators are fabricated using micro-electro-mechanical system (MEMS) technology to reduce the volume of the sorbent. These micropreconcentrators (μ PC) have been primarily used as an integral part of micro-gas chromatograph (μ GC) systems for field detection [172-176] or monitoring target VOCs in environmental air [177-180]. Micropreconcentrators can be loaded with different adsorbent materials to tailor affinities for target VOCs. Furthermore, μ PCs can enhance the LOD and also improve selectivity by reducing interfering compounds or filtering undesirable compounds from a sample matrix [181]. In a recent publication, a μ PC was mounted on an unmanned aerial vehicle to collect and concentrate VOCs in the air at different altitudes for subsequent analysis by GC-MS [182].

Although both microfabricated μ PC and SPME methods have been used for the analysis of VOCs in indoor and outdoor air, there is no study in which these two methods have been combined for the analysis of trace VOCs by GC-MS. Both methods face challenges for accurate analysis of sub-ppb level VOCs in the air by GC-MS because of the constraints of the detection limits of GC-MS for using SPME and large sample volume for using μ PC. In this study, a MEMS-fabricated μ PC was integrated with SPME to create

a two-stage concentration process for analysis of BTEX and TCE in environmental air by GC–MS [124]. Integration of these methods provides the advantages of using a smaller sample volume (less than a 2-liter sample) for preconcentrator and avoiding sample dilution on thermal desorption by SPME. The microfluidic channel of the μ PC device was filled with Carboxen 1000 to selectively trap gaseous BTEX and TCE. The adsorbed VOCs then were thermally desorbed to a small volume for extraction by SPME. This two-stage preconcentration method provides higher amounts of VOCs for GC-MS analysis than using either a μ PC or SPME alone. The performance of the μ PC device was characterized based on adsorption and desorption flow rates, recovery percentage, and thermal desorption efficiency. The two-stage preconcentration method was also examined for measurements of BTEX and TCE in the environmental air.

4.2 Materials and method

4.2.1 Chemicals and materials

Benzene, toluene, ethylbenzene, xylene (a mixture of o-, m-, and p-xylene), and TCE (analytical standard purity) were purchased from Sigma Aldrich. Tedlar bags, SPME holders, and fibers coated with Carboxen/polydimethylsiloxane (Car/PDMS) (75 μ m) coating, and Carboxen 1000 adsorbent were obtained from SUPELCO. Tedlar bags were cleaned by filling them with synthetic air and then evacuating and repeating the process three times. All chemicals used in this work were analytical grade and were used without further purification. Initially, a mixture of BTEX and TCE (1000 ppm) was prepared by injecting predetermined amounts of the chemicals into a Tedlar bag containing 1L synthetic

air. A serial dilution of this mixture was performed to achieve target concentrations for making calibration curves using SPME for extraction and GC-MS for analysis. Air-tight glass syringes were purchased from RESTEK. Freshly prepared standards were used for each experiment. Synthetic air (moisture < 4 ppm) was purchased from a local company (Welders Supply, Louisville, KY).

Table 4.1: Summary of miniaturized preconcentrator used to detect BTEX.

Ref	μ PC Device size	Adsorbent material	Adsorption parameter (sample volume, flow rate)	Desorption parameter (flow rate, Temperature)	Heating system	Separation Column, stationary phase & thickness	Detection system	LOD
[181, 182]	Borosilicate glass 2.54 cm x 2.54 cm x 1.4 cm	TENAX TA (\approx 7 mg)	180 mL, 90 sccm For environment analysis: 3.6 L, 30 sccm	25 sccm 260 °C	Cr/W metal	DB-VRX capillary column (20 m \times 0.18 mm \times 1 μ m, Agilent)	GC (HP 5890)/FID	22 ppb
[183]	Al 3 cm x 1.5 cm x 0.5 cm	Carbopack B (\approx 5 mg)	20 mL 5 sccm	2.5 sccm 330 °C	Ceramic heater	capillary column (20 m \times 0.18 mm \times 1 μ m, RXi-624 stationary phase, 1 μ m film thickness (Restek))	eVx Blue mini PID (Baseline MOCON, Lyons, CO, USA)	0.06 – 0.42 ppb
[184]	Glass tube 6.35 x 114.3 mm	TENAX GR (0.5g)	1 L 1.75 min	4 min 180 °C	Aluminum block with a 100 watt cartridge heater	15 m MXT-5 (0.53 mm ID x 0.25 μ m) and 30 m MXT-1301 columns (0.53 mm ID x 0.3 μ m) (Restek)	PID (Andrews Glass)	<1 ppb
[153]	Al 40 mm x 40 mm x 12.3 mm	Basolite C300	20 mL 5 sccm	150 °C	Three heating cartridges (Watlow, St. Louis, MO, USA)	20 m long capillary column (i.d. 0.18 mm, RXi-624 stationary phase, 1 μ m, Restek)	eVx Blue mini PID (Baseline MOCON, Lyons, CO, USA)	0.2 – 1.7 ppb
[172]	Tube ID: 0.065"	Restek Res-Sil B (75 mg)	Upto 4 L 100 – 300 sccm	180 °C	Cartridge heaters (McMaster)	MXT -1 (Restek)	PID (Alphasense)	1-5 ppt

[185]	Stainless steel tube (ID: 1.32 mm)	C-B (8 mg), C-X (2.5 mg), Carboxen 1000 (1.8 mg)	1 L	0.18 L/min for 5.5 min, 300 °C	Pt wire coil	Two columns: Rtx-1, 0.5 μm thickness, Rtx-200, thickness 0.25 μm (Restek, Bellefonte, PA).	Polymer coated surface acoustic wave (SAW) sensor array	<10 ppb
[186]	Si 13.6 mm × 4.1 mm	C-B (2 mg), C-X (2.3 mg)	5 – 10 mL 5 sccm	3 sccm 225 °C	Ti/Pt micro-heater	Two μcolumn chips, PDMS thickness 0.20 μm	Thiolate-monolayer protected gold nanoparticle coated Sensor array, FID (7890 Agilent, Santa Clara, CA, USA)	0.42 – 3 ppm
[180]	Si 25 mm × 12 mm × 1.3 mm	quinoxaline bridge cavitated	50 sccm	100 °C	TiN/Pt micro-heater	μcolumn chip, CarboGraph 2 + 0.2% Carbowax™	Metal oxide semiconductor (MOX) gas sensors	0.1 ppb
[187]	Stainless steel tube (ID: 1.2 mm, length: 8-cm)	C-B (3 mg), C-X (2 mg), Carboxen 1000 (1 mg)	1 L 100 sccm	1 sccm 320 °C	Ni/Cr wire coil	Silica capillary column, (0.25 mm i.d., DB-1 stationary phase, 0.5 μm thickness)	PID (PID-AH, Alphasense)	0.02-0.07 ppb
[57]	Si Glass 3 cm x 1.5 cm	metal organic framework (MOF-5) 20 mg	10 min 5 sccm	0.3 sccm 150 °C	Ti/Pt micro-heater	silica capillary column	FID (YL 6100, Young Lin Instrument)	< 1 ppm
[173]	Si-Glass 13 mm × 13 mm	Tenax TA film (thickness: ~200 nm)	10 min 10 mL 1 sccm	3 sccm 200 °C	Cr/Ni micro-heater	μcolumn chip, OV-1, ~250 nm	Micro-thermal conductivity detectors (μTCD)	~25 ppb

[188]	stainless steel tube (length 4.5 cm)	Carbopack B (0.75 mg), Carbopack X (0.75 mg)	200 mL 20 sccm	2.1 sccm NA	Cr/Ni wire coil	μcolumn chip, OV-1	μPID	0.14 – 0.23 ppt
[189]	stainless steel tube (1/16-inch diameter and 1-inch length)	porous graphitized carbon black	NA	NA 300 °C	Coil wire	UAC-CW (carbowax coated column, Quadrex) and UAC-502 (cyanopropylphenyl silicone coated column, Quadrex)	Microfabricated quartz tuning fork detector	~1 ppb
[190]	Si Glass 4 mm x 14 mm	Coated carbon flim (thickness 10 μm) 2 mg	50 mL 40 sccm	3 sccm 320 °C	Cr/Au	Capillary column (DB-5, 0.32 mm i.d., 15 m long, Supelco)	FID (Agilent 5890)	NA
[191]	Si Glass 1.4 × 4.1 cm	Carbopack B (2.0 mg), Carbopack X (2.3 mg)	5 – 10 mL 5 – 10 sccm	2 – 3 sccm 225 °C	Ti/Pt micro-heater	μSC chip, PDMS 0.2 μm	μCR array chip	16 - 600 ppb
[192]	Glass tube (4 mm I.D., 40 mm length)	Carbon nanotube sponge (5 mg)	90 mL 90 sccm	1.8 sccm 250 °C	NA	MXT-1 (Restek), dimethylpolysiloxane film thickness 1 μm	PID	0.13 – 0.28 ppb

4.2.2 MEMS preconcentrator fabrication procedure

Micropreconcentrator (14 mm x 8.5 mm x 1 mm) devices (Figure 4.1) were fabricated using a 0.5 mm thick 4-inch diameter double-side polished (DSP) silicon wafer. There are two main parts in the μ PC, namely the cavity area which contains adsorbent material and microheater. Two photomasks were used for the fabrication of μ PC. One photomask was for patterning the topside cavity and flow channel and another photomask was for designing the backside microheater. Figure 4.2 shows the two prepared photomasks used for μ PC fabrication. All the microdevices were fabricated using the microfabrication technique in the University of Louisville cleanroom facility (class 100/1000). Detailed fabrication steps (Figure 4.3) are discussed below.

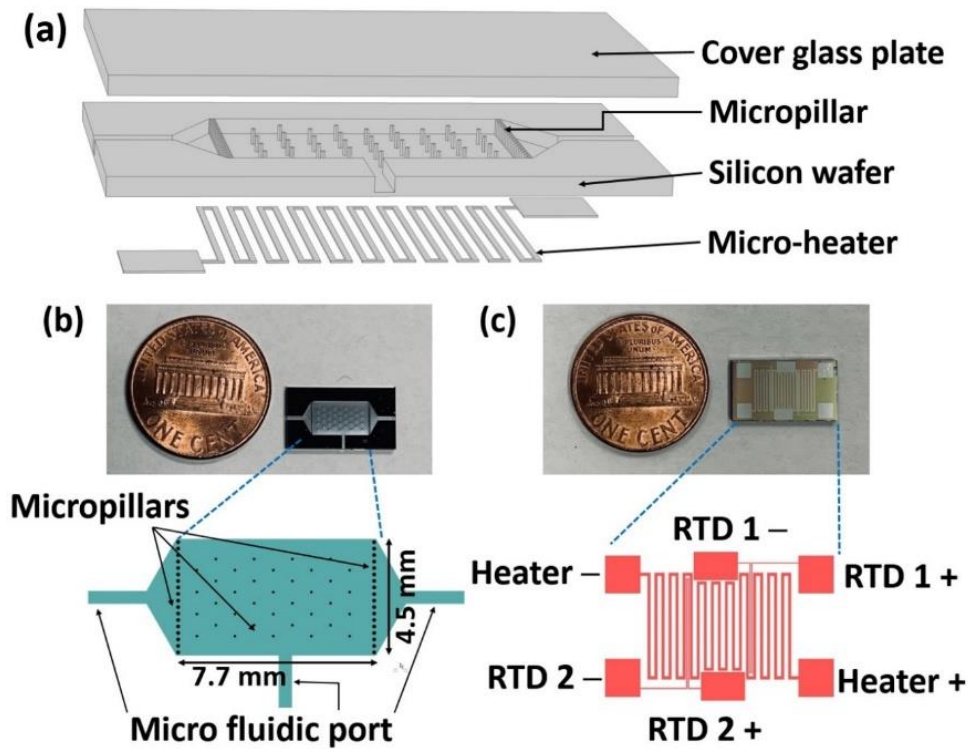
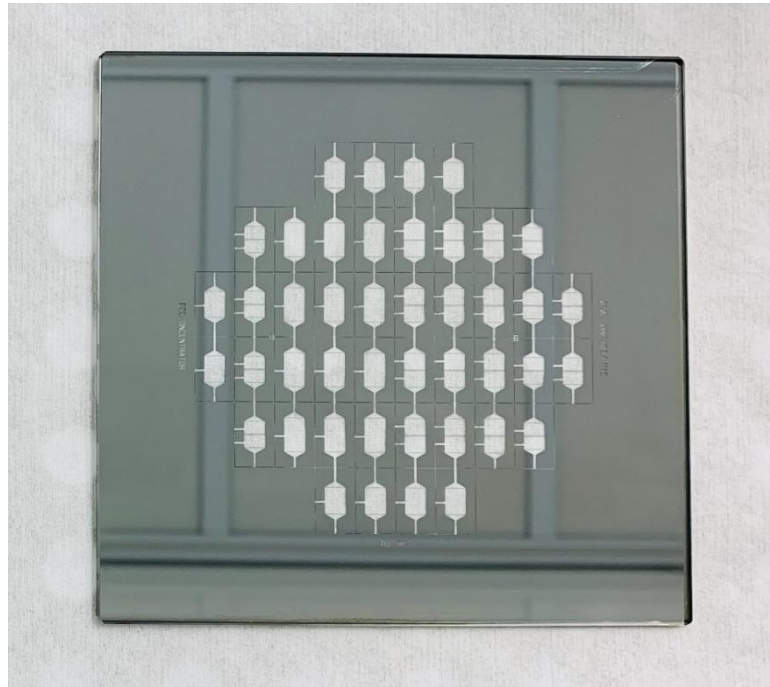


Figure 4.1: Micro gas preconcentrator (μ PC). (a) Three-dimensional view of layers. (b) Image of front faces of the μ PC containing cavity and micropillars. (c) Image of backside heater and RTD of the μ PC.

(a)



(b)

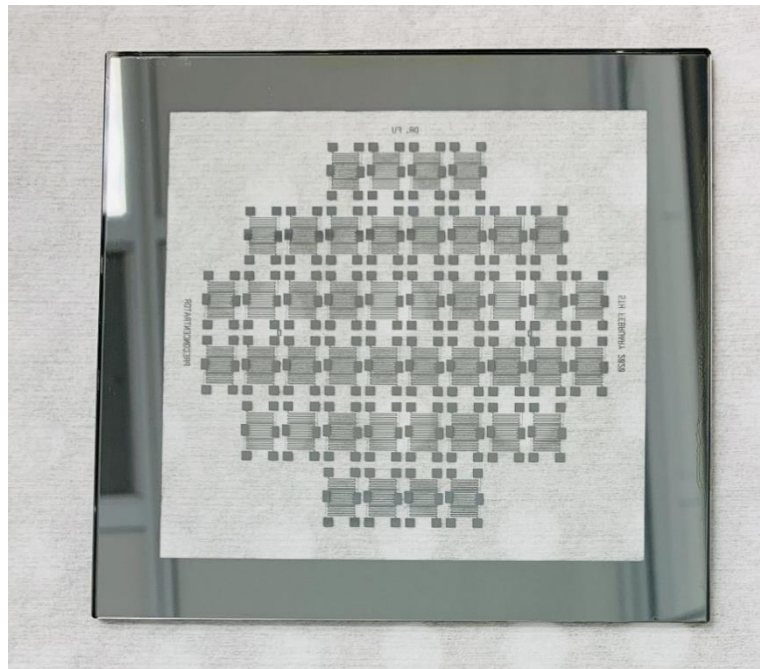


Figure 4.2: (a) Fabricated dark field photomask for creating cavity and flow channel in μ PC, (b) Fabricated light field photomask for microheater fabrication on the backside of μ PC.

Thermal oxidation:

The silicon dioxide layer was grown on both sides of the wafer because on one side SiO₂ served as a sacrificial layer for buffer oxide etch and on the other side it acts as an insulation for the microheater. First, the wafer was cleaned and dried using acetone, methanol, DI water, N₂ respectively to remove any trace contaminants on the surface such as dust, organic, ionic, and metallic compounds (Figure 4.3A). Then it was placed in a trash furnace to grow around 400 nm thick SiO₂ (Figure 4.3B). Wet thermal oxidation was run for 1.5 hours at 1000°C. 430 nm oxide layer thickness was measured on both sides of the wafer using a filmetrics system.

Photolithography:

A positive photoresist Shipley 1827 was coated on one side of the oxidized wafer at a spin speed of 500 rpm for 1 second and a spread speed of 4000 rpm for 30 seconds, causing the photoresist thickness of around 2.7 μm. The wafer was soft-baked at 90 °C for 2 minutes. The same steps were done for the other side of the wafer. Both sides were coated with photoresist as the photoresist on one side was patterned for cavity design by photolithography and the photoresist on another side prevented the SiO₂ layer from buffered oxide etchant.

One side of the wafer was then exposed to UV light using Karl Suss Mask Aligner MA6/BA6 which uses the contact exposure method. UV source was exposed on the wafer for 22 seconds at 12 W/cm² through a dark field photomask (Figure 4.3C). The UV-exposed area became soluble in the developer solvent. The wafer was then developed in

Microposit MF319 solution for 90 seconds followed by rinsing under a DI water bath and drying with N₂. The wafer was observed under an optical microscope to check the patterns.

The wafer was hard-baked for 2 minutes using the hotplate at 120°C.

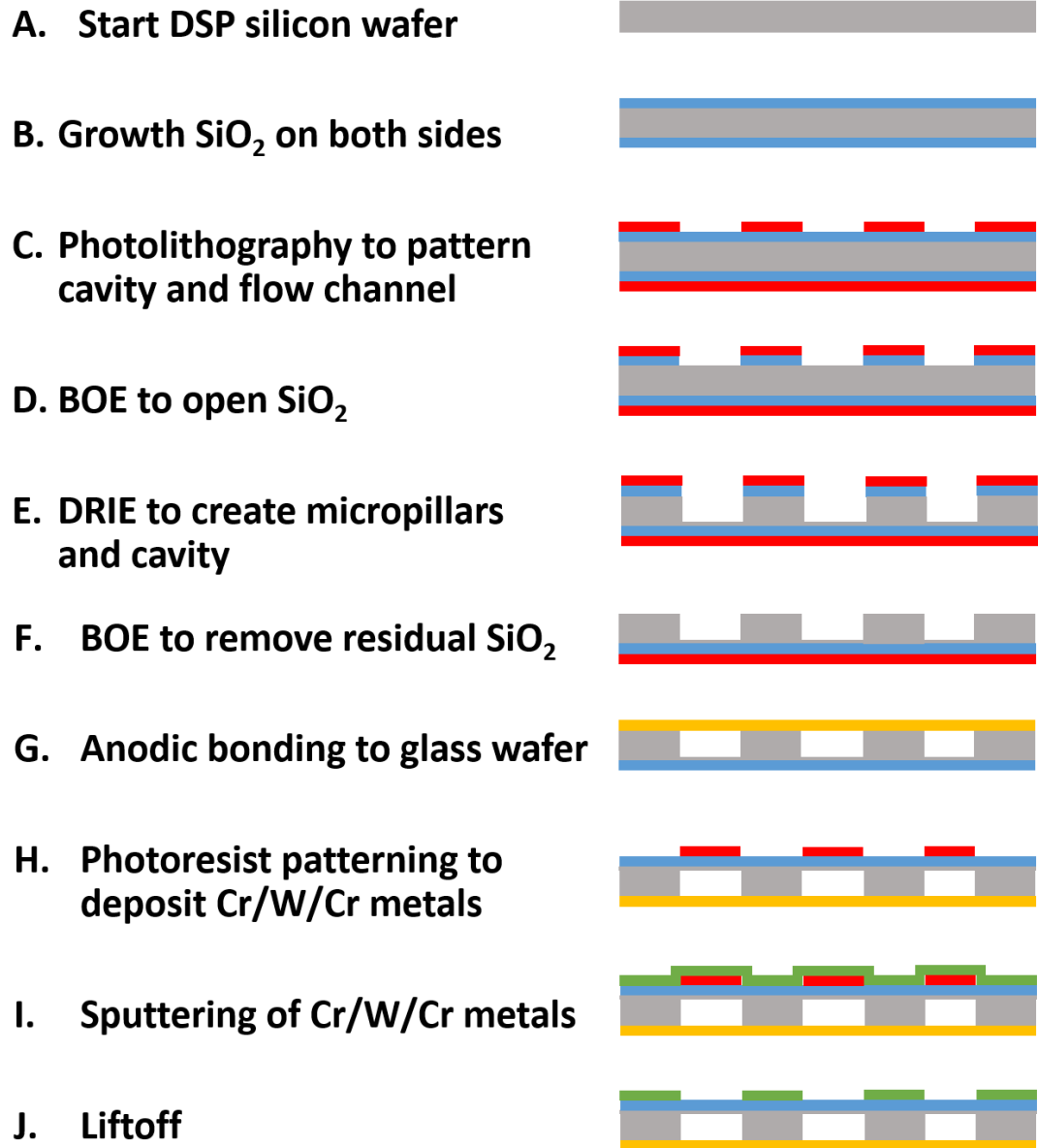


Figure 4.3: Schematic illustration of the μPC fabrication steps.

Silicon dioxide etching:

The thermal oxide in the patterned area was etched by a buffered oxide etching (BOE) solution. BOE solution is a wet etchant comprised of a 6:1 volume ratio of 40% ammonium fluoride (NH_4F) in water to hydrofluoric Acid (HF). The etch rate of BOE at 22 °C is 120 nm/min. The thickness of SiO_2 was 430 nm, so the wafer was immersed in BOE solution for 5 minutes to make sure that the SiO_2 layer under the UV patterned area was completely etched which opened the path for deep reactive ion etching (DRIE). After BOE, the wafer was rinsed for 2 minutes in a DI water bath, and dried with N_2 (Figure 4.3D). The coated photoresist on the other side of the wafer protected the SiO_2 layer from being etched away.

Deep reactive ion etching:

DRIE is a common tool for controllable anisotropic etching of MEMS devices to form high aspect ratio features. Sulfur Hexafluoride (SF_6) and Oxygen (O_2) plasma are used to etch through the silicon wafer. An STS MESC Multiplex ICP machine was used for DRIE. Before putting the wafer into the chamber, a 500 μm thick handle wafer was attached at the backside of the wafer to protect it from being ruptured as our target depth of cavity was around 400 μm . An adhesive glue was applied between these two wafers and heated up to 120 °C. After 20 min, the wafers were cooled and stuck together. Wafers were placed in a DRIE chamber and run for 120 minutes which created a 400 μm depth cavity with designed micropillars (Figure 4.3E). The depth was measured using a Dektak profilometer. Figure 4.4 shows the optical image of the wafer after DRIE.

Then the wafers were put in N-Methyl-2-pyrrolidone (NMP) bath at 60°C to strip the photoresist followed by oxygen plasma cleaning in the March RIE CS1701 for 10 minutes to completely remove any photoresist residues at a condition of 300 watts, Pressure 300 mTorr and O₂ flow (20% sccm). Sacrificial SiO₂ layers were completely cleaned by placing the wafers in BOE solution for 5 minutes (Figure 4.3F). After BOE, wafers were washed in a DI water bath and dried with N₂ flow.

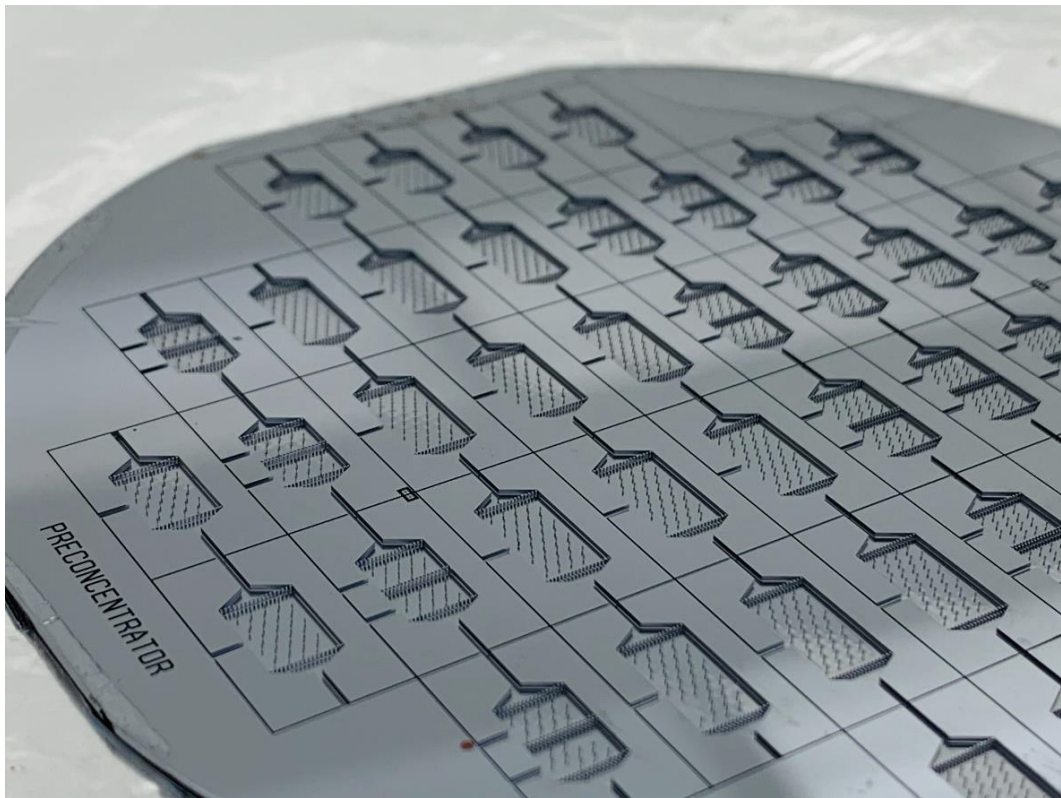


Figure 4.4: Optical image of the cleaned wafer before anodic bonding.

Anodic bonding:

The wafer was sealed by anodic bonding with a 500 μm thick glass wafer (Pyrex 7740 glass) using a Suss SB6e bonder. Before anodic bonding, the backside handle wafer was removed by applying heat at 150 °C. Then backside photoresist was removed by putting the wafer in the NMP bath at 60 °C for 10 minutes followed by rinsing in a DI water bath and drying with N_2 . Pyrex 7740 glass wafer was also cleaned by placing it in an NMP bath, rinsed in a DI water bath, dried by N_2 and hard-baked at 150 °C for 5 minutes. Then Si wafer and glass wafer were bonded by applying 1200 DC voltage at 450 °C (Figure 4.3G).

Photolithography with backside alignment:

The backside of the glass-bonded wafer was coated by Shipley 1827 photoresist at a spin speed of 500 rpm for 1 second and a spread speed of 4000 rpm for 30 seconds. The wafer was soft-baked at 90°C for 2 minutes. The wafer was placed in Karl Suss Mask Aligner MA6/BA6 and appropriate alignment was done by using the backside aligner and adjusting x, y, and theta orientation error between the alignment marks of the photomask and wafer. Then UV source was exposed on the wafer for 22 seconds at 12 W/cm^2 through a clear field photomask (Figure 4.3H).

YES Image reversal:

YES Image reversal was done to alternate the action of the photoresist. Also, this process improves the profile for the lift-off step by providing higher resolution, re-entrant sidewalls. The wafer was treated with ammonia exposure at 90°C and then flood exposure for 25 seconds using Karl Suss Mask Aligner MA6/BA6 which made photoresists in UV unexposed area soluble to the developer solvent. The wafer was developed in Microposit MF319 solution for 90 seconds followed by rinsing under a DI water bath and drying with N₂. The wafer was observed under an optical microscope to check the patterns. The wafer was hard-baked for 2 minutes using the hotplate at 130 °C.

Sputtering:

Before metal sputtering, the wafer surface was treated with O₂ plasma to remove any organics to promote better adhesion of metals to the wafer. March RIE CS1701 was used for this cleaning step and O₂ gas flowed at 20% sccm for 25 seconds. The wafer was then sputtered with Chromium (Cr) and Tungsten (W) metals for 2 minutes and 35 minutes respectively using a Kurt J. Lesker PVD 75 (Figure 4.3I). 550 nm thick metal layer was measured by Dektak profilometer.

Lift-off:

The undesired metal layers were removed by the lift-off process using acetone. Acetone was sprayed on the wafer and consequently, contact pads and microheater parts

on the wafer became visible. The wafer was then cleaned with methanol, DI water and dried with a spin drier and N₂ (Figure 4.3J).

The wafer was diced to get a complete μ PC which contains a flow channel and cavity with micropillars and at the backside of it, a microheater and RTD temperature sensors. The inlets and outlets of the μ PCs were connected with deactivated silica tubes (355 μ m O.D., 255 μ m I.D., Polymicro Technologies, AZ, USA) and secured with silicone adhesive (Duraseal®1531, Cotronics, NY, USA). 4.5 ± 0.1 mg of Carboxen 1000 adsorbent (surface area 1200 m²/g) was loaded into μ PC with the assistance of an applied vacuum. After filling with adsorbent, the port for loading the adsorbent was sealed with Duraseal 1531. The volume filled by the adsorbent was around 10×10^{-3} cm³. The packing density is 0.45 g/cm³.

4.2.3 Standard sample preparation and Calibration curves

The amounts of individual compounds of BTEX and TCE measured by GC-MS were calculated based on individual calibration curves. Different concentrations of standard analytes ranging from 1 to 50 ppb were prepared and transferred to a 50 mL air-tight glass syringe. A Car/PDMS SPME fiber was inserted into the glass syringe for a 15 min sampling time and then manually inserted into the GC-MS injection port for analysis. The 15 min sampling time was maintained for each concentration. The SPME fiber was thermally desorbed for cleaning before sampling and confirmed as VOC-free by the absence of any signals by GC-MS. Analyte peaks were well separated and less peak broadening was noticed. The xylene isomer sample showed two peaks corresponding to

m/p-xylene and o-xylene isomers, respectively and the peak area ratio of m/p-xylene to o-xylene was about 4:1. The total xylene peak area was counted by combining the areas of the m/p-xylene and o-xylene peaks. A calibration curve (Figure 4.5) was obtained by plotting the peak areas from GC-MS response versus concentrations for each analyte. The coefficient of determination (R^2) is higher than 0.99 for all analytes as shown in Table 4.2. The slopes of calibration lines are significantly different among the analytes because of differences in molecular weight and interaction between SPME surface coating and individual analytes.

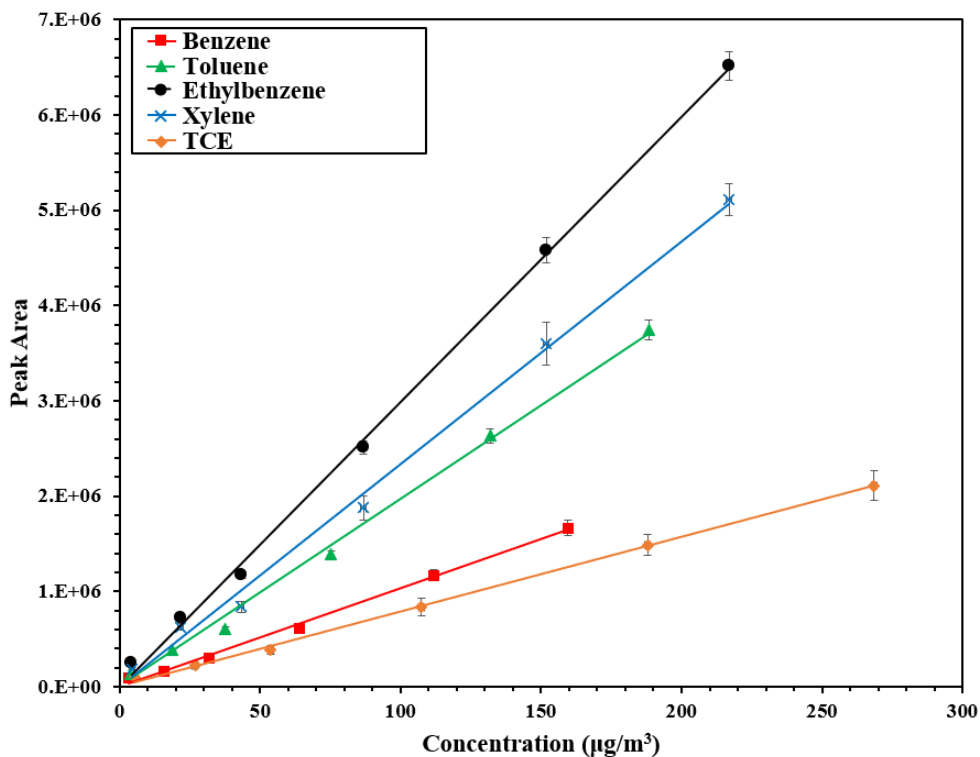


Figure 4.5: Calibration curves for BTEX and TCE analysis using SPME-GC-MS.

4.2.4 LOD, LOQ of GC–MS with SPME sampling

The LOD and limit of quantification (LOQ) for the SPME process were calculated from the calibration curves using a linear regression model. $LOD = 3.3 * (S_y/S)$ and $LOQ = 10 * (S_y/S)$, where S_y is the standard deviation of the response and S is the slope of the calibration curve. S_y is acquired by multiplying the square root of sample numbers with a standard error obtained from regression analysis. The calibration equations, LOD, and LOQ are presented in Table 4.2 for all analytes. The LODs of all compounds were a few $\mu\text{g}/\text{m}^3$. Because concentrations of BTEX and TCE in environmental air are at the levels of these LOD and LOQ when using SPME in conjunction with GC–MS, there is a need to increase the analyte concentrations to increase the amounts extracted by SPME for accurate quantitative analysis.

Table 4.2: Calibration equations, LOD and LOQ obtained for BTEX and TCE.

Compound	Calibration equation	R^2	LOD ($\mu\text{g}/\text{m}^3$)	LOQ ($\mu\text{g}/\text{m}^3$)
Benzene	$Y = 10,326 * X$	0.9963	2.66	8.07
Toluene	$Y = 19,690 * X$	0.9966	2.46	7.46
Ethylbenzene	$Y = 29,891 * X$	0.9985	1.67	5.04
Xylene	$Y = 23,349 * X$	0.9957	2.88	8.72
TCE	$Y = 7843.8 * X$	0.9985	1.63	4.95

Y and X correspond to the detector signal (peak area) and analyte concentration ($\mu\text{g}/\text{m}^3$), respectively.

4.2.5 Analytical procedure

Figure 4.6 shows a schematic of the experimental setup for the integration of μ PC and SPME as a two-stage preconcentration process. The overall process of analyzing standard BTEX and TCE samples includes four steps. The first step is to preconcentrate VOC analytes using the μ PC. The μ PC device was heated and flowed with synthetic air at 320 °C for 20 min to remove contaminants. A mixture of 1 ppb of each BTEX analyte and TCE was prepared from a 1000 ppm sample by dilution with synthetic air. Different volumes of this mixture were passed through the conditioned μ PC where the analytes were adsorbed on adsorbent at room temperature. Adsorption was examined at different sampling flow rates (20, 30, 40, and 50 mL/min) and an optimized flow rate was selected. The second step is the thermal desorption process of VOCs from the μ PC. The μ PC was placed on a preheated hotplate. The top surface of the μ PC reached 320 °C within 1 min. For these experiments, the microheater on the μ PC was not used due to high resistance and a maximum temperature of about 150 °C. A thermometer (Omega, model hh806au) with a K-type thermocouple was used to measure the temperature on the surface of the μ PC. When the temperature reached 320 °C, synthetic air from the cylinder was passed through the μ PC at an optimized flow rate of 40 mL/min. The first 50 mL of the desorbed sample was collected in a clean glass syringe. The third step is to utilize SPME extraction from the desorbed sample. The SPME fiber was conditioned before extraction to remove any background contaminants. The SPME fiber (Car/PDMS) then was inserted into the glass syringe with a short silicon rubber tube with a septum (RESTEK Septa Thermolite®Shimadzu Plug) to capture the analytes at room temperature. The last step is to analyze compounds from the SPME by GC–MS. The SPME fiber was immediately

transferred to the injection port of the GC. Thermal desorption of the analytes from the fiber was performed at 300 °C for 1.5 min.

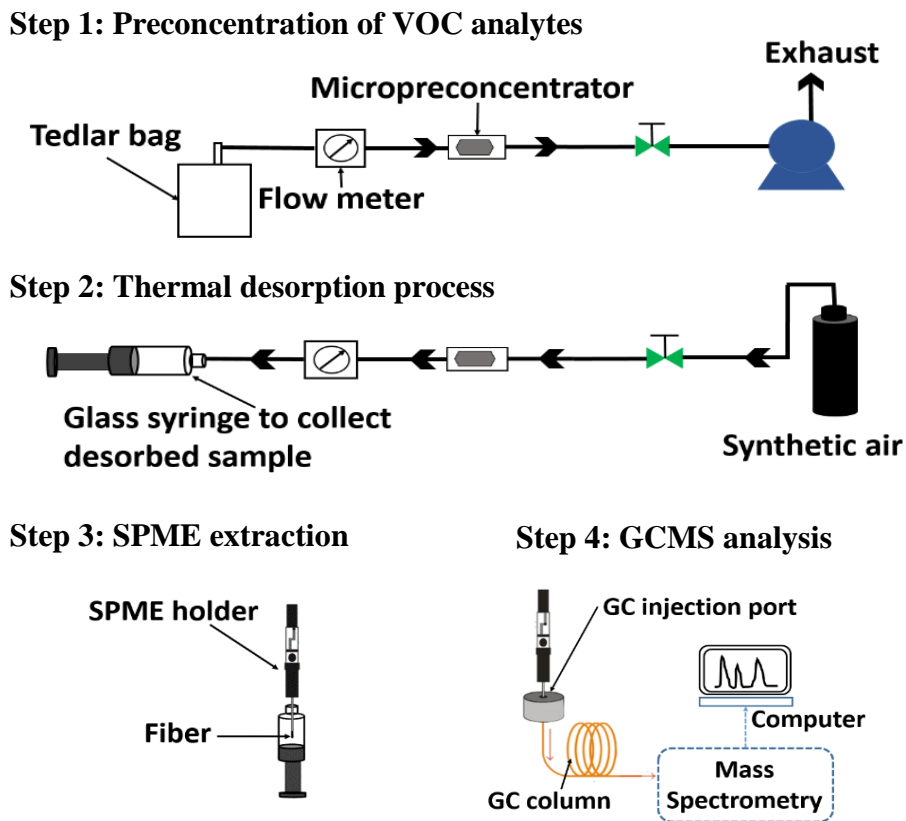


Figure 4.6: Scheme of the analytical procedure from adsorption of samples to GCMS analysis.

4.2.6 GC-MS parameters

Analysis was performed by a GCMS (Agilent 7820A GC system, 5975 Series MSD) equipped with an HP-1 column (30 m × 0.25 mm id, 0.25µm thickness). GC oven temperature was programmed to 40 °C, 3-min hold, then ramped to 120 °C at a rate of 10 °C/min following a 1-min hold. Helium was used as a carrier gas with a flow rate of 1

mL/min and split injection mode (split ratio 5:1) was used. The injection port temperature was set at 300 °C.

4.3 Results and discussion

4.3.1 Characterization of the preconcentrator–SPME for analysis of VOCs

The performance of a μ PC is determined by several variables including the device structure, types of adsorbents, adsorbent capacity, porosity, selectivity, power consumption, flow dynamics, and pressure drop across the device [193]. A preconcentration factor (PF) has been used to evaluate the performance of a μ PC. There is no standard definition of PF as researchers have used different criteria to calculate it. In general, PF is the ratio of the concentration of analytes after thermal desorption to the initial concentration of a gas sample [57]. Since the concentration of analytes after a preconcentration process depends on the initial sample volume and sampling conditions including sample flow rate and time, the PF depends on these variables. Alfeeli et al. defined PF as the ratio between peak areas generated by the detector (FID) with/without the μ PC [194]. Tian et al. used the ratio of volume in which gas is occupied initially to the volume after thermal desorption [195]. McCartney et al. used a correlation with flow rate and sampling time of adsorption and desorption to calculate PF [181]. In this study, we used the recovery percentage (%) of target analytes to measure the device performance instead of PF. The recovery percentage was determined by $(C_x \times V_x)/(C_i \times V_i) \times 100\%$, where C_x and V_x were the analyte concentration and volume after thermal desorption. C_i

and V_i were initial analyte concentration and volume before concentration process by the μ PC.

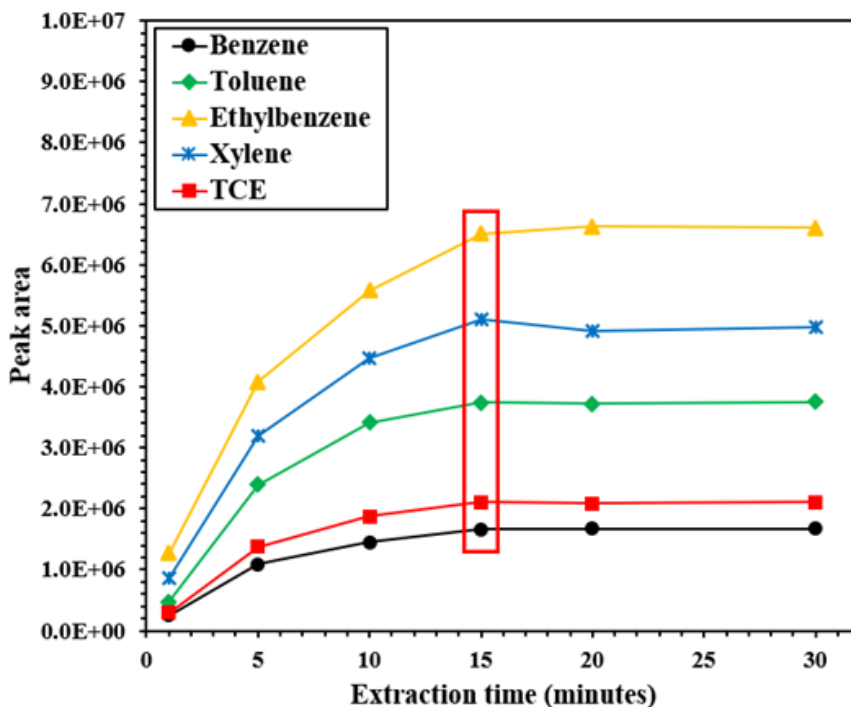


Figure 4.7: The effect of extraction time on GC-MS peak areas of 50 ppb BTEX & TCE mixture produced by SPME at room temperature.

To determine recovery percentages, different concentrations (0.5, 1, 2, and 3 ppb) of BTEX and TCE in 5 L synthetic air were passed through the device. The adsorption flow rate was set to 50 mL/min. The captured analytes then were collected by thermal desorption directly into a 50 mL air-tight syringe. The desorption flow rate and temperature were fixed at 40 mL/min and 320 °C, respectively. The optimization of desorption temperature and the flow rates for adsorption and desorption are discussed in later sections. The concentrations of the collected samples were measured after the SPME concentration

process and analysis by GC-MS using calibration curves. The SPME extraction time was fixed at 15 min based on our experimental data of optimized extraction time in Figure 4.7. Figure 4.8 represents the calculated recoveries for different analyte concentrations at a fixed sample volume of 5 L. The average recoveries were 99.6%, 98.8%, 69.6%, 66.5%, and 81.2% for benzene, toluene, ethylbenzene, xylene, and TCE, respectively.

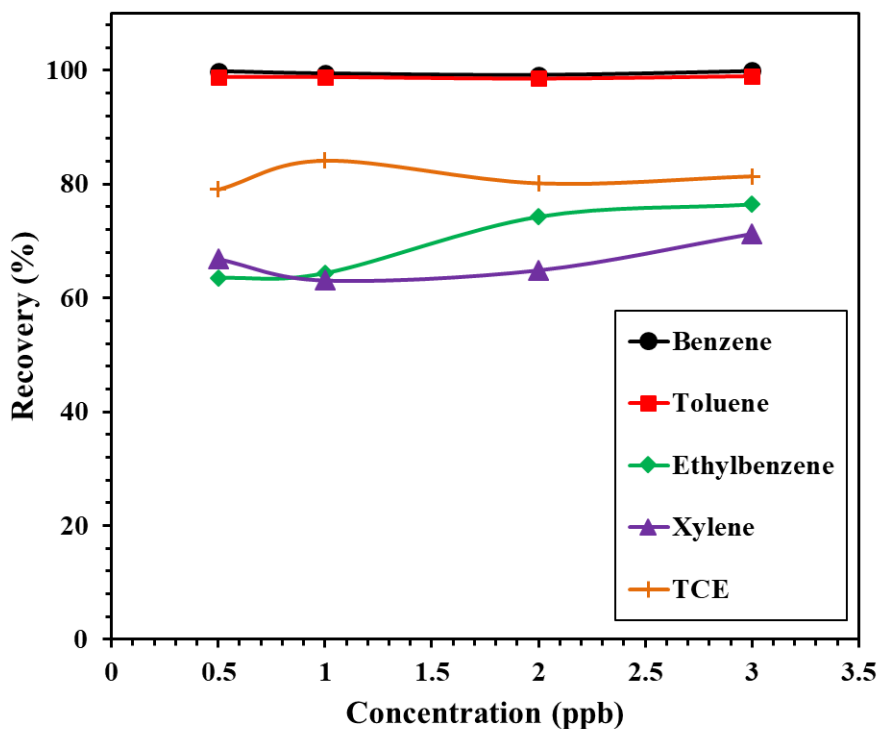


Figure 4.8: Recovery percentage of BTEX and TCE for a combination of μ PC and SPME at different initial concentrations (0.5, 1, 2, and 3 ppb) in 5 L samples.

For benzene and toluene, high recovery percentages were achieved, which indicates that most of these compounds adsorbed in the μ PC and then were collected after thermal desorption. Relatively lower values were observed for ethylbenzene, xylene, and TCE. One

possible reason could be related to the adsorbent property as the trapping capacity can vary with different compounds based on volatility. Also, some residues might not be desorbed completely. Nevertheless, similar recovery percentage results were acquired by using different concentrations of these analytes. The relative standard deviation in recoveries for these four different concentrations was lower than 8%, showing very good reproducibility for analysis.

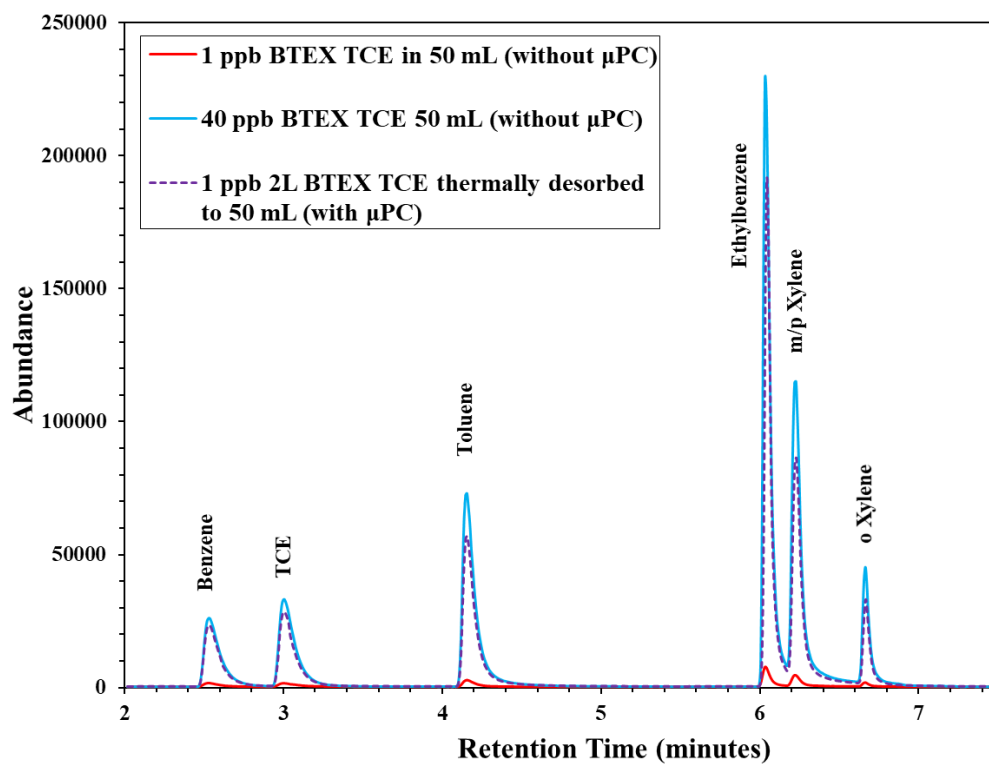


Figure 4.9: A comparison of detector signals for SPME of 1 ppb and 40 ppb BTEX TCE of 50 mL samples (without μ PC) with 1 ppb BTEX TCE of 2L concentrated by the μ PC and then thermally desorbed to 50 mL for SPME analysis.

Furthermore, SPME was carried out for 15 min on two 50 mL samples, one containing 1 ppb and the other containing 40 ppb of BTEX compounds and TCE. The GC–MS chromatograms for these analyses are shown in Figure 4.9. For comparison purposes, 1 ppb of BTEX and TCE in a 2 L sample was passed through the μ PC at a flow rate of 50 mL/min and then thermally desorbed at 320 °C. The desorbed sample was collected in 50 mL using a desorption flow rate of 40 mL/min. The desorbed sample was then extracted by SPME for 15 min and analyzed by GC–MS. Figure 4.9 shows the signals of BTEX and TCE from preconcentrated 2 L of 1 ppb using a combination of the μ PC and SPME. The results indicate that the μ PC with Carboxen 1000 adsorbent could concentrate 2 L of 1 ppb to 50 mL of 40 ppb for benzene, TCE, and toluene, but there was some loss for ethylene and xylene. According to SPME theory, the amounts of extracted analytes are proportional to the sample concentrations for the same SPME and sample volumes [44, 46]. Thus, increasing sample concentration by the μ PC is important for increasing the extracted amounts of analytes by SPME and consequently enhancing GC-MS signals. The results show the advantage of combining the μ PC with SPME for two-stage concentration and extraction to significantly increase GC-MS detection signals for accurate measurements of trace VOCs.

4.3.2 The effect flow rates for adsorption/thermal desorption of the μ PC

The flow rates for adsorption and thermal desorption are important parameters to characterize the μ PC device performance. A higher sample flow rate affects adsorption capacity. The packed adsorbent bed residence time is determined by the sample flow rate of the adsorption process. When the residence time is shorter than the critical residence

time, the adsorption capacity decreases and causes a breakthrough earlier. The maximum flow rate achieved for the μ PC was 50 mL/min using a KNF diaphragm vacuum pump. An optimized adsorption flow condition was determined using a range of adsorption flow rates (20 to 50 mL/min) for 4 ppb of BTEX and TCE in 2 L. Desorption flow rate and temperature for these experiments were set at 40 mL/min and 320 °C, respectively. After SPME, GC-MS chromatograms were obtained. There were no significant changes in recovery (%) for BTEX and TCE with increasing adsorption flow rate, as shown in Figure 4.10. The relative standard deviation (RSD, %) of recoveries for the above-mentioned flow ranges was lower than 5%. An optimum adsorption flow rate of 50 mL/min was chosen for the sample concentrations of BTEX and TCE less than 4 ppb for further experiments.

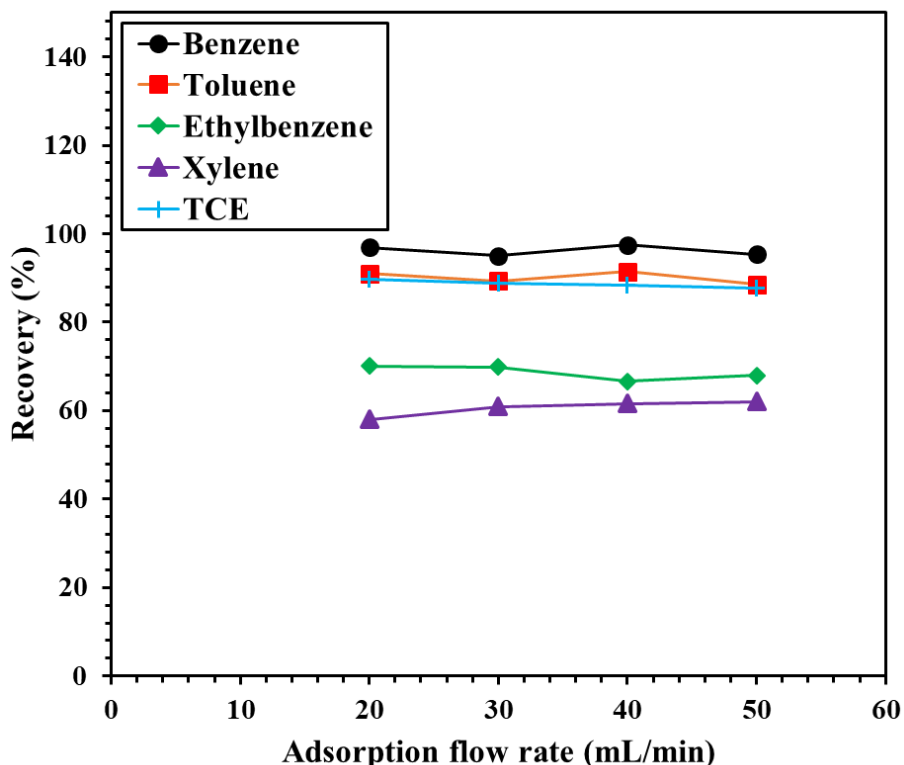


Figure 4.10: Recoveries obtained at different adsorption flow rates for 4 ppb of 2 L BTEX TCE preconcentrated into 50 mL samples.

The results in Figure 4.11 show the recoveries (%) at different desorption flow rates (10 to 40 mL/min) using 1 ppb of BTEX and TCE in 5 L. A constant adsorption flow rate of 50 mL/min and desorption temperature of 320 °C were maintained in this study. Desorbed analytes were collected to a volume of 50 mL of desorbed air from the μ PC. The results show that recoveries were lowest for the 10 mL/min desorption flow rate which indicates the lowest desorption efficiency. The recoveries were improved with higher flow rates of 20 to 40 mL/min. So, 40 mL/min was used in the desorption step for the next experiments. Also, desorption efficiency was checked by eluting all adsorbate inside the μ PC using a long thermal desorption process. The collected second 50 mL from thermal desorption was analyzed. It yielded no detectable BTEX and TCE peaks.

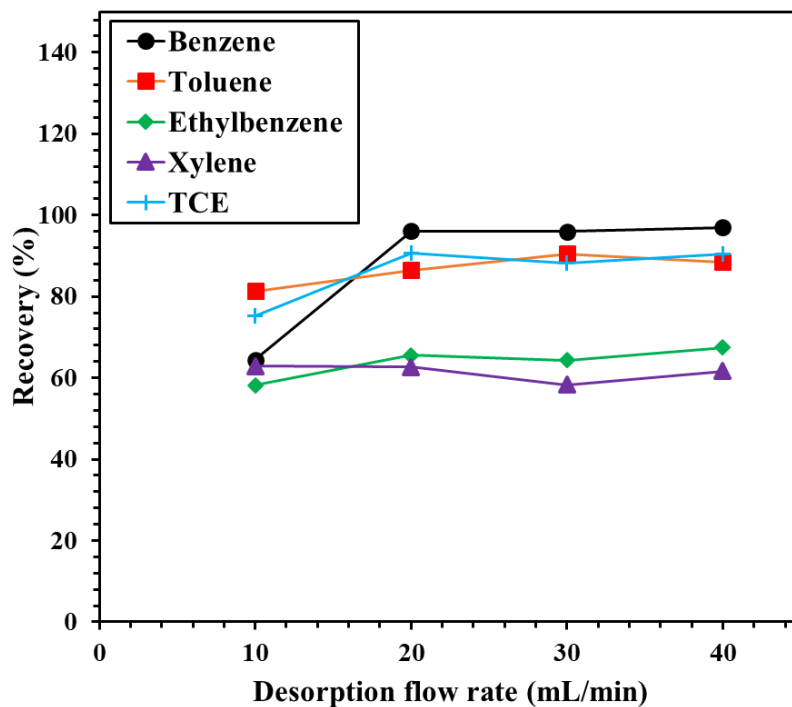


Figure 4.11: Recoveries obtained at different thermal desorption flow rates for 1 ppb of 5 L BTEX TCE pre-concentrated into 50 mL samples.

4.3.3 The effect of thermal desorption temperature of the μ PC

Desorption temperature is another important parameter that influences μ PC performance. Heat is applied to the device to increase the temperature to rapidly release any adsorbed analytes. However, increasing temperature above certain levels can cause a decomposition of captured analytes, which results in inaccurate sensing for analytes in the detection step. In this study, detector responses were measured at different desorption temperatures (200, 250, 280, 320, and 360 °C) with fixed preconcentration conditions (initial BTEX and TCE concentration of 2 ppb, sample volume of 2 L, adsorption and desorption flow rates at 50 mL/min and 40 mL/min, respectively, and a thermally desorbed sample volume of 50 mL). The desorption step started by keeping the μ PC device on a preheated hotplate and heated to gain the desired temperature. Within 1 min the temperature of the device reached the desired point. The temperature on the top surface of the device was measured by a K-type thermocouple. Then synthetic air was flowed at 40 mL/min and collected into a glass syringe. SPME and GC-MS analysis was performed to measure the analytes. Figure 4.12 shows the values of recoveries as a function of desorption temperature. The effect of desorption temperature on the recovery is obvious for all compounds. At 200 °C, low recoveries were observed for all analytes, indicating incomplete desorption of these analytes. Recoveries increased with higher temperatures; benzene and TCE reached maximum recovery at 280 °C. Similarly, toluene, ethylbenzene, and xylene recoveries increased with temperature up to 320 °C. Recoveries were observed to decrease at 360 °C desorption temperature. The recommended desorption temperature for the Carboxen-1000 adsorbent is 330 °C. Increasing the temperature beyond this temperature can cause the decomposition of analytes to result in a lower recovery. So, 320

°C was chosen for the desorption step to produce reliable and repeatable results for the analysis of environmental air samples.

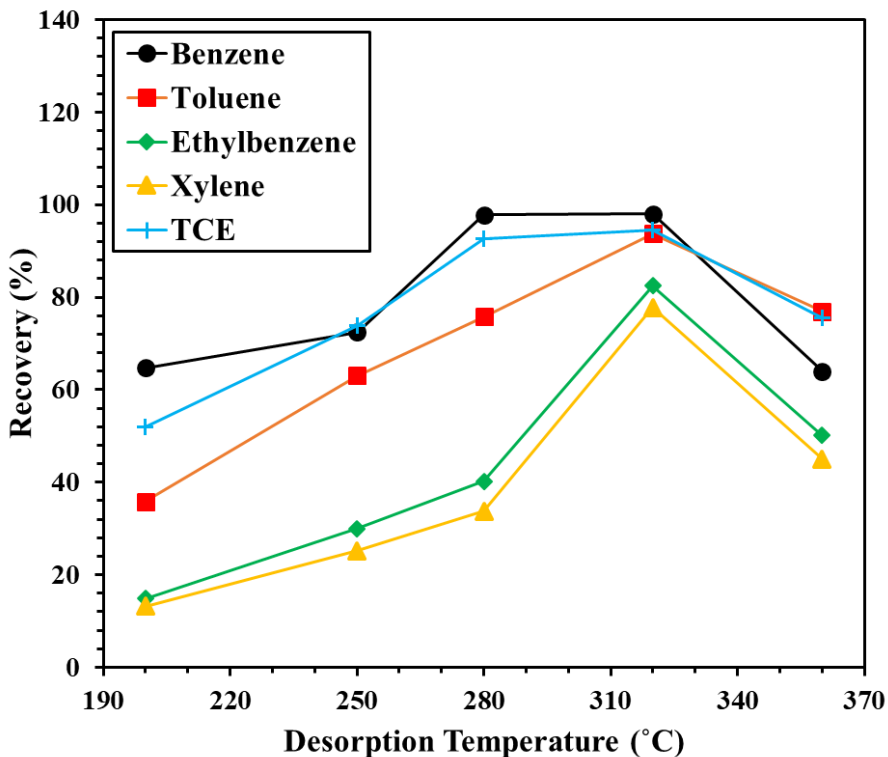


Figure 4.12: Recoveries obtained at different desorption temperatures for 2 ppb of 2 L BTEX and TCE preconcentrated into 50 mL samples.

4.3.4 Method precision

The reproducibility of different devices was tested to ensure reliable results in the long term. To evaluate reproducibility, three different μ PC devices were used to analyze 5 L of 2 ppb BTEX and TCE samples using the same experimental conditions of adsorption flow rate: 50 mL/min, desorption flow rate: 40 mL/min, desorption temperature of 320 °C, the desorbed volume of 50 mL for SPME extraction. These three devices yielded nearly

identical peak areas (RSD < 10%) for all target analytes which indicates the repeatability among different devices. Furthermore, 2 L of 1 ppb and 1 L of 2 ppb BTEX and TCE gaseous samples were analyzed using the two-stage preconcentration process using the same experimental conditions. The peak areas for all analytes were very close as shown in Figure 4.13.

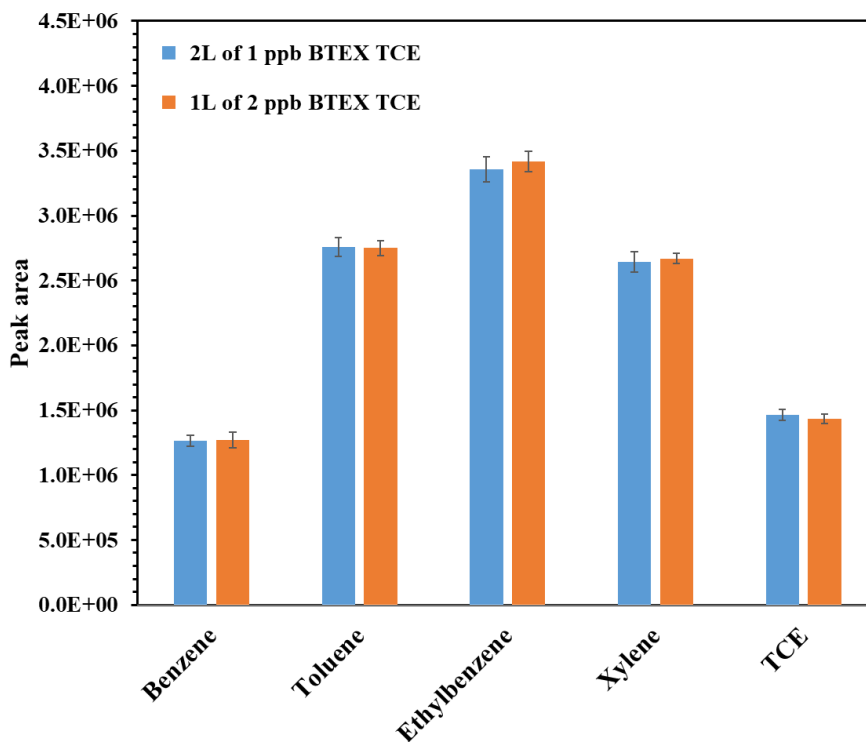


Figure 4.13: Comparison of GC-MS peak areas between 2 L of 1 ppb and 1 L of 2 ppb of BTEX and TCE samples using the two-stage preconcentration using μ PC and SPME for GC-MS analysis.

4.3.5 Application for real-world samples

This two-stage preconcentration approach was applied to detect BTEX and TCE in the environmental air. Air samples of 1 L were collected from a gas station near an exit of an interstate highway and a city roadside in Louisville, Kentucky at different times using cleaned Tedlar bags. Three air samples were taken from each location and each air sample was processed with different μ PCs. Table 4.3 shows the results obtained from a gas station near an interstate highway and a city roadside at two different times. All compound concentrations are in the ranges of the same compounds collected with passive sampling devices every two weeks for one year in Louisville, Kentucky in a recent publication [196]. The GC–MS chromatograms for the roadside are given as an example in Figure 4.14. Air samples with only SPME extraction were also tested by GC–MS for comparison and very tiny peaks were detected. The results show the advantage of the integration of the μ PC and SPME for increasing the GC–MS signals for quantitative analysis.

Toluene was found as the most abundant compound of BTEX in the environmental air. The mean levels of benzene and toluene were higher during the afternoon rush hours than in the morning as their source was principally car exhaust. The mean concentration of toluene near the gas station during rush hour was $1.731 \mu\text{g}/\text{m}^3$, while the mean concentration of this compound at the roadside during rush hour was $1.886 \mu\text{g}/\text{m}^3$. Other unknown peaks were obtained with different retention times, but because this work focused on method development and analysis of BTEX and TCE, these compounds are presently unidentified.

Table 4.3: Average concentrations ($\mu\text{g}/\text{m}^3$) and standard deviations ($n = 3$) of BTEX and TCE in ambient air with 1 L samples preconcentrated by the μPC and SPME.

Compound ($\mu\text{g}/\text{m}^3$)	Gas station (10 AM)	Gas station (5 PM)	Roadside (10 AM)	Roadside (5 PM)
Benzene	0.495 ± 0.019	0.48 ± 0.028	0.418 ± 0.026	$0.483 \pm .042$
Toluene	1.162 ± 0.034	1.731 ± 0.138	1.667 ± 0.062	1.886 ± 0.164
Ethylbenzene	0.451 ± 0.033	0.55 ± 0.009	0.182 ± 0.005	0.599 ± 0.039
Xylene	0.576 ± 0.012	0.918 ± 0.003	0.417 ± 0.024	0.689 ± 0.048
TCE	0.303 ± 0.006	0.287 ± 0.001	0.322 ± 0.026	0.384 ± 0.011

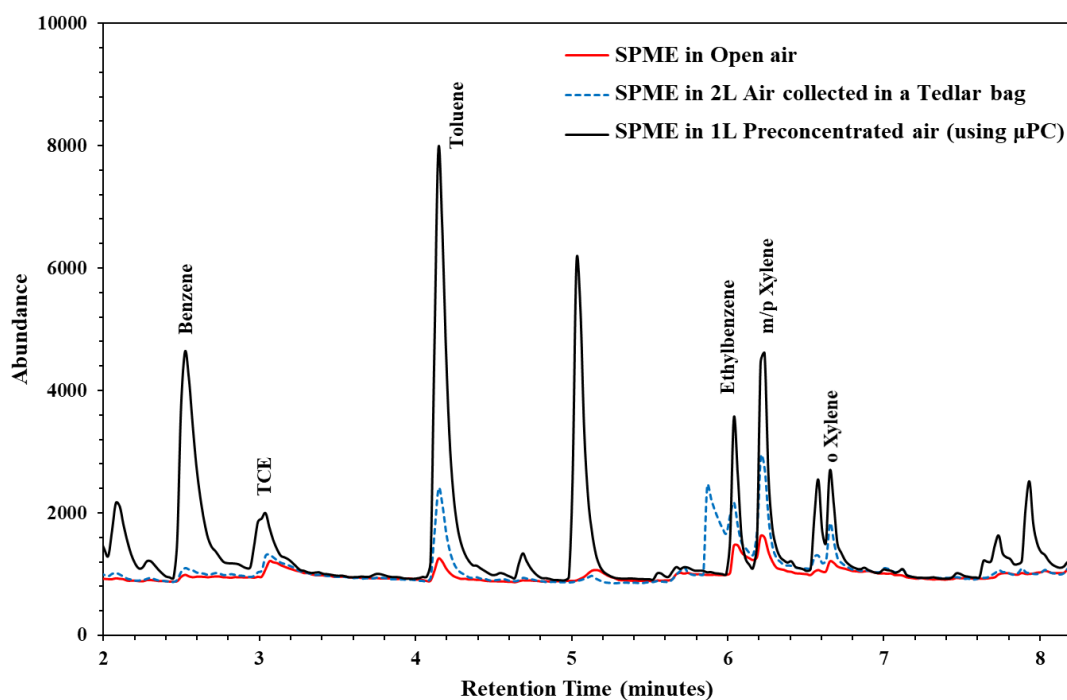


Figure 4.14: GC-MS spectra for environmental air sample; (a) red line: SPME for 15 min extraction in the open air (b) blue dash line: SPME for 15 min extraction in 2 L air collected in a Tedlar bag (c) black line: SPME for 15 min extraction of 50 mL sample preconcentrated from 1 L air using the μPC .

4.4 Conclusion

In this study, a MEMS preconcentrator was developed to integrate with SPME to significantly increase the amounts of extracted analytes for GC–MS analysis which in turn enables reliable measurements of VOCs at a few $\mu\text{g}/\text{m}^3$ levels in the environmental air. The performance of the μPC was characterized based on the optimized operation parameters of adsorption and thermal desorption for BTEX and TCE gaseous mixtures, which are toxic pollutants in the environmental air. Reproducible measurements were demonstrated with different μPC s and SPME. The optimized method has been applied to analyze trace BTEX and TCE in environmental air samples.

CHAPTER V

DEVELOPMENT OF A DUAL-COMPARTMENT
MICROPRECONCENTRATOR TO DETECT AIRBORNE VOCS

5.1 Introduction

Rising worldwide concern about the adverse effects of both indoor and outdoor air pollution on human health has promoted the development of innovative techniques for detecting toxic volatile organic compounds (VOCs) in the air. VOCs produce photochemical oxidants by participating in atmospheric photochemical reactions and possess boiling points from 50 °C to 260 °C at a standard atmospheric pressure of 101.3 kPa [7, 197]. VOCs are ubiquitous, generated from natural and anthropogenic sources. Biogenic VOCs contribute 60 – 70% of total VOCs emission, which are produced from vegetation, tropical woodlands, croplands, etc. [198, 199]. Most anthropogenic emissions are toxic, and these VOCs come from industrial solvents, cleaning agents, petroleum fuels, cooking oils, body spray, paint, automobile exhaust, etc. [9, 159, 200]. The severity of unpleasant health effects depends on the VOC types, concentration level, and exposure time. Aromatic compounds including benzene, toluene, ethylbenzene, and xylene (BTEX), are the prevalent VOCs present in urban and industrial areas [11, 12, 201]. Exposure to BTEX causes skin and eye irritation, leukemia, heart and kidney diseases, nervous system

dysfunction and cancer, etc. [11, 106, 124] while aldehydes including formaldehyde, acetaldehyde, and acrolein result in cardiovascular diseases, lung cancer, and chronic obstructive pulmonary diseases (COPD) for chronic exposure at high concentrations of these VOCs [36, 202]. Consequently, periodic monitoring of these toxic VOCs is required to prevent people from exposure to high levels of these toxic VOCs.

Gas chromatography (GC) coupled with different detectors such as mass spectrometry detector (MSD), flame ionization detector (FID), and photoionization detector (PID) are commonly used for VOC detection [203]. Because of trace levels of VOCs present in the air, a preconcentration process is required to increase the concentrations of target VOCs [124]. The quantification of VOCs first requires air sampling using sorbent tubes or cartridges, then elution of the target compounds followed by separation of compounds from the sample matrix and detection of each compound in a detector [204]. For trapping BTEX compounds on sorbents, several adsorbent materials, including porous carbon, polymeric Tenax, etc. were used [181, 205, 206]. In recent years, microfabricated preconcentrators are used for collecting airborne BTEX, which are suitable for onsite sampling and requires a small amount of sorbents [57, 124]. Moreover, micropreconcentrators (μ PC) fabricated by microelectromechanical system (MEMS) technology can afford lower fabrication costs, mass production, and high aspect ratio microdevices with low power consumption [57, 197, 207]. In addition, μ PC is filled or coated with suitable sorbents based on target analytes of interest. Tenax TA sorbent was used for air sampling during wildfires and analysis of BTEX compounds by gas chromatography-mass spectrometry (GC-MS) [182]. μ PC filled with carbopack B adsorbent was used for trapping BTEX and detection by GC-PID [183]. Besides thermal

desorption, solvents such as dichloromethane were also used for BTEX elution from adsorbents [41, 208]. Environmental Protection Agency (EPA) has a passive sampling technique (EPA method 325 A/B) to detect BTEX and other VOCs using a passive sampler packed with carbopack X [196].

The derivatization technique is used to transform a compound into a new compound by chemical reaction to promote better separation and detection [209]. Small aldehydes like formaldehyde and acetaldehyde are very volatile and difficult to use physical sorbent for capture. To measure carbonyl compounds in the air, derivatization before elution and analysis with GC or liquid chromatography (LC) is typically used. For instance, aldehydes reacted with 2,4-dinitrophenylhydrazine (DNPH) followed by liquid elution and then liquid chromatography for separation have been commonly used for the analysis of these compounds [34, 37, 210]. EPA TO-11A method is used for the analysis of formaldehyde in ambient air. The method involves DNPH coated silica gel cartridge for capturing formaldehyde and analysis of DNPH adducts by high-performance liquid chromatography (HPLC) with ultraviolet (UV) absorption for detection [37]. Another prevalent derivatizing reagent is *o*-(2,3,4,5,6-pentafluorobenzyl)-hydroxylamine hydrochloride (PFBHA) which forms stable oximes and amenable for GC-MS or GC electron-capture detector (ECD) analysis [38]. The reaction is swift, and the PFBHA derivatives form in seconds at ambient temperature [39]. EPA 556 method utilizes PFBHA to capture carbonyls in drinking water and GC-ECD for analysis [40].

Until present, BTEX and aldehydes in environmental air have been separately concentrated and analyzed by different methods. For example, EPA TO-15, and TO-14A methods were used for BTEX analysis and TO-11A method was applied for aldehyde

analysis separately [29, 33-37]. Passive sampling tubes containing activated charcoal were also used to capture BTEX and passive sampling tubes containing DNPH-coated silica were used for the derivatization of aldehydes [38-40]. Sampling environmental air for capturing BTEX or derivatizing carbonyls separately and detecting those in particular detectors is cumbersome and induces errors. Currently, there is no single sampling device and no single analytical method for analysis of BTEX and aldehydes together.

In the present work, a novel micropreconcentrator device is developed to capture a broad range of VOCs including BTEX and carbonyls, and analysis by GC-MS. The micropreconcentrator with a microfluidic channel has the advantages of faster reaction rates with an improved mass transfer rate that enables a short time for analysis, and a few microliters of solvent to elute captured compounds [36, 209]. The micropreconcentrator can be fabricated on silicon wafers by microelectromechanical system (MEMS) technology, which requires less power to operate [124, 202]. The micropreconcentrator contains two compartments, a set of micropillars for separating and fixing sorbents. One chamber is loaded with adsorbent carbopack X for trapping BTEX compounds, and the other is filled with silica gel particles. The silica gel particles are coated with PFBHA for capturing and derivatizing carbonyls. Dichloromethane (DCM) is used to elute all the captured compounds and analyzed by GC-MS, which takes less than 30 min to separate and detect BTEX and carbonyl compounds with a single GC-MS analysis. The micropreconcentrator provides an innovative approach for concentrating BTEX and carbonyls together and analysis by GC-MS.

5.2 Materials and Method

5.2.1 Chemicals and materials:

Benzene, toluene, ethylbenzene, xylene (a mixture of o-, m-, and p-xylene), formaldehyde, acetaldehyde, acetone, propanal, 2-butanone, butanal, 2-pentanone, pentanal, 2-hexanone, hexanal, and acrolein were purchased from Sigma Aldrich. Deuterated compounds acetone (d_6), propanal (d_2), 2-butanone (d_5), butanal (d_2), 2-pentanone (d_5), hexanal (d_{12}) were purchased from Sigma Aldrich. Tedlar bags were obtained from Supelco. PFBHA, carbopack X (60 – 80 mesh), silica gel (60 – 100 mesh), DCM, methanol, and hexane were bought from Sigma Aldrich. Septa and limited-volume inserts were bought from Restek. Synthetic air (moisture < 4 ppm) was purchased from a local gas company (Welders Supply, Louisville, KY).

5.2.2 Preparation of standards and calibration curve:

Deuterated propanal, 2-butanone, butanal, 2-pentanone and hexanal were diluted with methanol to prepare 100 mM concentration samples. A predetermined amount of these five samples were mixed to prepare a 1 mM concentration of each compound. Also, a 1 mM concentration of each deuterated carbonyl was prepared as standard. These samples were then reacted with PFBHA solution (PFBHA to carbonyl molar ratio 1.2: 1 to ensure all carbonyl reacted) to form PFBHA-carbonyl adducts. These standard solutions were stored at 4 °C. Calibration curves were prepared for investigation and characterization of a silica-loaded microdevice (Device A), carbopack X loaded microdevice (Device B) and both silica and carbopack X loaded dual-compartment microdevice (Device C). Deuterated

carbonyl compounds were used to characterize the capture efficiencies of Device A. Calibration curves (Figure 5.1a) for quantitative analysis of captured deuterated carbonyls by silica-loaded Device A were prepared by injecting 1–12 nmol of PFBHA adducts of propanal-d₂, 2-butanone-d₅, butanal-d₂, 2-pentanone-d₅, hexanal-d₁₂ into methanol (total volume 50 μL) and 5 nmol of PFBHA-acetone-d₆ was added into all samples as an internal reference (IR). Similarly, calibration curves (Figure 5.1b) for quantitative analysis of BTEX captured by carbopack X filled Device B was made by injecting 2 – 10 nmol of BTEX mixtures into methanol with 5 nmol of heptane-d₁₆ as an IR to estimate. Calibration curves were prepared (Figures 5.1c & 5.1d, separated in two figures to show all analytes) to analyze carbonyls (non-deuterated) and BTEX together using the Device C dual-compartment microfluidic device only for environmental air analysis. 0.25 – 1.25 nmol of BTEX and PFBHA adducts of formaldehyde, acetaldehyde, propanal, acetone, butanal, 2-butanone, pentanal, 2-pentanone, hexanal, 2-hexanone, and acrolein were mixed in a total volume of 50 μL methanol and 0.5 nmol of heptane-d₁₆ was added to each solution as an IR. PFBHA solutions were prepared by dissolving the required amount of PFBHA adducts in 1 mL of methanol. These solutions were prepared every week and stored at 4 °C.

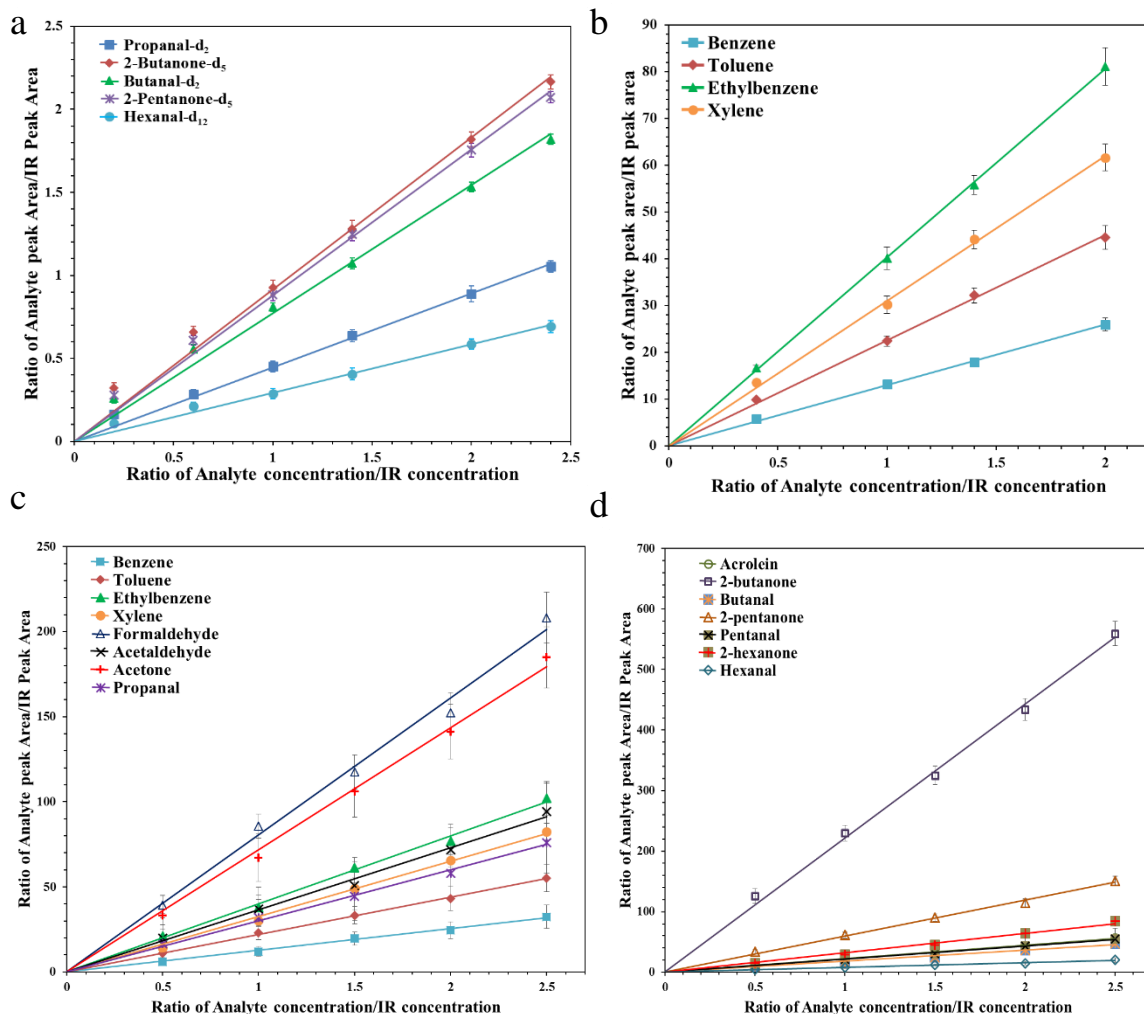


Figure 5.1: (a) Calibration curves for PFBHA-deuterated-propanal, 2-butanone, butanal, 2-pentanone, hexanal with IR PFBHA-acetone-d₆ to characterize device A; (b) Calibration curves for benzene, toluene, ethylbenzene and xylene with IR heptane-d₁₆ to characterize device B; (c) & (d) Calibration curves for benzene, toluene, ethylbenzene, xylene, PFBHA-(formaldehyde, acetaldehyde, acetone, propanal, acrolein, 2-butanone, butanal, 2-pentanone, pentanal, 2-hexanone and hexanal) with IR heptane-d₁₆ to characterize device C.

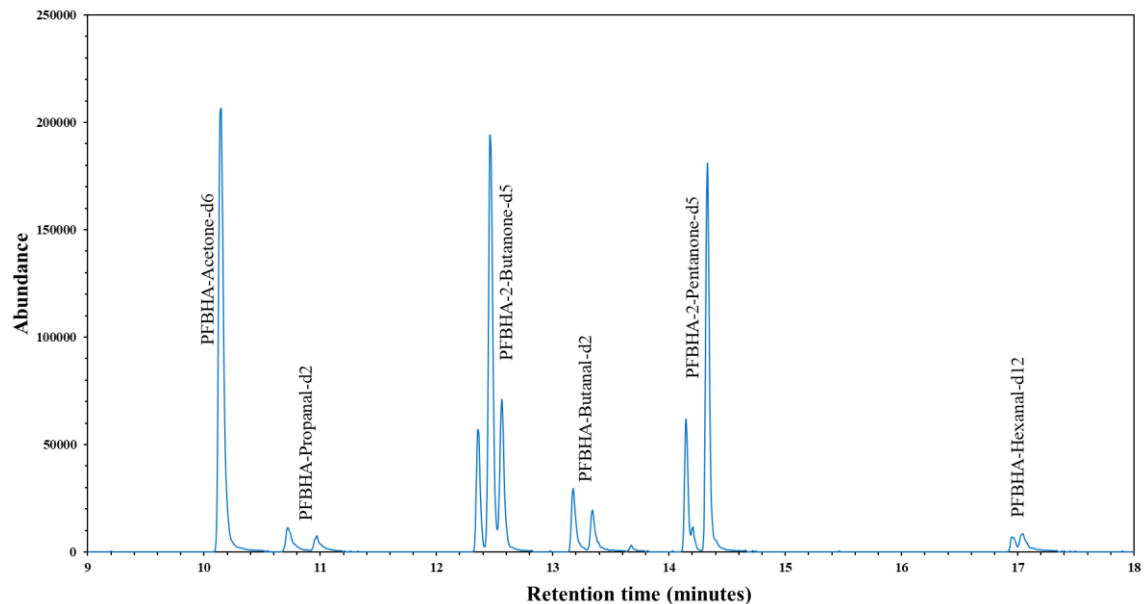


Figure 5.2: A GC-MS chromatogram of a standard sample containing 5 nmol of each PFBHA-deuterated-propanal, 2-butanone, butanal, 2-pentanone, hexanal and 5 nmol of PFBHA-acetone-d₆ as an IR in a total volume of 50 μ L methanol.

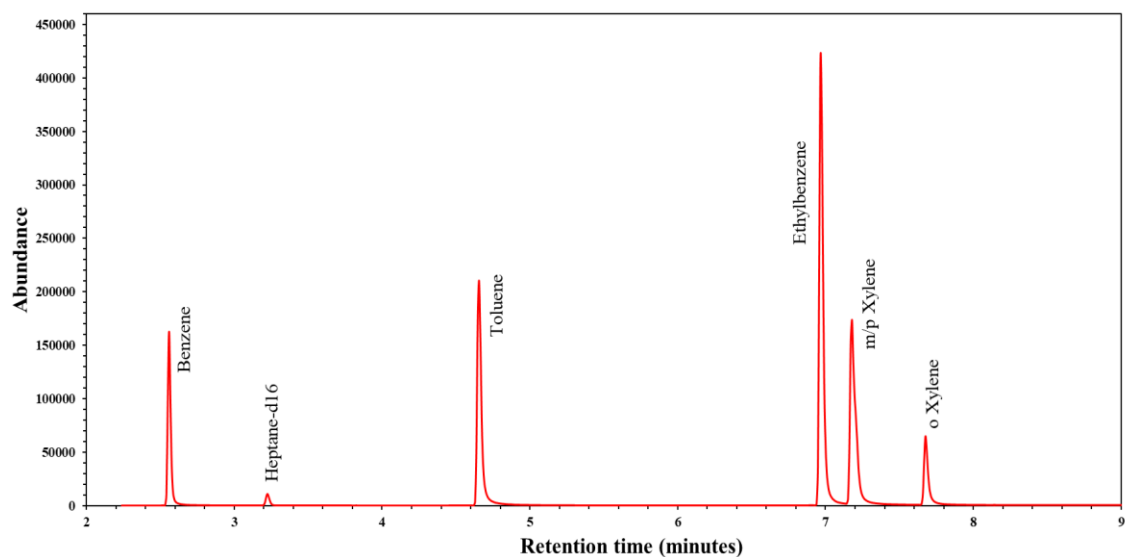


Figure 5.3: A GC-MS chromatogram of a standard sample containing 5 nmol of each benzene, toluene, ethylbenzene, xylene, and 5 nmol of heptane-d₁₆ as an IR in a total volume of 50 μ L methanol.

5.2.3 Design and fabrication of micropreconcentrator devices:

Two different designs of micropreconcentrators (Figure 5.4) were fabricated using single-side polished 1 mm thick 4-inch diameter silicon wafers. These micropreconcentrators are 14 mm x 8.5 mm x 1.5 mm. First, the cleaned wafer (Figure 5.5A) was placed in a furnace to grow around 400 nm thick SiO₂ (Figure 5.5B). Next, a positive photoresist was coated and exposed to UV light using a dark field photomask. The wafer was then developed in Microposit MF319 solution (Figure 5.5C). The thermal oxide

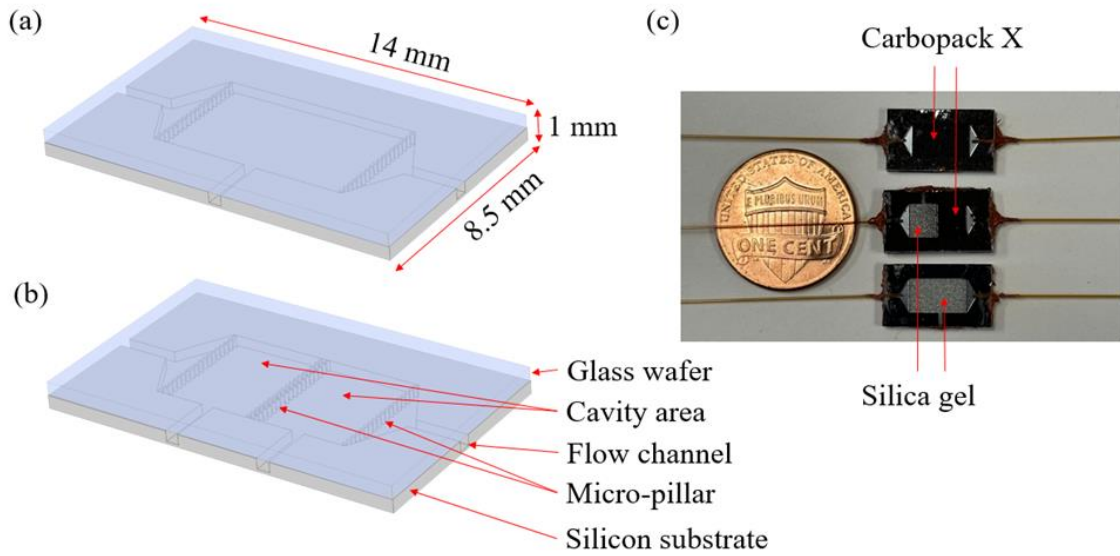


Figure 5.4: (a) Schematic of the single-compartment microdevice, (b) Schematic of the dual-compartment microdevice, (c) Optical pictures of silica gel and carbopack X loaded single and dual-compartment microdevices.

in the patterned area was removed by buffered oxide etchant (BOE) for deep reactive ion etching (DRIE) (Figure 5.5D). After BOE, DRIE was performed to create a flow channel, a central cavity with a set of micropillars near the inlet and outlet section to retain

adsorbents (Figure 5.5E). The depth (400 μm) was measured by a Dektak profilometer. Then, the wafers were put in N-Methyl-2-pyrrolidone (NMP) bath followed by oxygen plasma cleaning. Sacrificial SiO_2 layers were entirely removed by placing the wafer in a BOE solution (Figure 5.5F). Later, the wafer was sealed by anodic bonding with a 0.5 mm thick glass wafer (Pyrex 7740 glass) using a Suss SB6e bonder (Figure 5.5G). Finally, the wafer was diced to obtain individual microdevices. The fluidic channels were connected with deactivated fused silica tubes (355 μm O.D., 255 μm I.D., Polymicro Technologies) and sealed with silicone adhesive (Duraseal® 1531, Cotronics, NY USA).

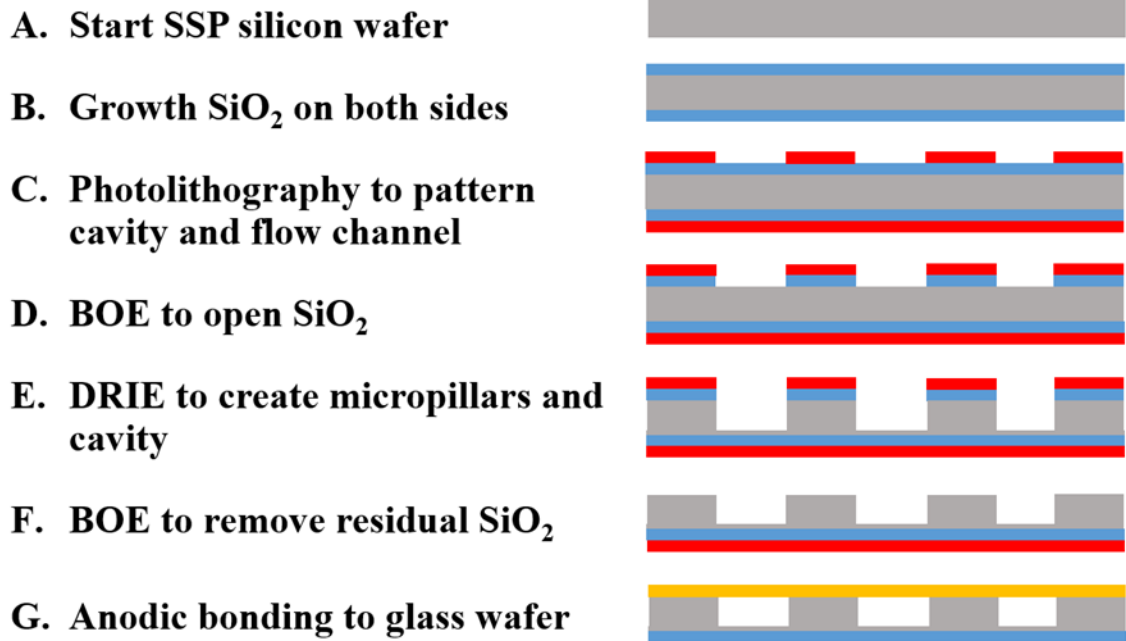


Figure 5.5: Schematic diagram of the microdevice fabrication steps.

5.2.4 Preparation of micropreconcentrator devices:

Micropreconcentrator device A and B (Figure 5.4a) contain a single cavity where device A was packed with silica gel (4.2 ± 0.2 mg), and device B was loaded with

carbopack X (4 ± 0.2 mg) by applying a vacuum. After filling with adsorbent, the loading port was sealed with Duraseal 1531. Device C (Figure 5.4b) contains two cavity compartments for filling silica gel (2.2 mg) & carbopack X (2 mg) separated by two parallel lines of micropillars with 50 μm in diameter and a gap of 50 μm between the closest micropillars. Since the amounts of sorbents in device C were less than that in devices A and B, device C was tested using similar VOC concentration levels present in the environmental air. Using trace concentration facilitates avoiding breakthroughs for sorbents. Recovery experiments for device C guide the evaluation of a breakthrough. Recovery (%) was defined as the percentage of a measured amount in eluate relative to the amount spiked into a Tedlar bag. Figure 5.4c shows these three types of microdevices loaded with adsorbents. Before all experiments, microdevices were cleaned by flushing with 1 mL of DCM and then dried by applying heat and flowing synthetic air. For carbonyl analysis, the silica gel of the micropreconcentrator was coated with 64–500 nmol of PFBHA. Afterward, both ends of the device were capped by septum to prevent background contamination.

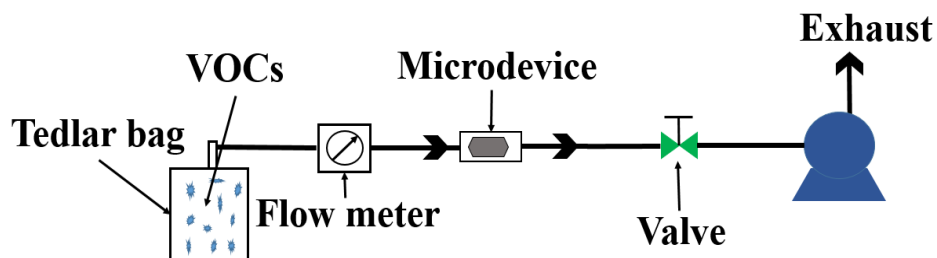


Figure 5.6: Schematic illustration of the experimental setup to capture or derivatize VOCs.

5.2.5 Experimental setup and analysis:

Figure 5.6 shows a schematic illustration of the experimental setup for capturing gaseous VOC samples. One end of the microdevice was connected with a Tedlar bag containing a gaseous sample, and the other end was connected with a diaphragm pump (KNF Neuberger Inc). A digital flow meter (Masterflex® 32908-55, Cole-Parmer Instrument Company) and a mechanical valve were connected to measure and adjust the flow rate. The sampling through the micropreconcentrator was performed at ambient temperature. For trapping carbonyls through Device A, gaseous mixtures of deuterated propanal, 2-butanone, butanal, 2-pentanone, and hexanal in 1L synthetic air were passed through the microdevices at different flow rates. After the evacuation of gaseous mixtures, the device was disconnected from the setup, and one end was connected with a collection vial containing a 200 μL volume insert. The reacted PFBHA adducts and unreacted PFBHA were eluted with 50 μL of DCM and collected in a sample vial. 5 nmol of PFBHA-acetone- d_6 was added as an IR in the eluted sample and later analyzed by GC-MS. The peak area ratio of analyte to IR was used and compared with calibration curves to calculate amounts in eluted samples. Similarly, for capturing BTEX through Device B, a gaseous mixture of BTEX compounds flowed through the device at different flow rates. After preconcentration, the captured compounds were eluted with 50 μL of DCM and 5 nmol of heptane- d_{16} was added in it as an IR. The collected sample was used for analysis by GC-MS. For Device C loaded with two sorbents to capture BTEX and carbonyls, a mixture of BTEX and target carbonyls (formaldehyde, acetaldehyde, propanal, acetone, butanal, 2-butanone, pentanal, 2-pentanone, hexanal, 2-hexanone, and acrolein) in air sample was passed at an optimized flow rate of 50 mL/min. Then, the trapped compounds were

collected with an optimized amount of DCM, 0.5 nmol of heptane-d₁₆ was added as an IR and analyzed by GC-MS. The eluted amounts were calculated similarly by using the peak area ratio of analyte to IR compared with calibration curves.

5.2.6 GC-MS parameter:

Analyses were performed by a 7820A GC (Agilent Technologies, USA) coupled with a 7975 series MSD (Agilent Technologies, USA). The column used was an HP-1 column (30 m × 0.25 mm id, 0.25 μm thickness) with Helium as a carrier gas. A split injection mode of a 10:1 ratio was used. The injection port temperature was set at 250°C. The injected volume was 2 μL. Selected ion monitoring (SIM) mode with ions 78, 91, 106, 116, and 181 m/z was applied. As the PFBHA derivatization process forms E and Z isomers from carbonyl compounds, both peaks were used for quantification. The GC oven temperature profile was different for analyzing samples from these device A, B and C.

Device A: initial 60 °C with 1 min hold, then ramped to 90 °C at 10 °C/min rate with 5 min hold, then ramped to 180 °C at 8 °C/min rate following a 1 min hold and finally raised to 250 °C at a rate of 20 °C/min with 1 minute hold.

Device B: initial 35 °C with 4 min hold, then ramped to 90 °C at 10 °C/min rate with 5 min hold, then ramped to 150 °C at 8 °C/min rate with a 1 min hold.

Device C: initial 35°C with 4 min hold, then raised to 90°C at a rate of 10°C/min with 5 min hold, then raised to 180°C at a rate of 8°C/min with 1 min hold and finally raised to 220°C at a rate of 20°C/min with 1 min hold.

5.3 Results and Discussion

5.3.1 Characterization of Device A for capturing carbonyl compounds:

Device A contains a single cavity that was loaded with silica gel. Different amounts of PFBHA solution were used to coat the silica gel. The effects of sampling flow rate, coating amount, reaction temperature, humidity, etc. on vapor–solid derivatization reaction were studied.

5.3.1.1 Solvent selection for PFBHA adducts elution

Both PFBHA and its carbonyl adducts are water-soluble compounds. However, water is not an appropriate solvent to elute these compounds for this study because aqueous solutions cannot be injected into GC-MS [209]. Instead, several organic solvents, including hexane, DCM, chloroform, acetonitrile, ethanol, ethyl acetate, and methanol have been studied to elute PFBHA carbonyl adducts [209, 211-215]. In this experiment, we tested DCM, methanol, and hexane solvent to elute PFBHA carbonyl adducts from the microdevice loaded with silica gel particles. Device A was coated with 250 nmol of PFBHA. 5 nmol of each deuterated propanal (d_2), 2-butanone (d_5), butanal (d_2), 2-pentanone (d_5), and hexanal (d_{12}) were injected into 1L synthetic air in Tedlar bags. After complete evaporation, the gaseous samples were passed through micropreconcentrators at a 40 mL/min flow rate. Then, the derivatized adducts were collected with the first and second 50 μ L of these three solvents. 5 nmol of PFBHA-acetone- d_6 was added to each sample as an internal reference to calculate the eluted amounts of injected compounds. Figure 5.7 shows the influence of solvent elution on the recovery (%) of collected

derivatized carbonyl compounds. The results indicate that DCM was the most efficient solvent for eluting carbonyl adducts using only 50 μL compared with the other two solvents. Since PFBHA dissolves more in methanol than hexane due to its polar properties, methanol can elute PFBHA-carbonyl adducts easily from silica gel. DCM eluted most of the adducts using a small volume of 50 μL . Also, DCM contained fewer adducts detected than other solvents in the second 50 μL of eluted solvent. So, DCM was chosen for the optimum elution. The results are consistent with reported studies [211, 214].

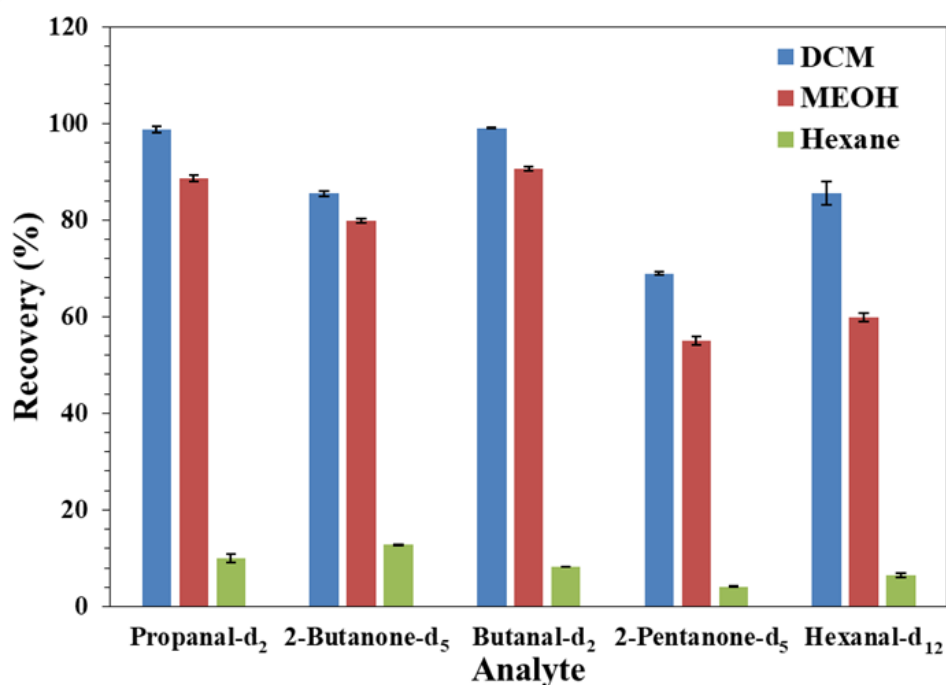


Figure 5.7: Comparison of recovery (%) for target deuterated carbonyls using 250 nmol of PFBHA coated on silica gel loaded (4.2 ± 0.2 mg) single-compartment microdevices extracted with 50 μL of three different solvents.

5.3.1.2 Effect of Flow rate on derivatization

The flow rate is an essential parameter for the reaction of gaseous carbonyl compounds with PFBHA on silica particles. The mass transfer rate is significantly low at a lower flow rate, and it limits the reaction and capture of the carbonyl compounds. As the flow rate is increased, the mass transfer rate will increase and the reaction rate becomes to limit the reaction [216]. If the flow rate is too high, the bed residence time is too short to retain the reactants in the reaction chamber [217, 218]. Therefore, both low and very high sampling flow rates affect the recovery (%) of derivatized adducts of carbonyl compounds from silica-loaded microdevices.

Different flow rates of carbonyl compounds varying from 2 to 120 mL/min were evaluated for the recovery. 5 nmol of each deuterated propanal (d_2), 2-butanone (d_5), butanal (d_2), 2-pentanone (d_5), hexanal (d_{12}) were injected into 1L synthetic air. The mixture of these gaseous samples was evacuated at room temperature of 22°C through microdevices that were coated with 250 nmol of PFBHA. Then the derivatized adducts were collected with 50 μ L of DCM. 5 nmol of PFBHA-acetone- d_6 was added to each eluate as IR and analyzed in GC-MS. As shown in Figure 5.8, at a low flow rate from 2 to 10 mL/min the recovery was lower for these compounds. The recovery was increased higher than 95% for propanal- d_2 and butanal- d_2 when the flow rate exceeded 10 mL/min and remained the same until the flow rate of 80 mL/min. The maximum recovery for hexanal- d_{12} was 90%. The recovery increased gradually with an increasing flow rate of up to 20 mL/min for 2-butanone- d_5 and 2-pentanone- d_5 and reached a plateau in the flow rate range of 20 – 80 mL/min. The maximum recovery observed for 2-butanone- d_5 and 2-pentanone- d_5 were around 85% and 65%, respectively. The recovery decreased likewise after 80

mL/min flow rate. The degree of maximum recovery was compound-dependent. Shen et al. tested recovery at a sample flow rate of 10, 50, and 100 mL/min for carbonyl derivatization with PFBHA coated on Tenax TA in tube cartridges and observed reduced recovery with a higher flow rate of 100 mL/min [215]. Also, Ho et al. obtained decreased recovery as the flow rate increased from 20 to 100 mL/min flow rate with PFBHA coated on Tenax TA [218]. Our results followed a similar pattern for 20 – 120 mL/min flow rates. However, both groups did not test recovery below 10 mL/min flow rate even though lower flow rates are not desirable or favorable. The low recovery of carbonyl adducts at a flow rate below 10 mL/min in this work indicates the mass transfer rate limit region and above a flow rate of 80 mL/min flow rate for the reaction limit region.

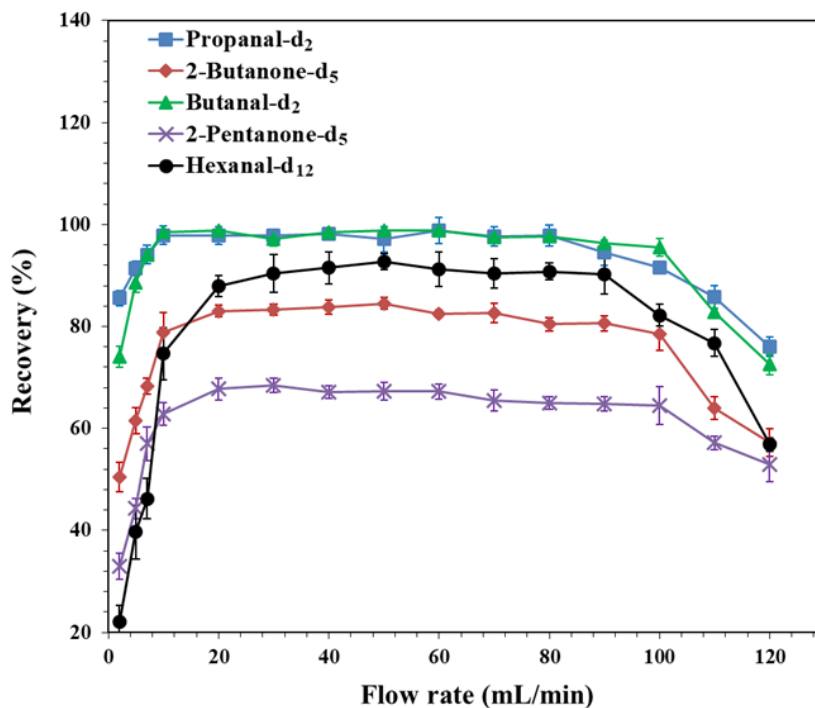


Figure 5.8: Recovery (%) for target deuterated carbonyls using 250 nmol PFBHA coated silica gel loaded (4.2 ± 0.2 mg) single-chamber microdevices at different flow rates (2 – 120 mL/min) extracted with 50 μ L of DCM.

5.3.1.3 Effect of PFBHA coating amount on recovery

The amount of PFBHA coated into the micropreconcentrator affects the reaction kinetics. The capture efficiency of carbonyl compounds is lower if the coating amount is insufficient for vapor-solid reaction at a specific flow rate [219]. However, coating too much PFBHA results in a higher amount of unreacted PFBHA in eluate and causes lower GC peak resolution with a higher baseline. Notably, a higher amount of PFBHA in the GC column could cause the shoulder peak or even unresolved PFBHA-acetaldehyde derivative, which elutes right after PFBHA, making acetaldehyde quantification inaccurate or even impossible [218]. Microdevices were coated with different amounts of PFBHA ranging from 64–500 nmol of PFBHA. The gaseous mixture of five tested deuterated

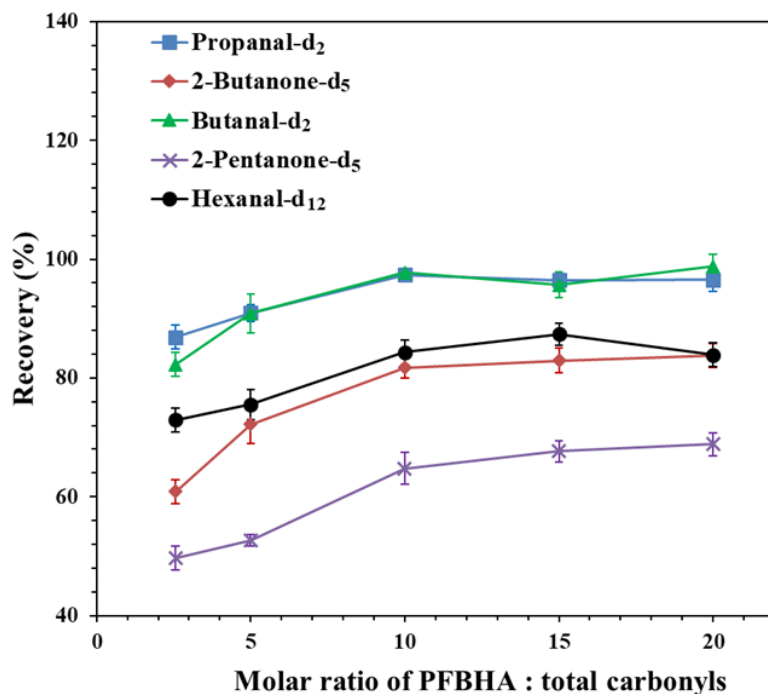


Figure 5.9: Recovery (%) for target deuterated carbonyls using different amounts (64 – 500 nmol) of PFBHA coated silica gel loaded (4.2 ± 0.2 mg) into single-chamber preconcentrator extracted with 50 μ L of DCM.

carbonyls (5 nmol of each in 1L synthetic air) were evacuated through microdevices with a 40 mL/min flow rate and eluted similarly described before. Figure 5.9 represents the effect of PFBHA coating on the recovery. The recovery was lower when the PFBHA coating amount was 64 nmol, and the corresponding molar ratio of PFBHA/total carbonyls was 2.56. The recovery was increased with a higher amount of PFBHA coating. When PFBHA/total carbonyl molar ratio was larger than 10 (coated with 250 nmol of PFBHA), more than 95% of propanal-d₂ and butanal-d₂ were recovered. Also, in this condition, 2-butanone-d₅ and 2-pentanone-d₅ recoveries were 82% and 65%, respectively. The lower recoveries of ketones are related to the lower reaction kinetics of ketones in comparison with aldehydes. The recovery was similar for aldehydes but increased slightly for ketones after PFBHA/total carbonyl ratio exceeded 10.

5.3.1.4 Humidity effect

The effect of moisture was investigated at different humidity levels. The microdevices were coated with 250 nmol of PFBHA. Predetermined amounts of water were injected into Tedlar bags containing 1L synthetic air to prepare 25%, 50%, 75%, and 100% relative humidity (RH). In those bags, 5 nmol of each tested deuterated carbonyl was injected and evaporated. The gaseous mixture of water vapor and carbonyls were passed through the microdevices at 40 mL/min, and derivatives were eluted by 50 μ L of DCM. Similarly, 5 nmol of PFBHA-acetone-d₆ was added as IR in there for quantitative analysis and analyzed by GC-MS. Figure 5.10 depicts the outcome of humidity on recovery. There was no noteworthy difference in recovery at different humidity levels. Also, compared with the dry VOCs mixture, recovery values were almost similar, consistent with those by Shen

and Ho [215, 220]. So, the environmental air containing relative humidity ranging from 65 – 95% does not affect recovery.

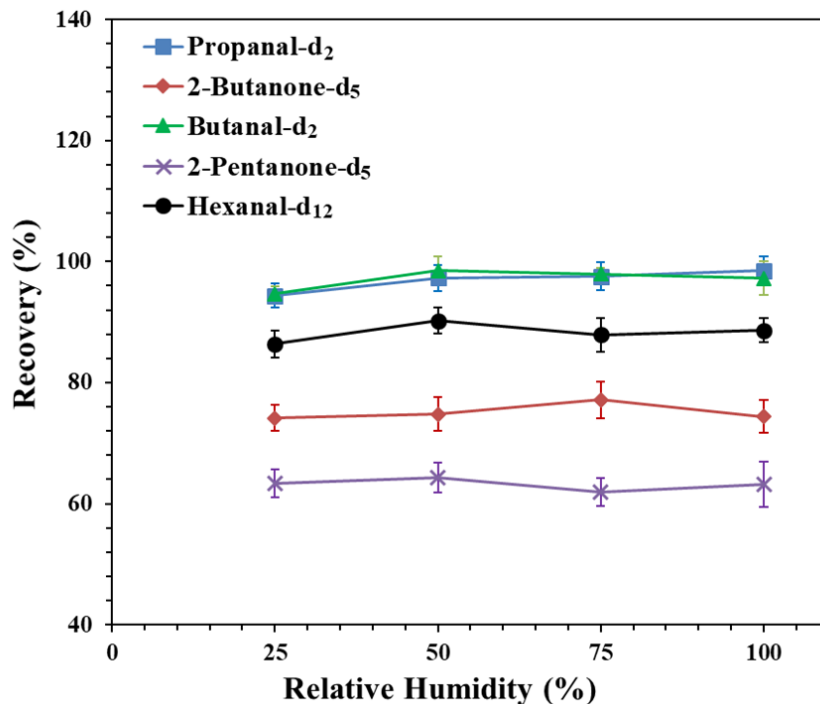


Figure 5.10: Recovery (%) for target deuterated carbonyls at different humidity levels (25 – 100 % RH) using 250 nmol of PFBHA-coated silica gel loaded with 4.2 ± 0.2 mg single-compartment microdevices extracted with 50 μ L of DCM.

5.3.1.5 Temperature effect on derivatization reaction

Temperature influences the equilibrium and reaction rate [221]. Both high and low temperatures may affect the reaction kinetics and sampling efficiency. Shen et al. tested PFBHA-coated Tenax TA sorbents to capture formaldehyde at three different temperatures (7, 25, and 40 °C) at a 50 mL/min flow rate [215]. They observed no significant differences ($p \leq 0.05$) among the recoveries of oxime products. Ho et al. achieved $\geq 92\%$ collection

efficiency of five tested carbonyl compounds using PFBHA-coated Tenax TA that sampling were carried out at room temperature (~22 °C). Also, Lomonaco et al. used PFBHA-coated Tenax GR sorbents to detect carbonyl compounds in exhaled breath and reported that derivatization temperature was non-significant for their experiments [222]. So, based on their studies, we did not expect a significant temperature effect on the recovery of carbonyls and thus ran our experiments at ambient temperature (~22 °C).

5.3.2 Characterization of Device B for capturing BTEX:

Device B contains one cavity that was loaded with carbopack X. The gaseous mixture of BTEX was passed through the microdevice at different flow rates, and a suitable solvent with an optimized amount was used to elute captured compounds. Cucciniello et al. observed higher than 97% of recovery of BTEX from charcoal in optimized conditions using DCM [41]. As carbopack X is a carbon-based adsorbent, we used this solvent to assess the performance of this device on trapping BTEX with the highest recovery.

5.3.2.1 Adsorption flow rate effect

These microdevices were evaluated to analyze BTEX compounds at different flow rates (20 – 80 mL/min). A slower flow rate takes a longer time for sampling. However, a higher evacuation flow rate affects adsorption capacity. When the residence time is shorter than the critical bed residence time, the adsorption capacity decreases and causes breakthroughs earlier [124]. BTEX mixture with 5 nmol of each compound was injected into 1L synthetic air. The gaseous mixture of BTEX flowed through device B at a room

temperature of 22 °C. The captured BTEX were eluted with the first and second 50 μL of DCM. After elution, 5 nmol of heptane- d_{16} was added as an IR to calculate the amounts in the eluate. From Figure 5.11, the recovery remained almost similar (relative standard deviation (RSD) < 5%) for these compounds at different flow rates. This result suggests that adsorption flow rates in these ranges did not impact recovery. Also, this outcome is consistent with our previous study of using carboxen-1000 adsorbent to capture BTEX [124]. Therefore, benzene and toluene were eluted more than 90% in the first 50 μL , and ethylbenzene and xylene amounts were higher than 85%. So, we used 50 μL of DCM for further experiments for this microdevice B.

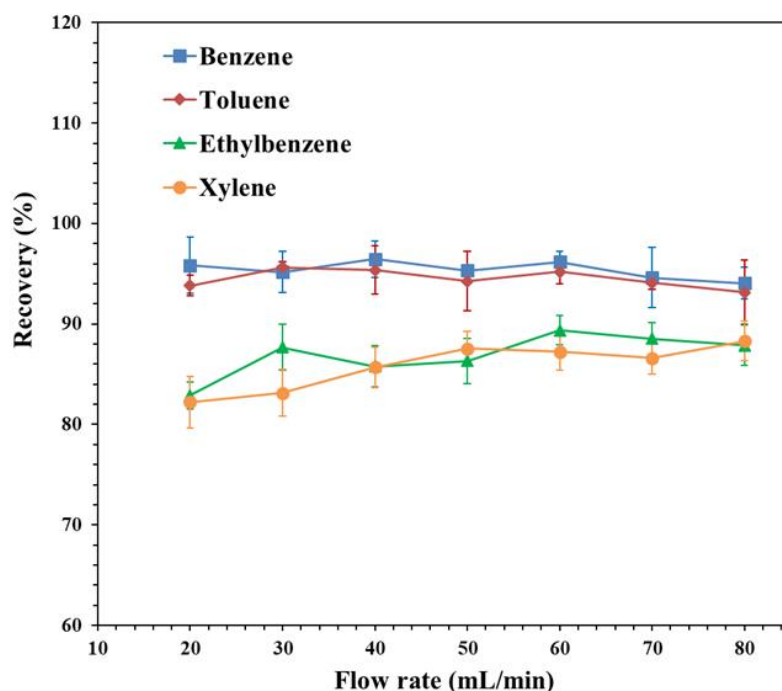


Figure 5.11: Recovery (%) for BTEX compounds at different flow rates (20 – 80 mL/min) using single-chamber microdevices loaded with 4 ± 0.2 mg of carbopack X adsorbent.

5.3.2.2 Humidity effect

Carbopack X is a hydrophobic carbon adsorbent barely affected by moisture [223, 224]. We studied the effect of moisture on capturing BTEX. Different amounts of water were injected into Tedlar bags containing 1L of synthetic air to prepare 25 – 100% RH, and 5 nmol of each compound of BTEX was added to it. Then gaseous mixture passed through device B at a 40 mL/min flow rate. After evacuation, the captured BTEX were collected with 50 μ L of DCM. Figure 5.12 represents the calculated recovery at different RH. There was no impact on recovery after increasing the moisture levels.

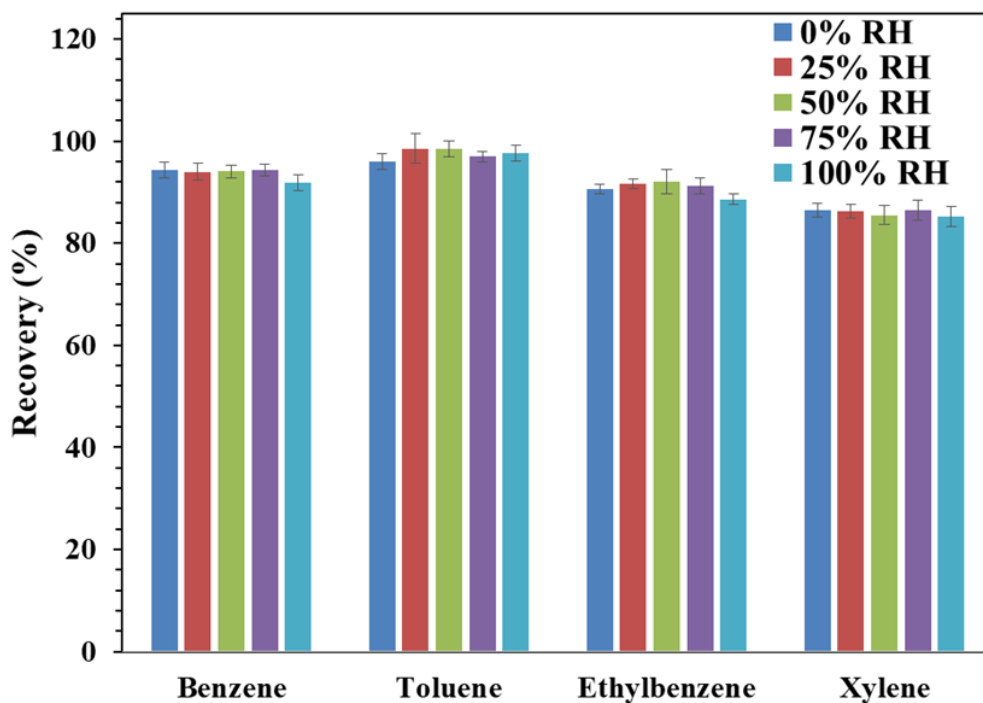


Figure 5.12: Recovery (%) for BTEX compounds at different humidity levels 25 – 100% Relative humidity (RH) using single-compartment microdevices loaded with 4 ± 0.2 mg of carbopack X adsorbent.

5.3.3 Characterization of device C with dual compartments for capturing both BTEX and carbonyls

Device C contains two compartments loaded with carbopack X and silica gel for capturing BTEX and carbonyls. Only silica gel was coated with PFBHA solution for capturing carbonyl compounds via oximation. Carbopack X adsorbent captures BTEX by physical adsorption. A gaseous mixture of standard BTEX and target carbonyls (formaldehyde, acetaldehyde, propanal, acetone, butanal, 2-butanone, pentanal, 2-pentanone, hexanal, 2-hexanone, and acrolein) was passed through the micropreconcentrator at the room temperature of 22 °C. The captured BTEX on carbopack X adsorbent and PFBHA-carbonyl adducts on silica gel were eluted by elution with DCM solvent. Heptane-d₁₆ was added to the eluate as an IR. The samples were analyzed by GC-MS in a single run. The peak area ratio of analyte to IR was used to calculate the amounts in the eluate compared with calibration equations presented in Table 5.1.

5.3.3.1 Calibration Curves and Limit of Detection

Calibration curves in Figure 5.1c & 5.1d and Table 5.1 for target compounds were prepared by taking three replicates of 5, 10, 15, 20 and 25 μM concentration levels where IR heptane-d₁₆ concentration was fixed (10 μM) in all samples. Figure 5.13 represents a GC-MS chromatogram of a standard sample (concentration 10 μM). Calibration equations were determined from ratios between peak areas of analyte and heptane-d₁₆ (Y-axis, $A_{\text{Analyte}}/A_{\text{IR}}$) versus the concentration ratio (X-axis, $C_{\text{Analyte}}/C_{\text{IR}}$). Table 5.1 presents the

calibration equation, coefficients of determination (R^2), and limit of detection (LOD). The linearity was observed in these compounds with the R^2 ranging from 0.9883 to 0.9986. The

Table 5.1: Retention time of analytes in GC-MS, calibration equation, coefficient of determination (R^2), limit of detection (LOD), and calculated (%) recovery of these VOCs.

Compound	Retention time (min)	Calibration equation	R^2	LOD ($\mu\text{g}/\text{m}^3$)	Recovery (%)
Benzene	2.55	$Y = 12.691 * X$	0.9949	0.11	88 ± 2
Heptane-d ₁₆	3.16				
Toluene	4.82	$Y = 22 * X$	0.9986	0.69	90 ± 2
Ethylbenzene	7.16	$Y = 39.931 * X$	0.9957	0.07	89 ± 2
Xylene	7.37, 7.87	$Y = 32.605 * X$	0.9945	0.07	88 ± 2
Formaldehyde-PFBHA	10.2	$Y = 80.479 * X$	0.9902	1.29	93 ± 2
PFBHA	12.15				
Acetaldehyde-PFBHA	12.71, 13.02	$Y = 36.475 * X$	0.9914	0.11	92 ± 2
Acetone-PFBHA	15.25	$Y = 71.828 * X$	0.9952	0.39	89 ± 1.5
Propanal-PFBHA	15.9, 16.18	$Y = 30.01 * X$	0.9943	0.08	84 ± 1.5
Acrolein-PFBHA	15.95, 16.4	$Y = 22.131 * X$	0.9948	0.07	84 ± 2.5
2-Butanone-PFBHA	17.73, 17.84	$Y = 221.6 * X$	0.9962	0.35	68 ± 2
Butanal-PFBHA	18.5, 18.69	$Y = 18.179 * X$	0.9907	0.22	73 ± 2
2-Pentanone-PFBHA	19.56, 19.74	$Y = 59.61 * X$	0.9938	0.18	50 ± 2
Pentanal-PFBHA	20.61, 20.74	$Y = 21.594 * X$	0.9955	0.06	68 ± 3
2-Hexanone-PFBHA	21.31, 21.51	$Y = 32.063 * X$	0.9883	0.03	53 ± 4
Hexanal-PFBHA	22.44, 22.54	$Y = 7.8091 * X$	0.9901	0.03	62 ± 3

X represents the concentration ratio of the analyte to IR heptane-d₁₆

Y represents the peak area of the analyte to IR heptane-d₁₆

LODs for analytes were calculated in accordance with International Union of Pure and Applied Chemistry (IUPAC) guidelines as three times the standard deviation of blank samples [222, 225]. A total of six blank samples were analyzed. The LOD values were 0.11, 0.69, 0.07, 0.07, 1.29, 0.11, 0.39, 0.08, 0.07, 0.35, 0.22, 0.18, 0.06, 0.03, 0.03 $\mu\text{g}/\text{m}^3$ for benzene, toluene, ethylbenzene, toluene, Formaldehyde, Acetaldehyde, Acetone, Propanal, Acrolein, 2-Butanone, Butanal, 2-Pentanone, Pentanal, 2-Hexanone, Hexanal adducts, respectively.

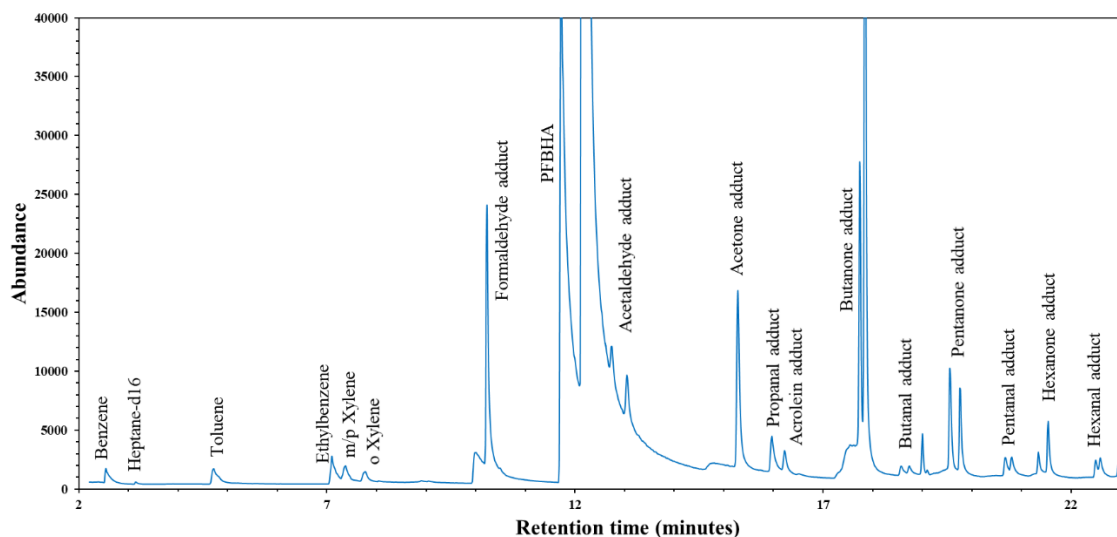


Figure 5.13: A GC-MS chromatogram of a standard sample containing 0.5 nmol of each compound (benzene, toluene, ethylbenzene, xylene, PFBHA adducts of formaldehyde, acetaldehyde, propanal, acetone, butanal, 2-butanone, pentanal, 2-pentanone, hexanal, 2-hexanone, acrolein) and 0.5 nmol of heptane-d₁₆ as an IR in a total volume of 50 μL methanol.

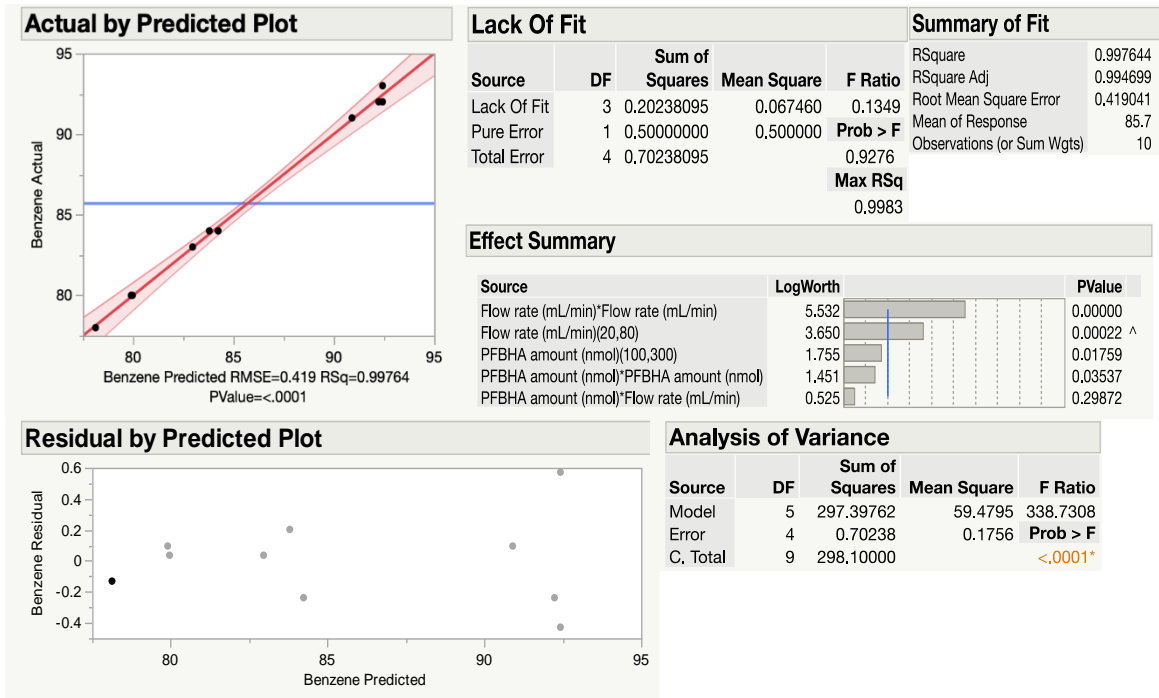
5.3.3.2 Optimization of operation conditions for device C

Since target VOCs are present in environmental air at trace levels, standard gaseous samples with low concentrations were prepared to characterize the device that requires less amount of solvent to elute captured compounds. The compartment dimensions and loaded sorbent amounts in micropreconcentrator C were different from devices A & B. Therefore, an experimental design was performed to obtain optimum conditions and compare them with single-compartment device performances. It is observed from the characterization of Devices A & B that the flow rate and PFBHA coating amount were important variables in determining device performance. As the objective was to maximize the recovery, a response surface design for two factors was designed. Response surface methodology (RSM) is used to obtain a large amount of information from a limited number of experiments by studying the main effects of factors and their interaction with the response [226]. The objective of using RSM is to optimize operating conditions with an increasing yield at a low cost or run fewer experiments [227]. We used a 10-run central composite design for two factors: sampling flow rate and PFBHA coating amount. Factor levels for flow rate were 20 & 80 mL/min and for PFBHA coating amounts were 100 and 300 nmol with two replicate center points (flow rate 50 mL/min and PFBHA amount 200 nmol). A total of 10 experiments were performed in random order. The recoveries of benzene and formaldehyde were the response variables. Results were analyzed by JMP[®]16 software.

A gaseous mixture of benzene and formaldehyde (0.25 nmol of each compound in 1L synthetic air) was formulated for this experiment. For the first run, a dual-compartment microdevice was prepared by coating the silica gel loaded into one compartment with 100 nmol of PFBHA and a 50 mL/min evacuation flow rate was used. 300 nmol of PFBHA

coating amount and 20 mL/min sampling flow rate were used for the second run. Similarly, a total of 10 runs were carried out varying the PFBHA coating amounts and sampling flow rate in random order. All experiments were performed at a room temperature of 22°C. 25 uL of DCM was used to elute captured compounds from sorbents in the microdevices. 0.5 nmol of heptane-d₁₆ was added to the eluted samples and analyzed by GC-MS. The peak area ratio of analyte to IR was used to calculate the recovery. The model was run to fit benzene and formaldehyde separately. A prediction profiler was performed for both variables and hit maximum desirability. The analysis results are presented in Figure 5.14 & 5.15. This model had two main effects, the interaction between the flow rate and PFBHA amount, and two quadratic effects. The model was significant ($p < 0.05$ for both benzene and formaldehyde) and there was very little unexplained variation (from analysis of variance results, the sum of squares for error was very small than the model). Most of the variation in benzene and formaldehyde recovery was explained by the model. The lack of fit test showed the model fit adequately ($p > 0.05$) to describe the relationship between factors and responses. R_{square} and $R_{\text{square,adj}}$ values were close to 1. The root-mean-square error was less than 0.5. The predicted plot and the residual plots did not show any unusual patterns or outliers. So, this model was used to find the optimum factors settings that provided the most desirable values for maximizing recovery. It was found that the desired flow rate should be around 50 mL/min and the PFBHA coating amount should be about 250 nmol (Figure 5.15). Therefore, these optimized conditions were used for further experiments for device C.

(a)



(b)

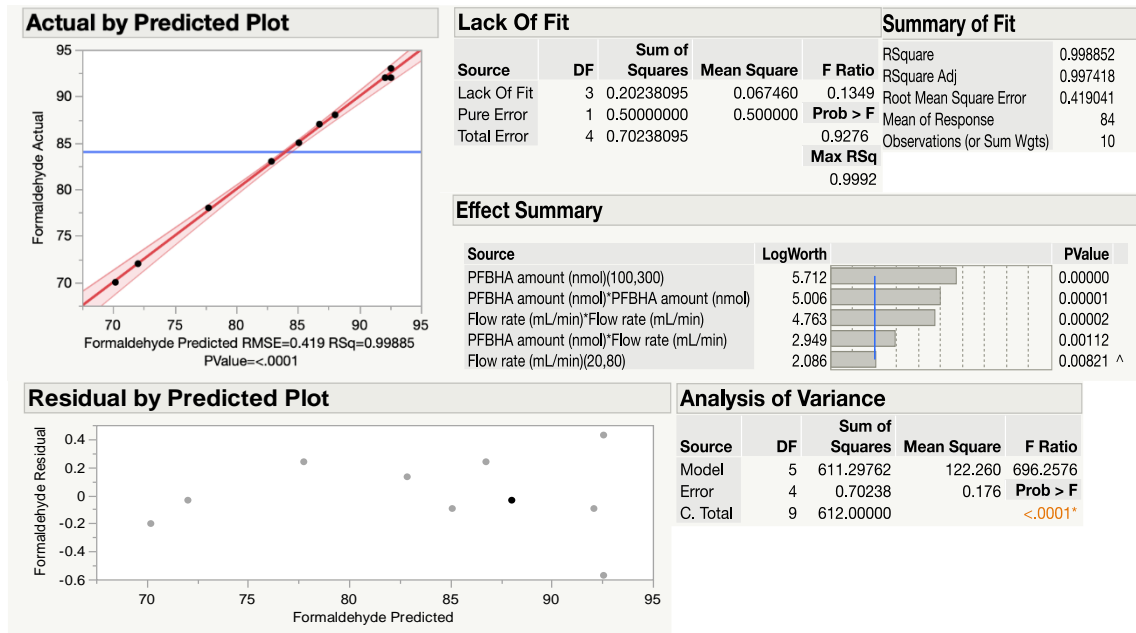


Figure 5.14: Actual by predicted plot, lack of fit, a summary of fit, analysis of variance, effect summary, and residual by the predicted plot for (a) benzene and (b) formaldehyde;

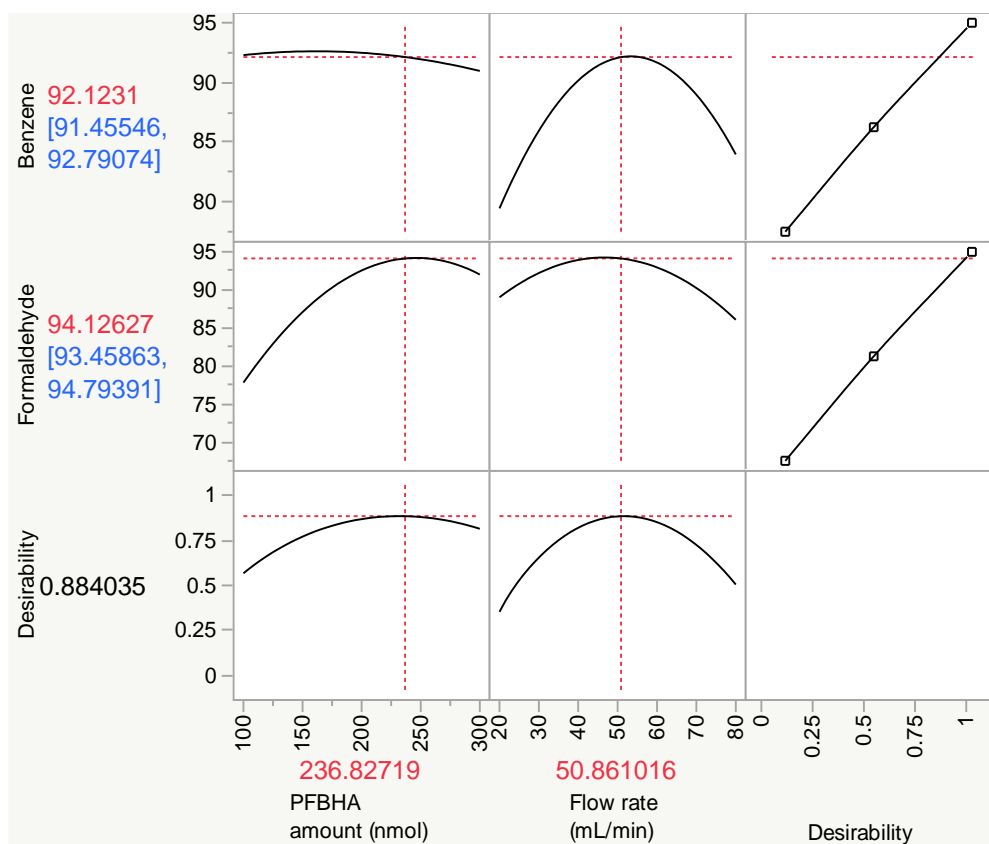


Figure 5.15: Prediction profiler to obtain maximum desirability.

5.3.3.3 Recovery (%) of analytes for device C

0.25 – 0.5 nmol of each gaseous BTEX and target carbonyls in 1L synthetic air were passed through 250 nmol PFBHA-coated dual-compartment microdevices at 50 mL/min at room temperature of 22°C. Then microdevices were eluted with the first and second 25 uL of DCM. 0.5 nmol of heptane-d₁₆ was added to the eluted samples and analyzed by GC-MS. The recovery was measured similarly. Table 5.1 represents the

calculated recovery of the BTEX and target carbonyls in the first 25 μL DCM eluate amounts. Most of the compounds were eluted in the first 25 μL of DCM, and less than 5% of these captured compounds were obtained in the second 25 μL . Thus 25 μL of DCM was used for the elution of device C for environmental air analysis.

5.3.3.4 Method Precision

Three replicate gaseous samples of BTEX and target carbonyls (0.25 nmol of each compound in 1L synthetic air) passed through 250 nmol of PFBHA-coated device C at a 50 mL/min flow rate. After elution with 25 μL of DCM and the addition of IR (0.5 nmol of heptane- d_{16}), the peak area ratios of analyte to IR of individual compounds in different samples were compared. The relative standard deviation (RSD, %) of the ratio for each compound was less than 4% which is the measure of method precision. In addition, six replicate gaseous samples containing 0.1 nmol of each compound of BTEX and target carbonyls in 1L synthetic air flowed at a 50 mL/min flow rate through device C coated with 250 nmol of PFBHA for three consecutive days to test reproducibility. The calculated recoveries of these compounds were in the same range presented in table 5.1 with a 4% maximum RSD. These results indicate that the steps of coating, sampling, elution and analysis are reproducible.

5.3.3.5 Effect of background contamination

A PFBHA-coated dual-compartment micropreconcentrator prepared within 24 hours without any active flow of environmental air was eluted with DCM and analyzed in

GC-MS. A few compounds were detected in a noticeable range, including toluene, formaldehyde, acetone, etc. because these compounds are ubiquitous in environmental air, even in lab air. However, the peak areas of these compounds were less than 10% of that of the detected same compounds from 5L environmental air samples. These results indicate that background contamination of the microdevices can be neglected because of relatively low levels of background VOC contamination.

5.3.3.6 Application for analyzing environmental air samples

The optimized experimental condition was applied for analyzing VOCs in the environmental air. 5L air samples were collected in Tedlar bags from a city roadside and Rubbertown area in Louisville, Kentucky. Rubbertown area is a neighborhood of chemical industries, a power plant, and a toxic landfill site. Figure 5.16 shows three sampling locations in the Rubbertown area (site 1, 2, and 3) and a Superfund site (Lee's Lane, site 4). Air samples were collected from the Rubbertown area during 1 – 2 pm on three different days (8/22/2022, 10/27/2022, and 12/10/2022). Also, air samples were collected from a city roadside at 10 am and 5 pm on the same day (9/14/2022). Triplet air samples were collected from each location. The weather conditions are mostly sunny, sunny, and cloudy days in the summer, autumn, and winter season, respectively. Detailed weather conditions are reported in Table 5.2. First, dual-compartment microdevices were prepared by coating silica gel with 250 nmol of PFBHA. The collected air samples were passed through devices at a 50 mL/min flow rate. The captured and derivatized VOCs were eluted with 25 μ L of DCM. 0.5 nmol of IR heptane-d₁₆ was added to all eluted samples and analyzed by GC-

MS. The amounts of VOCs in the eluted samples were determined using the peak area ratio of analyte to IR compared with calibration curves.

Table 5.2: Weather condition, season, ambient temperature (°C), UV index, wind speed, direction and humidity of the environmental air sample collection dates with sampling time.

Date	Sample collection time	Weather condition	Season	Ambient Temperature (°C)	UV index	Wind	Humidity
8/22/2022	1 PM	Mostly Sunny	Summer	28	10	SSW 4 mph	76%
9/14/2022	10 AM, 5 PM	Mostly Sunny	Autumn	25	7	NNE 4 mph	63%
10/27/2022	1 PM	Sunny	Autumn	10	4	NE 8 mph	69%
12/10/2022	1 PM	Cloudy	Winter	2	1	ENE 2 mph	53%

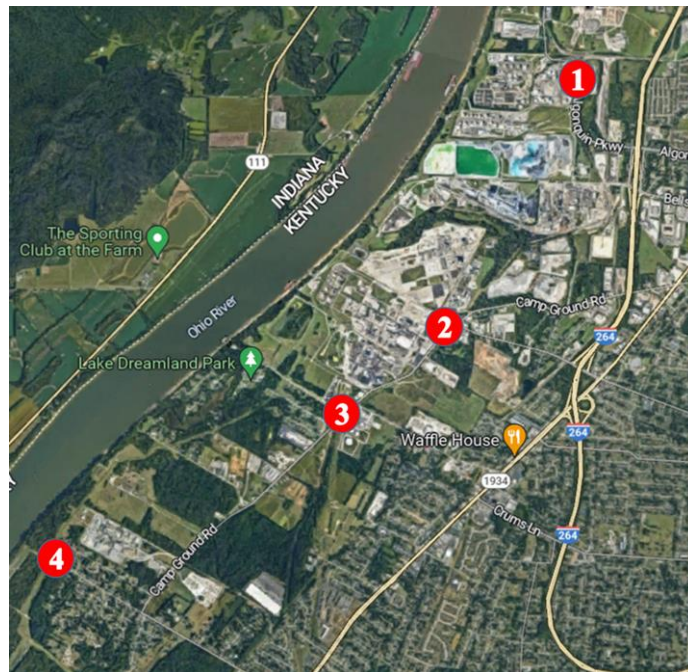


Figure 5.16: Air samples collection sites in the Rubbertown area, Louisville, Kentucky.

Figure 5.17 shows a typical chromatogram of well-separated peaks of detected BTEX and PFBHA-carbonyl derivatives. Table 5.3 represents the average amounts of target VOCs present in these locations on different dates. The total BTEX concentrations in sites 1, 2, 3, and 4 were 7.66, 6.88, 6.73, and 5.83 $\mu\text{g}/\text{m}^3$, respectively for a mostly sunny day in the summer season (08/22/2022). It is observed that the total BTEX amounts in sites 1, 2, and 3 were higher for that mostly sunny day with higher ambient temperature (28 °C) than other sampling days in the autumn and winter season. This could be the indication of higher evaporation of aromatic VOCs from their sources at a higher temperature. Mohammadi et al. obtained a higher amount of total BTEX in the summer season than in winter in their study of analyzing VOCs in Urmia, Iran [228]. However, Jiang et al. observed a higher concentration of BTEX in the winter season than in summer at a semi-urban site in Orleans, France from October 2010 to August 2011 [229]. In the summer season, the BTEX concentration could decrease due to photochemical degradation that breaks down BTEX into less harmful substances. So, it is noteworthy to mention that the levels of BTEX in the environment air can be affected by many factors, including weather conditions, wind speed, direction, humidity, traffic patterns, and industrial emissions.

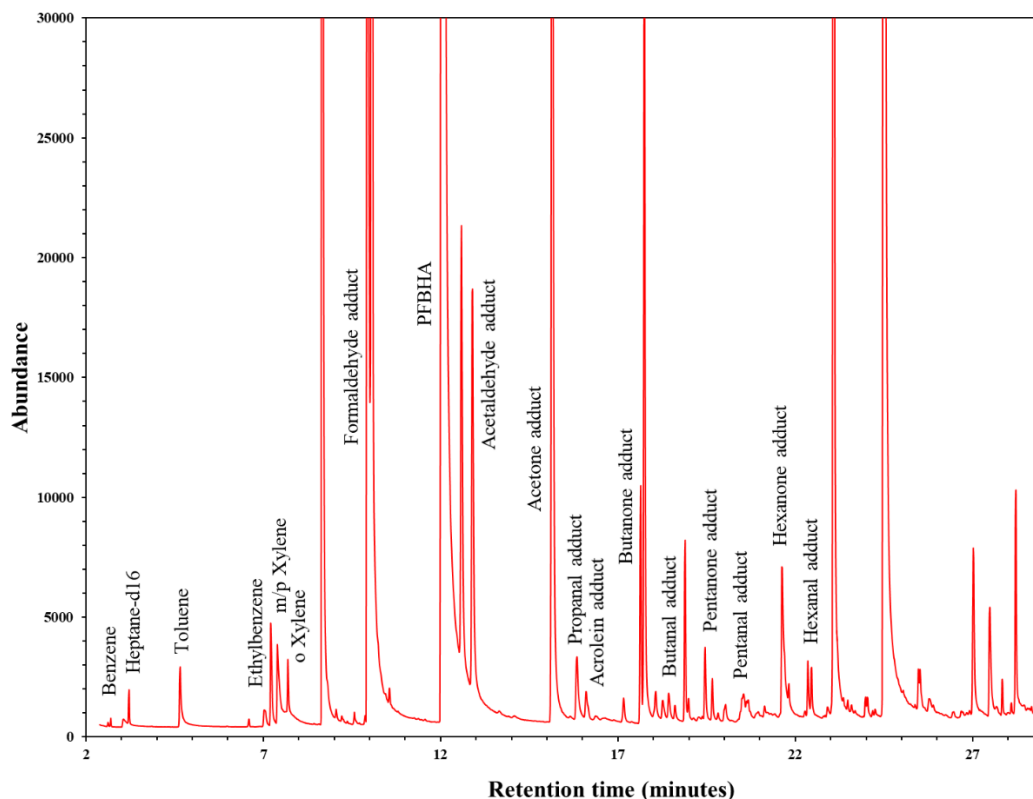


Figure 5.17: A GC-MS chromatogram of 5L environmental air sample analyzed by a dual-compartment microdevice loaded with carbopack X and 250 nmol PFBHA coated silica gel.

In comparison with BTEX, the amounts of carbonyls detected in these locations showed a complex relationship with weather conditions. The concentration of carbonyl compounds could increase in sunny weather due to photochemical reactions that occur in the atmosphere. Sunlight can promote the formation of ozone, which can react with other pollutants to form carbonyl VOCs. The three most abundant carbonyl compounds in these sites were formaldehyde, acetone and acetaldehyde. The concentrations of these compounds were at the same levels as previously measured levels although the

environmental air samples were collected from the same city, but different sites and dates [13]. The concentrations of acrolein are very similar to that of propanal. As a comparison of VOC levels among four different sites, site 1 contained higher amounts of BTEX than the other 3 sites which are consistent with the reported data [196]. There are several petrochemical storage tanks near site 1. Mukerjee et al. used a passive sampling technique to detect BTEX at similar locations in the Rubbertown area from September 12, 2017 to September 12, 2018. The values of BTEX in Table 5.3 were in these ranges of their reported concentrations [196]. Carbonyl compounds such as formaldehyde and acetaldehyde were higher in site 2. Site 4 is away from the chemical industries near sites 1 and 2, it showed less amount of VOCs than the other sites. But, site 4 presented a higher amount of toluene and formaldehyde on 10/27/2022 (autumn season, sunny day) which might be a reason for a wind flowing from the northeast direction (NE 8 mph). Also, BTEX and carbonyl amounts are presented in Table 5.3 for comparing VOC exposure on a roadside during rush hour and off-rush hour. It is obvious that the total VOCs amount ($46.79 \mu\text{g}/\text{m}^3$) during rush hour (5 pm) was higher due to car exhaust than the total VOCs amount ($34.48 \mu\text{g}/\text{m}^3$) at off-rush hour time (10 am) which was consistent with published results [202].

Table 5.3: Average concentrations ($\mu\text{g}/\text{m}^3$) (N=3) of BTEX and carbonyl compounds detected from 5L ambient air samples collected from four different locations in Rubbertown industrial areas on three different seasons and a city roadside at two different times on the same day, Louisville, Kentucky using the dual-compartment microdevices loaded with 2 mg carbopack X and 2.2 mg silica gel coated with 250 nmol of PFBHA.

Compound ($\mu\text{g}/\text{m}^3$)	Site 1			Site 2			Site 3			Site 4			Roadside	
	8/22 /202 2	10/2 7/20 22	12/1 0/20 22	8/22 /202 2	10/2 7/20 22	12/1 0/20 22	8/22 /202 2	10/2 7/20 22	12/1 0/20 22	8/22 /202 2	10/2 7/20 22	12/1 0/20 22	9/14 /202 2 (off - rush hou r)	9/14 /202 2 (rus h hou r)
Benzene	0.86	1.06	1.19	0.83	0.85	0.75	0.76	0.59	0.81	0.78	0.84	0.66	0.64	0.98
Toluene	3.86	3.16	3.52	3.45	2.99	2.93	3.27	3.31	3.43	2.75	3.08	2.80	3.22	4.05
Ethylbenzene	1.15	0.94	0.91	1.08	1.22	0.92	1.11	0.99	0.94	1.08	1.19	1.11	1.24	1.66
Xylene	1.79	1.42	1.70	1.52	1.55	1.49	1.59	1.31	1.27	1.22	1.30	1.29	1.09	1.40
Formaldehyde	12.0	11.7	13.2	13.0	13.8	12.2	12.6	11.6	10.2	11.2	14.2	10.6	7.90	11.3
Acetaldehyde	3.79	3.50	3.54	3.60	4.21	3.02	3.40	3.27	3.50	3.31	3.46	3.74	3.20	4.90
Acetone	6.38	5.41	4.88	5.43	6.90	5.58	5.64	5.52	6.13	6.53	6.18	6.16	5.55	6.97
Propanal	0.91	0.81	0.97	0.86	1.02	0.63	0.86	0.83	0.92	0.84	0.94	0.89	0.70	0.96
Acrolein	0.81	0.88	0.93	0.87	0.88	0.87	0.76	0.75	0.81	0.85	0.98	0.81	0.71	0.96
2-butanone	2.75	2.66	2.70	3.06	2.88	2.88	3.11	3.08	3.24	2.92	3.06	3.17	2.47	3.31
Butanal	4.27	5.09	5.34	4.40	5.06	4.91	3.95	4.26	4.40	4.91	3.84	4.62	4.13	5.30
2-pentanone	0.85	0.86	0.95	0.92	0.85	0.84	0.86	0.84	0.85	0.79	0.86	0.90	0.65	0.80
Pentanal	0.55	0.46	0.53	0.56	0.56	0.46	0.45	0.46	0.56	0.51	0.57	0.47	0.41	0.54
2-hexanone	0.28	0.28	0.18	0.23	0.21	0.24	0.15	0.21	0.25	0.23	0.26	0.19	0.18	0.26
Hexanal	3.15	3.15	3.08	2.96	3.16	3.22	3.40	3.12	3.31	3.37	3.28	3.04	2.38	3.44

5.4 Conclusion

A simple, unique, and rapid technique has been developed to detect BTEX and carbonyls together using a dual-compartment microfluidic device loaded with carbopack X and PFBHA-coated silica gel. The captured and derivatized compounds were analyzed in a single run by GC-MS. The optimized conditions for carbonyl derivatization reaction in a microdevice were explored. Evacuation flow rate, PFBHA coating amount, and solvent amount affect the capture efficiencies of these compounds. Similarly, favorable conditions for capturing BTEX in microdevices loaded with carbopack X were examined. This dual-compartment microdevice demonstrated good reproducibility, reusability, and stability. This method was applied to detect BTEX and carbonyls in the environmental air. These results are very promising for future applications to monitor VOCs in environmental air, exhaled breath, and e-cigarette aerosols.

CHAPTER VI

CONCLUSION AND FUTURE WORK

This dissertation has described three research projects relating to the development of microsensor array and micropreconcentrators for detection and quantification of airborne toxic VOCs.

6.1 Conclusion

Thiol-functionalized gold nanoparticle-based sensing materials provide a new opportunity to develop a gas sensor array with enhanced sensitivity and selectivity. The device is portable, inexpensive and convenient to use for real-time analysis. In this dissertation, a sensor array was fabricated on a silicon substrate to accommodate and test four sensing materials simultaneously. MEMS technology was used to fabricate the sensor array on a silicon chip which affords lower fabrication cost, less usage of materials and faster sensing response. Thiol-functionalized Au MPCs were characterized to develop a sensor array for aromatic and chlorinated VOC detection. Different alkali metal ions such as Li, Na and K were integrated onto the surface of Au MPCs to explore the cation- π interaction for sensing aromatic VOCs. Several aromatic and non-aromatic VOCs were exposed to these sensors for testing selectivity and sensitivity toward electron-rich aromatic compounds. Also, Cs-linked Au MPCs were tested for gaseous chlorinated compounds

because of the coordination between Cs^+ and Cl^- . Cs^+ sensor response towards gaseous chlorinated, polar, and non-polar compounds was analyzed to understand the sensing mechanism. All these sensors showed linear and reversible responses with increasing concentrations of analytes. The interference of these sensors with humidity was investigated and suggested to use of a sorbent tube or a preconcentrator to eliminate moisture and to trap target compounds and thermally desorbed to produce a moisture-free concentrated VOCs mixture.

A micropreconcentrator (μPC) was designed and fabricated using microfabrication techniques. This device was developed to capture benzene, toluene, ethylbenzene, xylene, and trichloroethylene with Carboxen 1000 adsorbent. The adsorption and thermal desorption flow rates and desorption temperature were optimized to obtain the maximum recovery of the analytes from the μPC . The μPC was integrated with solid-phase microextraction (SPME) to increase the sensitivity and improve the detection limit for the detector of GC-MS. The combination of μPC with SPME was applied for analyzing airborne VOCs using GC-MS. This microdevice would facilitate to increase the sensitivity of our developed sensor array containing metalated carboxylate-linked Au MPCs.

Further, a dual-compartment micropreconcentrator has been developed to preconcentrate and detect a wide range of VOCs using a single analysis with GC-MS. Currently, there is no analytical sampling technique to analyze BTEX and carbonyls together which promotes quick detection of a large group of compounds. Carboxen X and silica gel were loaded into the two separate compartments of the μPC . Physical adsorption of BTEX was carried out on the surface of carboxen X and derivatization of carbonyls was performed via oximation reacting with O-(2,3,4,5,6-pentafluorobenzyl)

hydroxylamine (PFBHA) reagent that was coated on the surface of silica gel. Dichloromethane solvent was used to elute all captured compounds from the μ PC. The reaction parameters for carbonyl derivatization such as sampling flow rate, PFBHA coating amount, and humidity effect were investigated using single-compartment μ PC loaded with silica gel. Similarly, the effects of adsorption flow rate and humidity to capture BTEX were examined for carbopack X loaded single-compartment μ PC. Finally, the sampling flow rate, PFBHA coating amount and solvent elution amount were optimized for dual-compartment μ PC to obtain maximum recovery. The optimized conditions were applied for environmental air analysis using a 5L air sample. These results are very promising for future utilizations to detect a wide range of VOCs for biomedical applications and hazardous gas monitoring.

6.2 Future work and recommendation

This dissertation identifies the following five potential areas for further investigation to develop a portable device for real-time analysis of airborne VOCs. This includes:

1. Design a sensor array chip that could accommodate 8 sensing materials and perform simultaneous testing. 8 different sensors with different selectivity could be used for real-time analysis of target airborne VOCs including BTEX, TCE and formaldehyde. The application of machine learning or principle component analysis (PCA) can distinguish analytes of interest using sensor response patterns.

2. Integration of the micropreconcentrator with the existing sensor array can be utilized for detection of trace target VOCs. The thermally desorbed sample from the micropreconcentrator can be exposed to a sensor array containing metalated Au MPCs because this sample does not contain any moisture. This approach not only prevents the interferences coming from humidity but also screens and increases the concentration of target analytes.
3. Different sorbents can be investigated to select a suitable one for target VOCs. There are several polymer-based porous sorbents such as Hayesep® which can be conveniently used for a wide range of compounds and thermally desorbed at a lower temperature (below 200 °C).
4. The dual-compartment micropreconcentrator can be used for frequent monitoring of airborne VOCs in particular regions such as industrial areas, airports, gas stations, etc. in different weather conditions, and seasons. As indoor air contains higher amounts of VOCs, this device can be used for indoor air quality assessment too.
5. The dual-compartment μ PC can be integrated with a portable detector such as a photo-ionization detector for field application. This will provide on-site sampling and analysis by saving time on sample collection.

REFERENCES

- [1] G.D. Thurston, Outdoor air pollution: sources, atmospheric transport, and human health effects, *International Encyclopedia of Public Health*, (2008) 700-712.
- [2] Y. Liu, M. Shao, L. Fu, S. Lu, L. Zeng, D. Tang, Source profiles of volatile organic compounds (VOCs) measured in China: Part I, *Atmospheric Environment*, 42 (2008) 6247-6260.
- [3] N.S. Chary, A.R. Fernandez-Alba, Determination of volatile organic compounds in drinking and environmental waters, *TrAC Trends in Analytical Chemistry*, 32 (2012) 60-75.
- [4] T. Cheng, Chemical evaluation of electronic cigarettes, *Tobacco control*, 23 (2014) ii11-ii17.
- [5] A. Srivastava, D. Majumdar, Monitoring and reporting VOCs in ambient air, *Air quality monitoring, assessment management*, 1 (2011).
- [6] A. Mirzaei, S. Leonardi, G. Neri, Detection of hazardous volatile organic compounds (VOCs) by metal oxide nanostructures-based gas sensors: A review, *Ceramics international*, 42 (2016) 15119-15141.
- [7] P. Wolkoff, G.D. Nielsen, Organic compounds in indoor air—their relevance for perceived indoor air quality?, *Atmospheric Environment*, 35 (2001) 4407-4417.

- [8] C.-J. Lu, W.H. Steinecker, W.-C. Tian, M.C. Oborny, J.M. Nichols, M. Agah, J.A. Potkay, H.K. Chan, J. Driscoll, R.D. Sacks, First-generation hybrid MEMS gas chromatograph, *Lab Chip*, 5 (2005) 1123-1131.
- [9] Q. Zhong, W.H. Steinecker, E.T. Zellers, Characterization of a high-performance portable GC with a chemiresistor array detector, *Analyst*, 134 (2009) 283-293.
- [10] V. Soni, P. Singh, V. Shree, V. Goel, Effects of VOCs on human health, *Air pollution control*, (2018) 119-142.
- [11] M. Kampa, E. Castanas, Human health effects of air pollution, *Environmental pollution*, 151 (2008) 362-367.
- [12] M. Miri, M.R.A. Shendi, H.R. Ghaffari, H.E. Aval, E. Ahmadi, E. Taban, A. Gholizadeh, M.Y. Aval, A. Mohammadi, A. Azari, Investigation of outdoor BTEX: Concentration, variations, sources, spatial distribution, and risk assessment, *Chemosphere*, 163 (2016) 601-609.
- [13] J.C. Robinson, D.G. Paxman, S.M. Rappaport, Implications of OSHA's reliance on TLVs in developing the air contaminants standard, *American journal of industrial medicine*, 19 (1991) 3-13.
- [14] M.T. Smith, Advances in understanding benzene health effects and susceptibility, *Annual review of public health*, 31 (2010) 133-148.
- [15] V. Benignus, Health effects of toluene: a review, *Neurotoxicology*, 2 (1981) 567-588.

- [16] C. Gericke, B. Hanke, G. Beckmann, M.M. Baltes, K.-P. Köhl, D. Neubert, Multicenter field trial on possible health effects of toluene: III. Evaluation of effects after long-term exposure, *Toxicology*, 168 (2001) 185-209.
- [17] A.L. Bolden, C.F. Kwiatkowski, T. Colborn, New look at BTEX: are ambient levels a problem?, *Environmental science technology*, 49 (2015) 5261-5276.
- [18] M. Banton, J. Bus, J. Collins, E. Delzell, H.-P. Gelbke, J. Kester, M. Moore, R. Waites, S. Sarang, Evaluation of potential health effects associated with occupational and environmental exposure to styrene—an update, *Journal of Toxicology Environmental Health, Part B*, 22 (2019) 1-130.
- [19] K. Matsumura, M. Opiekun, H. Oka, A. Vachani, S.M. Albelda, K. Yamazaki, G.K. Beauchamp, Urinary volatile compounds as biomarkers for lung cancer: a proof of principle study using odor signatures in mouse models of lung cancer, *PloS one*, 5 (2010) e8819.
- [20] Z. Wang, C. Wang, Is breath acetone a biomarker of diabetes? A historical review on breath acetone measurements, *Journal of breath research*, 7 (2013) 037109.
- [21] H.P. Chan, C. Lewis, P.S. Thomas, Exhaled breath analysis: novel approach for early detection of lung cancer, *Lung Cancer*, 63 (2009) 164-168.
- [22] Z. Zhang, G. Li, A review of advances and new developments in the analysis of biological volatile organic compounds, *Microchemical journal*, 95 (2010) 127-139.

- [23] L. Mølhave, G. Clausen, B. Berglund, J. De Ceaurriz, A. Kettrup, T. Lindvall, M. Maroni, A. Pickering, U. Risse, H. Rothweiler, Total volatile organic compounds (TVOC) in indoor air quality investigations, *Indoor Air*, 7 (1997) 225-240.
- [24] A.T. Hodgson, A review and a limited comparison of methods for measuring total volatile organic compounds in indoor air, *Indoor Air*, 5 (1995) 247-257.
- [25] A. Kot-Wasik, B. Zabiegała, M. Urbanowicz, E. Dominiak, A. Wasik, J. Namieśnik, Advances in passive sampling in environmental studies, *Analytica chimica acta*, 602 (2007) 141-163.
- [26] T. Górecki, J. Namieśnik, Passive sampling, *TrAC Trends in Analytical Chemistry*, 21 (2002) 276-291.
- [27] S. Seethapathy, T. Gorecki, X. Li, Passive sampling in environmental analysis, *J Chromatogr A*, 1184 (2008) 234-253.
- [28] J. Wang, Gas Chromatographic Microsystems for Airborne and Aqueous Volatile Organic Compound Determinations, in, 2019.
- [29] G. Ouyang, J. Pawliszyn, Configurations and calibration methods for passive sampling techniques, *J Chromatogr A*, 1168 (2007) 226-235.
- [30] M.R. Ras, F. Borrull, R.M. Marcé, Sampling and preconcentration techniques for determination of volatile organic compounds in air samples, *TrAC Trends in Analytical Chemistry*, 28 (2009) 347-361.

- [31] J. Bang, D.-W. You, Y. Jang, J.-S. Oh, K.-W. Jung, A carbon nanotube sponge as an adsorbent for vapor preconcentration of aromatic volatile organic compounds, *J Chromatogr A*, 1605 (2019) 460363.
- [32] C.S.L. Koh, H.K. Lee, X. Han, H.Y.F. Sim, X.Y. Ling, Plasmonic nose: integrating the MOF-enabled molecular preconcentration effect with a plasmonic array for recognition of molecular-level volatile organic compounds, *Chemical Communications*, 54 (2018) 2546-2549.
- [33] B. Alfeeli, L.T. Taylor, M. Agah, Evaluation of Tenax TA thin films as adsorbent material for micro preconcentration applications, *Microchemical Journal*, 95 (2010) 259-267.
- [34] J.E. Szulejko, K.-H. Kim, Derivatization techniques for determination of carbonyls in air, *TrAC Trends in Analytical Chemistry*, 64 (2015) 29-41.
- [35] A. Lattuati-Derieux, O. Ramalho, C. Egasse, S. Thao-Heu, A.-L. Dupont, Evaluation of solid-phase microextraction on-fiber derivatization for the analysis of paper degradation compounds, *E-Preservation Science*, 12 (2015) 38-49.
- [36] Y. Chen, Q. Li, Z. Xie, X.-a. Fu, Characterization of DNPH-coated microreactor chip for analysis of trace carbonyls with application for breath analysis, *Journal of Chromatography B*, 1106 (2019) 58-63.
- [37] C. Jia, J. Foran, Air toxics concentrations, source identification, and health risks: An air pollution hot spot in southwest Memphis, TN, *Atmospheric environment*, 81 (2013) 112-116.

- [38] J. Zapata, L. Mateo-Vivaracho, J. Cacho, V. Ferreira, Comparison of extraction techniques and mass spectrometric ionization modes in the analysis of wine volatile carbonyls, *Analytica Chimica Acta*, 660 (2010) 197-205.
- [39] C. Deng, X. Zhang, A simple, rapid and sensitive method for determination of aldehydes in human blood by gas chromatography/mass spectrometry and solid-phase microextraction with on-fiber derivatization, *Rapid communications in mass spectrometry*, 18 (2004) 1715-1720.
- [40] C. Tessini, N. Müller, C. Mardones, D. Meier, A. Berg, D. von Baer, Chromatographic approaches for determination of low-molecular mass aldehydes in bio-oil, *J Chromatogr A*, 1219 (2012) 154-160.
- [41] R. Cucciniello, A. Proto, F. Rossi, N. Marchettini, O. Motta, An improved method for BTEX extraction from charcoal, *Analytical Methods*, 7 (2015) 4811-4815.
- [42] P. Bruno, M. Caputi, M. Caselli, G. De Gennaro, M. De Rienzo, Reliability of a BTEX radial diffusive sampler for thermal desorption: field measurements, *Atmospheric Environment*, 39 (2005) 1347-1355.
- [43] G. Ouyang, J. Pawliszyn, SPME in environmental analysis, *Anal bioanal chem*, 386 (2006) 1059-1073.
- [44] G. Ouyang, J. Pawliszyn, Recent developments in SPME for on-site analysis and monitoring, *TrAC Trends in Analytical Chemistry*, 25 (2006) 692-703.

- [45] A. Spietelun, M. Pilarczyk, A. Kloskowski, J. Namieśnik, Current trends in solid-phase microextraction (SPME) fibre coatings, *Chemical Society Reviews*, 39 (2010) 4524-4537.
- [46] J. Pawliszyn, Theory of solid-phase microextraction, in: *Handbook of solid phase microextraction*, Elsevier, 2012, pp. 13-59.
- [47] J. Pawliszyn, *Solid phase microextraction: theory and practice*, John Wiley & Sons, 1997.
- [48] M. de Fatima Alpendurada, Solid-phase microextraction: a promising technique for sample preparation in environmental analysis, *J Chromatogr A*, 889 (2000) 3-14.
- [49] B.A. Weggler, B. Gruber, P. Teehan, R. Jaramillo, F.L. Dorman, Inlets and sampling, in: *Separation science and technology*, Elsevier, 2020, pp. 141-203.
- [50] C.-H. Wu, C.-T. Feng, Y.-S. Lo, T.-Y. Lin, J.-G. Lo, Determination of volatile organic compounds in workplace air by multisorbent adsorption/thermal desorption-GC/MS, *Chemosphere*, 56 (2004) 71-80.
- [51] C. Dass, *Fundamentals of contemporary mass spectrometry*, John Wiley & Sons, 2007.
- [52] K. Dettmer, P.A. Aronov, B.D. Hammock, Mass spectrometry-based metabolomics, *Mass spectrometry reviews*, 26 (2007) 51-78.
- [53] K. Badjagbo, S. Sauv e, S. Moore, Real-time continuous monitoring methods for airborne VOCs, *TrAC Trends in Analytical Chemistry*, 26 (2007) 931-940.

- [54] A. Ribes, G. Carrera, E. Gallego, X. Roca, M.J. Berenguer, X. Guardino, Development and validation of a method for air-quality and nuisance odors monitoring of volatile organic compounds using multi-sorbent adsorption and gas chromatography/mass spectrometry thermal desorption system, *J Chromatogr A*, 1140 (2007) 44-55.
- [55] B.M. Lerner, J.B. Gilman, K.C. Aikin, E.L. Atlas, P.D. Goldan, M. Graus, R. Hendershot, G.A. Isaacman-VanWertz, A. Koss, W.C. Kuster, An improved, automated whole air sampler and gas chromatography mass spectrometry analysis system for volatile organic compounds in the atmosphere, *Atmospheric Measurement Techniques*, 10 (2017) 291-313.
- [56] G. Lubec, L. Afjehi-Sadat, Limitations and pitfalls in protein identification by mass spectrometry, *Chemical reviews*, 107 (2007) 3568-3584.
- [57] J. Lee, J. Lee, S.-H. Lim, Micro gas preconcentrator using metal organic framework embedded metal foam for detection of low-concentration volatile organic compounds, *Journal of Hazardous Materials*, 392 (2020) 122145.
- [58] T. Seiyama, *Chemical Sensor Technology: Volume 2*, Elsevier, 2013.
- [59] S. Afreen, N. Talreja, M. Ashfaq, D. Chauhan, Carbon nanostructure-based sensor: a promising tools for monitoring crops, in: *Nanotechnology-Based Sustainable Alternatives for the Management of Plant Diseases*, Elsevier, 2022, pp. 287-300.
- [60] V. Schroeder, S. Savagatrup, M. He, S. Lin, T.M. Swager, Carbon nanotube chemical sensors, *Chemical reviews*, 119 (2018) 599-663.

- [61] S. Abdul, T. Judit, F. Ilona, M. Nikoletta, Chapter 16-Functional thin films and nanostructures for sensors. Fundamentals of Nanoparticles. Barhoum A, Hamdy Makhoulouf AS, Eds, in, Elsevier, 2018.
- [62] J.R. Stetter, W.R. Penrose, Understanding chemical sensors and chemical sensor arrays (electronic noses): Past, present, and future, *Sensors update*, 10 (2002) 189-229.
- [63] K.J. Albert, N.S. Lewis, C.L. Schauer, G.A. Sotzing, S.E. Stitzel, T.P. Vaid, D.R. Walt, Cross-reactive chemical sensor arrays, *Chemical reviews*, 100 (2000) 2595-2626.
- [64] M. Penza, F. Antolini, M.V. Antisari, Carbon nanotubes as SAW chemical sensors materials, *Sensors & Actuators B: Chemical*, 100 (2004) 47-59.
- [65] J. Zhang, A. Boyd, A. Tselev, M. Paranjape, P. Barbara, Mechanism of NO₂ detection in carbon nanotube field effect transistor chemical sensors, *Applied Physics Letters*, 88 (2006) 123112.
- [66] J.W. Fergus, Sensing mechanism of non-equilibrium solid-electrolyte-based chemical sensors, *Journal of Solid State Electrochemistry*, 15 (2011) 971-984.
- [67] D.K. Aswal, S.K. Gupta, Science and technology of chemiresistor gas sensors, Nova Publishers, 2007.
- [68] R.K. Paul, S. Badhulika, N.M. Saucedo, A. Mulchandani, Graphene nanomesh as highly sensitive chemiresistor gas sensor, *Anal Chem*, 84 (2012) 8171-8178.
- [69] S. Pandey, Highly sensitive and selective chemiresistor gas/vapor sensors based on polyaniline nanocomposite: A comprehensive review, *Journal of Science: Advanced Materials Devices*, 1 (2016) 431-453.

- [70] S. Srinives, T. Sarkar, R. Hernandez, A. Mulchandani, A miniature chemiresistor sensor for carbon dioxide, *Analytica chimica acta*, 874 (2015) 54-58.
- [71] M.A. Carpenter, S. Mathur, A. Kolmakov, *Metal oxide nanomaterials for chemical sensors*, Springer Science & Business Media, 2012.
- [72] P.-C. Chen, G. Shen, C. Zhou, Chemical sensors and electronic noses based on 1-D metal oxide nanostructures, *IEEE Transactions on Nanotechnology*, 7 (2008) 668-682.
- [73] T.A. Saleh, G. Fadillah, Recent trends in the design of chemical sensors based on graphene–metal oxide nanocomposites for the analysis of toxic species and biomolecules, *TrAC Trends in Analytical Chemistry*, 120 (2019) 115660.
- [74] S. Lee, J. Oh, D. Kim, Y. Piao, A sensitive electrochemical sensor using an iron oxide/graphene composite for the simultaneous detection of heavy metal ions, *Talanta*, 160 (2016) 528-536.
- [75] J.M. George, A. Antony, B. Mathew, Metal oxide nanoparticles in electrochemical sensing and biosensing: a review, *Microchimica Acta*, 185 (2018) 1-26.
- [76] J. Zhang, H. Lu, C. Yan, Z. Yang, G. Zhu, J. Gao, F. Yin, C. Wang, Fabrication of conductive graphene oxide-WO₃ composite nanofibers by electrospinning and their enhanced acetone gas sensing properties, *Sensors and Actuators B: Chemical*, 264 (2018) 128-138.
- [77] J. Huang, S. Virji, B.H. Weiller, R.B. Kaner, Nanostructured polyaniline sensors, *Chemistry–A European Journal*, 10 (2004) 1314-1319.

- [78] J. Liu, Y. Lin, L. Liang, J.A. Voigt, D.L. Huber, Z.R. Tian, E. Coker, B. Mckenzie, M.J. Mcdermott, Templateless assembly of molecularly aligned conductive polymer nanowires: a new approach for oriented nanostructures, *Chemistry—A European Journal*, 9 (2003) 604-611.
- [79] J. Chen, Y. Zhu, J. Huang, J. Zhang, D. Pan, J. Zhou, J.E. Ryu, A. Umar, Z. Guo, Advances in responsively conductive polymer composites and sensing applications, *Polymer Reviews*, 61 (2021) 157-193.
- [80] J. Janata, M. Josowicz, Conducting polymers in electronic chemical sensors, *Nature materials*, 2 (2003) 19-24.
- [81] H. Bai, G. Shi, Gas sensors based on conducting polymers, *Sensors*, 7 (2007) 267-307.
- [82] H. Yoon, J. Jang, Conducting-polymer nanomaterials for high-performance sensor applications: issues and challenges, *Advanced Functional Materials*, 19 (2009) 1567-1576.
- [83] F. Garnier, Functionalized conducting polymers—Towards intelligent materials, *Angewandte Chemie*, 101 (1989) 529-533.
- [84] K. Białas, D. Moschou, F. Marken, P. Estrela, Electrochemical sensors based on metal nanoparticles with biocatalytic activity, *Microchimica Acta*, 189 (2022) 172.
- [85] F.J. Ibanez, F.P. Zamborini, Chemiresistive sensing with chemically modified metal and alloy nanoparticles, *Small*, 8 (2012) 174-202.

- [86] G. Korotcenkov, V. Brinzari, B.K. Cho, Conductometric gas sensors based on metal oxides modified with gold nanoparticles: a review, *Microchimica Acta*, 183 (2016) 1033-1054.
- [87] O. Lupan, N. Ababii, D. Santos-Carballal, M.-I. Terasa, N. Magariu, D. Zappa, E. Comini, T. Pauporte, L. Siebert, F. Faupel, Tailoring the selectivity of ultralow-power heterojunction gas sensors by noble metal nanoparticle functionalization, *Nano Energy*, 88 (2021) 106241.
- [88] Y. Wang, Z. Zhao, G. Li, Y. Yan, C. Hao, A 2D covalent organic framework as a sensor for detecting formaldehyde, *Journal of Molecular Modeling*, 24 (2018) 1-7.
- [89] X. Song, Y. Wang, C. Wang, D. Wang, G. Zhuang, K.O. Kirlikovali, P. Li, O.K. Farha, Design rules of hydrogen-bonded organic frameworks with high chemical and thermal stabilities, *Journal of the American Chemical Society*, 144 (2022) 10663-10687.
- [90] A. Star, V. Joshi, S. Skarupo, D. Thomas, J.-C.P. Gabriel, Gas sensor array based on metal-decorated carbon nanotubes, *The Journal of Physical Chemistry B*, 110 (2006) 21014-21020.
- [91] K.J. Johnson, S.L. Rose-Pehrsson, Sensor array design for complex sensing tasks, *Annual Review of Analytical Chemistry*, 8 (2015) 287-310.
- [92] B. Shan, Y.Y. Broza, W. Li, Y. Wang, S. Wu, Z. Liu, J. Wang, S. Gui, L. Wang, Z. Zhang, W. Liu, S. Zhou, W. Jin, Q. Zhang, D. Hu, L. Lin, Q. Zhang, W. Li, J. Wang, H. Liu, Y. Pan, H. Haick, Multiplexed nanomaterial-based sensor array for detection of COVID-19 in exhaled breath, *ACS nano*, 14 (2020) 12125-12132.

- [93] A.K. Pavlou, N. Magan, C. McNulty, J.M. Jones, D. Sharp, J. Brown, A.P. Turner, Use of an electronic nose system for diagnoses of urinary tract infections, *Biosensors Bioelectronics*, 17 (2002) 893-899.
- [94] J.W. Grate, Acoustic wave microsensors for vapor sensing, *Chemical reviews*, 100 (2000) 2627-2648.
- [95] N.A. Rakow, K.S. Suslick, A colorimetric sensor array for odour visualization, *Nature*, 406 (2000) 710-713.
- [96] J.-S. Yang, T.M. Swager, Fluorescent porous polymer films as TNT chemosensors: electronic and structural effects, *Journal of the American Chemical Society*, 120 (1998) 11864-11873.
- [97] I. Heller, A.M. Janssens, J. Männik, E.D. Minot, S.G. Lemay, C. Dekker, Identifying the mechanism of biosensing with carbon nanotube transistors, *Nano letters*, 8 (2008) 591-595.
- [98] E.S. Snow, F. Perkins, J.A. Robinson, Chemical vapor detection using single-walled carbon nanotubes, *Chemical Society Reviews*, 35 (2006) 790-798.
- [99] Y. Cui, Q. Wei, H. Park, C.M. Lieber, Nanowire nanosensors for highly sensitive and selective detection of biological and chemical species, *Science*, 293 (2001) 1289-1292.
- [100] A. Kolmakov, Y. Zhang, G. Cheng, M. Moskovits, Detection of CO and O₂ using tin oxide nanowire sensors, *Advanced materials*, 15 (2003) 997-1000.

- [101] M.C. Leopold, R.L. Donkers, D. Georganopoulou, M. Fisher, F.P. Zamborini, R.W. Murray, Growth, conductivity, and vapor response properties of metal ion-carboxylate linked nanoparticle films, *Faraday Discussions*, 125 (2004) 63-76.
- [102] L. Han, X. Shi, W. Wu, F.L. Kirk, J. Luo, L. Wang, D. Mott, L. Cousineau, I. Stephanie, I. Lim, Nanoparticle-structured sensing array materials and pattern recognition for VOC detection, *Sensors and Actuators B: Chemical*, 106 (2005) 431-441.
- [103] T. Lin, X. Lv, Z. Hu, A. Xu, C. Feng, Semiconductor metal oxides as chemoresistive sensors for detecting volatile organic compounds, *Sensors*, 19 (2019) 233.
- [104] Z. Pang, J. Fu, P. Lv, F. Huang, Q. Wei, Effect of CSA concentration on the ammonia sensing properties of CSA-doped PA6/PANI composite nanofibers, *Sensors*, 14 (2014) 21453-21465.
- [105] G.H. Woehrle, L.O. Brown, J.E. Hutchison, Thiol-functionalized, 1.5-nm gold nanoparticles through ligand exchange reactions: Scope and mechanism of ligand exchange, *Journal of the American Chemical Society*, 127 (2005) 2172-2183.
- [106] P.K. Adhietty, S. Halder, J.B. Jasinski, X.-A. Fu, M.H. Nantz, Harnessing the cation- π interactions of metalated gold monolayer-protected clusters to detect aromatic volatile organic compounds, *Talanta*, 253 (2023) 123915.
- [107] N.R. Devi, M. Sasidharan, A.K. Sundramoorthy, Gold nanoparticles-thiol-functionalized reduced graphene oxide coated electrochemical sensor system for selective detection of mercury ion, *Journal of the Electrochemical Society*, 165 (2018) B3046-B3053.

- [108] F.J. Ibañez, U. Gowrishetty, M.M. Crain, K.M. Walsh, F.P. Zamborini, Chemiresistive vapor sensing with microscale films of gold monolayer protected clusters, *Anal Chem*, 78 (2006) 753-761.
- [109] S.D. Evans, S.R. Johnson, Y.L. Cheng, T. Shen, Vapour sensing using hybrid organic–inorganic nanostructured materials, *Journal of Materials Chemistry*, 10 (2000) 183-188.
- [110] H. Zhang, S. Evans, J. Henderson, R. Miles, T. Shen, Vapour sensing using surface functionalized gold nanoparticles, *Nanotechnology*, 13 (2002) 439.
- [111] J.B. Chang, V. Liu, V. Subramanian, K. Sivula, C. Luscombe, A. Murphy, J. Liu, J.M. Frechet, Printable polythiophene gas sensor array for low-cost electronic noses, *Journal of Applied Physics*, 100 (2006) 014506.
- [112] R. Bogue, Recent developments in MEMS sensors: A review of applications, markets and technologies, *Sensor review*, (2013).
- [113] R. Bogue, MEMS sensors: past, present and future, *Sensor Review*, (2007).
- [114] H. Miyajima, M. Mehregany, High-aspect-ratio photolithography for MEMS applications, *J Microelectromech S*, 4 (1995) 220-229.
- [115] N.P. Pham, J.N. Burghartz, P.M. Sarro, Spray coating of photoresist for pattern transfer on high topography surfaces, *Journal of Micromechanics Microengineering*, 15 (2005) 691.
- [116] S. Barnes, S. CRUZ, W. Quarter, Image Reversal of Positive Photoresists, (1987).

- [117] M. Brust, M. Walker, D. Bethell, D.J. Schiffrin, R. Whyman, Synthesis of thiol-derivatised gold nanoparticles in a two-phase liquid–liquid system, *Journal of the Chemical Society, Chemical Communications*, (1994) 801-802.
- [118] Y. Joseph, A. Peić, X. Chen, J. Michl, T. Vossmeier, A. Yasuda, Vapor sensitivity of networked gold nanoparticle chemiresistors: importance of flexibility and resistivity of the interlinkage, *The Journal of Physical Chemistry C*, 111 (2007) 12855-12859.
- [119] F.P. Zamborini, M.C. Leopold, J.F. Hicks, P.J. Kulesza, M.A. Malik, R.W. Murray, Electron hopping conductivity and vapor sensing properties of flexible network polymer films of metal nanoparticles, *Journal of the American Chemical Society*, 124 (2002) 8958-8964.
- [120] J.M. Walker, S.A. Akbar, P.A. Morris, Synergistic effects in gas sensing semiconducting oxide nano-heterostructures: A review, *Sensors Actuators B: Chemical*, 286 (2019) 624-640.
- [121] G. Di Francia, B. Alfano, E. Massera, M.L. Miglietta, T. Polichetti, *Chemical Sensors: Conductometric Gas Sensors*, *Encyclopedia of Sensors and Biosensors*, 1 (2023) 189-208.
- [122] D.M. Wilson, S. Hoyt, J. Janata, K. Booksh, L. Obando, Chemical sensors for portable, handheld field instruments, *IEEE Sensors Journal*, 1 (2001) 256-274.
- [123] C. Zhu, R.E. Gerald II, Y. Chen, J. Huang, Metal-organic framework portable chemical sensor, *Sensors and Actuators B: Chemical*, 321 (2020) 128608.

- [124] S. Halder, Z. Xie, M.H. Nantz, X.-A. Fu, Integration of a micropreconcentrator with solid-phase microextraction for analysis of trace volatile organic compounds by gas chromatography-mass spectrometry, *J Chromatogr A*, (2022) 463083.
- [125] S. Hazrati, R. Rostami, M. Farjaminezhad, M. Fazlzadeh, Preliminary assessment of BTEX concentrations in indoor air of residential buildings and atmospheric ambient air in Ardabil, Iran, *Atmospheric Environment*, 132 (2016) 91-97.
- [126] W.A. Chiu, J. Jinot, C.S. Scott, S.L. Makris, G.S. Cooper, R.C. Dzubow, A.S. Bale, M.V. Evans, K.Z. Guyton, N. Keshava, Human health effects of trichloroethylene: key findings and scientific issues, *Environmental health perspectives*, 121 (2013) 303-311.
- [127] N.M. Julkapli, S. Bagheri, Nanosensor in gas monitoring: a review, *Nanotechnology in Environmental Science*, (2018) 443-472.
- [128] R.J. Rath, S. Farajikhah, F. Oveissi, F. Dehghani, S. Naficy, Chemiresistive Sensor Arrays for Gas/Volatile Organic Compounds Monitoring: A Review, *Advanced Engineering Materials*, 25 (2023) 2200830.
- [129] M. Righettoni, A. Tricoli, S.E. Pratsinis, Si: WO₃ sensors for highly selective detection of acetone for easy diagnosis of diabetes by breath analysis, *Anal Chem*, 82 (2010) 3581-3587.
- [130] W.H. Steinecker, M.P. Rowe, E.T. Zellers, Model of vapor-induced resistivity changes in gold– thiolate monolayer-protected nanoparticle sensor films, *Anal Chem*, 79 (2007) 4977-4986.

- [131] W. Zheng, Y. Fu, L. Liu, Q. Guo, Hydrogen bonding interaction between ureas or thioureas and carbonyl compounds, *Acta Physico-Chimica Sinica*, 23 (2007) 1018-1024.
- [132] V. Montes-García, M.A. Squillaci, M. Diez-Castellnou, Q.K. Ong, F. Stellacci, P. Samori, Chemical sensing with Au and Ag nanoparticles, *Chemical Society Reviews*, 50 (2021) 1269-1304.
- [133] Z. Xie, M.V. Ramakrishnam Raju, P.K. Adihetty, X.-A. Fu, M.H. Nantz, Effect of Thiol Molecular Structure on the Sensitivity of Gold Nanoparticle-Based Chemiresistors toward Carbonyl Compounds, *Sensors*, 20 (2020) 7024.
- [134] H. Wohltjen, A.W. Snow, Colloidal metal–insulator–metal ensemble chemiresistor sensor, *Anal Chem*, 70 (1998) 2856-2859.
- [135] Y.J. Kim, H.-B. Pyo, S.H. Park, Response Properties of the Gold Nanoparticle Sensors toward Benzene and Toluene Vapors, in: *SENSORS, 2006 IEEE*, IEEE, 2006, pp. 1078-1080.
- [136] Y. Joseph, N. Krasteva, I. Besnard, B. Guse, M. Rosenberger, U. Wild, A. Knop-Gericke, R. Schlögl, R. Krustev, A. Yasuda, Gold-nanoparticle/organic linker films: self-assembly, electronic and structural characterisation, composition and vapour sensitivity, *Faraday Discussions*, 125 (2004) 77-97.
- [137] M. Kimura, M. Yokokawa, S. Sato, T. Fukawa, T. Mihara, Volatile organic compound sensing by gold nanoparticles capped with calix [4] arene ligand, *Chemistry Letters*, 40 (2011) 1402-1404.

- [138] J.S. Cooper, H. Kiiveri, L.J. Hubble, E. Chow, M.S. Webster, K.-H. Müller, A. Sosa-Pintos, A. Bendavid, B. Raguse, L. Wieczorek, Quantifying BTEX in aqueous solutions with potentially interfering hydrocarbons using a partially selective sensor array, *Analyst*, 140 (2015) 3233-3238.
- [139] J.C. Ma, D.A. Dougherty, The cation- π interaction, *Chemical reviews*, 97 (1997) 1303-1324.
- [140] Z. Liang, Q.X. Li, π -Cation interactions in molecular recognition: Perspectives on pharmaceuticals and pesticides, *Journal of agricultural food chemistry*, 66 (2018) 3315-3323.
- [141] S. Mecozzi, A.P. West, D.A. Dougherty, Cation- π interactions in simple aromatics: electrostatics provide a predictive tool, *Journal of the American Chemical Society*, 118 (1996) 2307-2308.
- [142] J.P. Gallivan, D.A. Dougherty, A computational study of cation- π interactions vs salt bridges in aqueous media: implications for protein engineering, *Journal of the American Chemical Society*, 122 (2000) 870-874.
- [143] M.S. Marshall, R.P. Steele, K.S. Thanthiriwatte, C.D. Sherrill, Potential energy curves for cation- π interactions: off-axis configurations are also attractive, *The Journal of Physical Chemistry A*, 113 (2009) 13628-13632.
- [144] V. Aggarwal, H. Li, S.A. Boyd, B.J. Teppen, Enhanced sorption of trichloroethene by smectite clay exchanged with Cs⁺, *Environmental science technology*, 40 (2006) 894-899.

- [145] P.K. Adhietty, Surface-functionalized chemiresistive films that exploit h-bonding, cation- π , and metal-halide interactions, (2022).
- [146] K.K. Bania, A.K. Guha, P.K. Bhattacharyya, S. Sinha, Effect of substituent and solvent on cation- π interactions in benzene and borazine: a computational study, Dalton transactions, 43 (2014) 1769-1784.
- [147] M. France, S. Pullins, M. Duncan, Spectroscopy of the Ca⁺-acetylene π complex, The Journal of chemical physics, 108 (1998) 7049-7051.
- [148] S. Yamada, T. Misono, S. Tsuzuki, Cation- π interactions of a thiocarbonyl group and a carbonyl group with a pyridinium nucleus, Journal of the American Chemical Society, 126 (2004) 9862-9872.
- [149] S. Mecozzi, A.P. West Jr, D.A. Dougherty, Cation- π interactions in aromatics of biological and medicinal interest: electrostatic potential surfaces as a useful qualitative guide, Proceedings of the National Academy of Sciences, 93 (1996) 10566-10571.
- [150] G.N. Vayssilov, J.A. Lercher, N. Rösch, Interaction of methanol with alkali metal exchanged molecular sieves. 2. Density functional study, The Journal of Physical Chemistry B, 104 (2000) 8614-8623.
- [151] G. Smith, Poly [μ 6-4-amino-3, 5, 6-trichloropyridine-2-carboxylato) aquacaesium], Acta Crystallographica Section E: Structure Reports Online, 69 (2013) m22-m23.
- [152] A. Allouch, S. Le Calvé, C.A. Serra, Portable, miniature, fast and high sensitive real-time analyzers: BTEX detection, Sensors and Actuators B: Chemical, 182 (2013) 446-452.

- [153] I. Lara-Lbeas, A. Rodríguez-Cuevas, C. Andrikopoulou, V. Person, L. Baldas, S. Colin, S. Le Calvé, Sub-ppb level detection of BTEX gaseous mixtures with a compact prototype GC equipped with a preconcentration unit, *Micromachines*, 10 (2019) 187.
- [154] Y. Ueno, T. Horiuchi, T. Morimoto, O. Niwa, Microfluidic device for airborne BTEX detection, *Anal Chem*, 73 (2001) 4688-4693.
- [155] K. Na, K.-C. Moon, Y.P. Kim, Source contribution to aromatic VOC concentration and ozone formation potential in the atmosphere of Seoul, *Atmospheric environment*, 39 (2005) 5517-5524.
- [156] R.R. Hoque, P. Khillare, T. Agarwal, V. Shridhar, S. Balachandran, Spatial and temporal variation of BTEX in the urban atmosphere of Delhi, India, *Science of the total environment*, 392 (2008) 30-40.
- [157] A. Zalel, D.M. Broday, Revealing source signatures in ambient BTEX concentrations, *Environmental pollution*, 156 (2008) 553-562.
- [158] N. Yassaa, E. Brancaloni, M. Frattoni, P. Ciccioi, Isomeric analysis of BTEXs in the atmosphere using β -cyclodextrin capillary chromatography coupled with thermal desorption and mass spectrometry, *Chemosphere*, 63 (2006) 502-508.
- [159] R. Atkinson, Atmospheric chemistry of VOCs and NO_x, *Atmospheric Environment*, 34 (2000) 2063-2101.
- [160] P. Romagnoli, C. Balducci, M. Perilli, F. Vichi, A. Imperiali, A. Cecinato, Indoor air quality at life and work environments in Rome, Italy, *Environmental Science and Pollution Research*, 23 (2016) 3503-3516.

- [161] G. Lewis, U. Winsford, Continuous monitoring of benzene, toluene, ethyl benzene, and xylenes (BTEX) in air with the Thermo Scientific Sentinel PRO Environmental Mass Spectrometer, Thermo Fisher Scientific, (2014) 0-3.
- [162] S. Tumbiolo, J.-F. Gal, P.-C. Maria, O. Zerbinati, Determination of benzene, toluene, ethylbenzene and xylenes in air by solid phase micro-extraction/gas chromatography/mass spectrometry, *Anal Bioanal Chem*, 380 (2004) 824-830.
- [163] J. Namieśnik, B. Zygmunt, A. Jastrzębska, Application of solid-phase microextraction for determination of organic vapours in gaseous matrices, *J Chromatogr A*, 885 (2000) 405-418.
- [164] L. Spinelle, M. Gerboles, G. Kok, S. Persijn, T. Sauerwald, Review of portable and low-cost sensors for the ambient air monitoring of benzene and other volatile organic compounds, *Sensors*, 17 (2017) 1520.
- [165] J. Koziel, M. Jia, A. Khaled, J. Noah, J. Pawliszyn, Field air analysis with SPME device, *Analytica chimica acta*, 400 (1999) 153-162.
- [166] S. Merkle, K.K. Kleeberg, J. Fritsche, Recent developments and applications of solid phase microextraction (SPME) in food and environmental analysis—a review, *Chromatography*, 2 (2015) 293-381.
- [167] N. Baimatova, J.A. Koziel, B. Kenessov, Quantification of benzene, toluene, ethylbenzene and o-xylene in internal combustion engine exhaust with time-weighted average solid phase microextraction and gas chromatography mass spectrometry, *Analytica chimica acta*, 873 (2015) 38-50.

- [168] N. Baimatova, B. Kenessov, J.A. Koziel, L. Carlsen, M. Bektasov, O.P. Demyanenko, Simple and accurate quantification of BTEX in ambient air by SPME and GC–MS, *Talanta*, 154 (2016) 46-52.
- [169] N. Riboni, J.W. Trzcinski, F. Bianchi, C. Massera, R. Pinalli, L. Sidisky, E. Dalcanale, M. Careri, Conformationally blocked quinoxaline cavitand as solid-phase microextraction coating for the selective detection of BTEX in air, *Analytica chimica acta*, 905 (2016) 79-84.
- [170] J.A. Koziel, J. Pawliszyn, Air sampling and analysis of volatile organic compounds with solid phase microextraction, *Journal of the Air & Waste Management Association*, 51 (2001) 173-184.
- [171] V. Larroque, V. Desauziers, P. Mocho, Development of a solid phase microextraction (SPME) method for the sampling of VOC traces in indoor air, *Journal of environmental monitoring*, 8 (2006) 106-111.
- [172] K.M. Skog, F. Xiong, H. Kawashima, E. Doyle, R. Soto, D.R. Gentner, Compact, automated, inexpensive, and field-deployable vacuum-outlet gas chromatograph for trace-concentration gas-phase organic compounds, *Anal Chem*, 91 (2019) 1318-1327.
- [173] A. Garg, M. Akbar, E. Vejerano, S. Narayanan, L. Nazhandali, L.C. Marr, M. Agah, Zebra GC: A mini gas chromatography system for trace-level determination of hazardous air pollutants, *Sensors and Actuators B: Chemical*, 212 (2015) 145-154.
- [174] P.R. Lewis, P. Manginell, D.R. Adkins, R.J. Kottenstette, D.R. Wheeler, S.S. Sokolowski, D.E. Trudell, J.E. Byrnes, M. Okandan, J.M. Bauer, Recent advancements in the gas-phase MicroChemLab, *IEEE Sensors Journal*, 6 (2006) 784-795.

- [175] T. Sukaew, H.W. Chang, G. Serrano, E.T. Zellers, Multi-stage preconcentrator/focuser module designed to enable trace level determinations of trichloroethylene in indoor air with a microfabricated gas chromatograph, *Analyst*, 136 (2011) 1664-1674.
- [176] J. Bryant-Genevier, E.T. Zellers, Toward a microfabricated preconcentrator-focuser for a wearable micro-scale gas chromatograph, *J Chromatogr A*, 1422 (2015) 299-309.
- [177] H. Lahlou, X. Vilanova, X. Correig, Gas phase micro-preconcentrators for benzene monitoring: A review, *Sensors and Actuators B: Chemical*, 176 (2013) 198-210.
- [178] E. Camara, P. Breuil, D. Briand, N. De Rooij, C. Pijolat, A micro gas preconcentrator with improved performance for pollution monitoring and explosives detection, *Analytica chimica acta*, 688 (2011) 175-182.
- [179] E. Camara, P. Breuil, D. Briand, L. Guillot, C. Pijolat, N. de Rooij, A Micro Gas Preconcentrator with improved performances for environmental monitoring, *TRANSDUCERS 2009 - 2009 International Solid-State Sensors, Actuators and Microsystems Conference*, IEEE, 2009, pp. 983-986.
- [180] S. Zampolli, I. Elmi, F. Mancarella, P. Betti, E. Dalcanale, G. Cardinali, M. Severi, Real-time monitoring of sub-ppb concentrations of aromatic volatiles with a MEMS-enabled miniaturized gas-chromatograph, *Sensors and Actuators B: Chemical*, 141 (2009) 322-328.
- [181] M.M. McCartney, Y. Zrodnikov, A.G. Fung, M.K. LeVasseur, J.M. Pedersen, K.O. Zamuruyev, A.A. Aksenov, N.J. Kenyon, C.E. Davis, An easy to manufacture micro gas preconcentrator for chemical sensing applications, *ACS sensors*, 2 (2017) 1167-1174.

- [182] L.A. Simms, E. Borrás, B.S. Chew, B. Matsui, M.M. McCartney, S.K. Robinson, N. Kenyon, C.E. Davis, Environmental sampling of volatile organic compounds during the 2018 Camp Fire in Northern California, *Journal of Environmental Sciences*, 103 (2021) 135-147.
- [183] A. Rodríguez-Cuevas, I. Lara-Ibeas, A. Leprince, M. Wolf, S. Le Calvé, Easy-to-manufacture micro gas preconcentrator integrated in a portable GC for enhanced trace detection of BTEX, *Sensors and Actuators B: Chemical*, 324 (2020) 128690.
- [184] I. Frausto-Vicencio, A. Moreno, H. Goldsmith, Y.-K. Hsu, F.M. Hopkins, Characterizing the performance of a compact BTEX GC-PID for near-real time analysis and field deployment, *Sensors*, 21 (2021) 2095.
- [185] C.-J. Lu, J. Whiting, R.D. Sacks, E.T. Zellers, Portable gas chromatograph with tunable retention and sensor array detection for determination of complex vapor mixtures, *Anal Chem*, 75 (2003) 1400-1409.
- [186] J.Q. Wang, J. Bryant-Genevier, N. Nunovero, C.Y. Zhang, B. Kraay, C.H. Zhan, K. Scholten, R. Nidetz, S. Buggaveeti, E.T. Zellers, Compact prototype microfabricated gas chromatographic analyzer for autonomous determinations of VOC mixtures at typical workplace concentrations, *Microsyst Nanoeng*, 4 (2018).
- [187] R.-S. Jian, Y.-S. Huang, S.-L. Lai, L.-Y. Sung, C.-J. Lu, Compact instrumentation of a μ -GC for real time analysis of sub-ppb VOC mixtures, *Microchemical Journal*, 108 (2013) 161-167.

- [188] M. Wei-Hao Li, A. Ghosh, A. Venkatasubramanian, R. Sharma, X. Huang, X. Fan, High-Sensitivity Micro-Gas Chromatograph–Photoionization Detector for Trace Vapor Detection, *ACS Sensors*, (2021).
- [189] C. Chen, F. Tsow, K.D. Campbell, R. Iglesias, E. Forzani, N. Tao, A wireless hybrid chemical sensor for detection of environmental volatile organic compounds, *IEEE sensors journal*, 13 (2013) 1748-1755.
- [190] M.-Y. Wong, W.-R. Cheng, M.-H. Liu, W.-C. Tian, C.-J. Lu, A preconcentrator chip employing μ -SPME array coated with in-situ-synthesized carbon adsorbent film for VOCs analysis, *Talanta*, 101 (2012) 307-313.
- [191] J. Wang, N. Nuñovero, R. Nidetz, S.J. Peterson, B.M. Brookover, W.H. Steinecker, E.T. Zellers, Belt-mounted micro-gas-chromatograph prototype for determining personal exposures to volatile-organic-compound mixture components, *Anal Chem*, 91 (2019) 4747-4754.
- [192] D.-W. You, Y.-S. Seon, Y. Jang, J. Bang, J.-S. Oh, K.-W. Jung, A portable gas chromatograph for real-time monitoring of aromatic volatile organic compounds in air samples, *J Chromatogr A*, 1625 (2020) 461267.
- [193] B. Alfeeli, M. Agah, Toward handheld diagnostics of cancer biomarkers in breath: Micro preconcentration of trace levels of volatiles in human breath, *IEEE Sensors Journal*, 11 (2011) 2756-2762.
- [194] B. Alfeeli, D. Cho, M. Ashraf-Khorassani, L.T. Taylor, M. Agah, MEMS-based multi-inlet/outlet preconcentrator coated by inkjet printing of polymer adsorbents, *Sensors and Actuators B: Chemical*, 133 (2008) 24-32.

- [195] W.C. Tian, S.W. Pang, C.J. Lu, E.T. Zellers, Microfabricated preconcentrator-focuser for a microscale gas chromatograph, *J Microelectromech S*, 12 (2003) 264-272.
- [196] S. Mukerjee, L.A. Smith, E.D. Thoma, D.A. Whitaker, K.D. Oliver, R. Duvall, T.A. Cousett, Spatial analysis of volatile organic compounds using passive samplers in the Rubbertown industrial area of Louisville, Kentucky, USA, *Atmospheric pollution research*, 11 (2020) 81-86.
- [197] H. Lan, K. Hartonen, M.-L. Riekkola, Miniaturised air sampling techniques for analysis of volatile organic compounds in air, *TrAC Trends in Analytical Chemistry*, 126 (2020) 115873.
- [198] A. Kansal, Sources and reactivity of NMHCs and VOCs in the atmosphere: A review, *Journal of hazardous materials*, 166 (2009) 17-26.
- [199] A.H. Goldstein, I.E. Galbally, Known and unexplored organic constituents in the earth's atmosphere, *Environmental science technology*, 41 (2007) 1514-1521.
- [200] R. Koppmann, *Volatile organic compounds in the atmosphere*, John Wiley & Sons, 2008.
- [201] R. Montero-Montoya, R. López-Vargas, O. Arellano-Aguilar, Volatile organic compounds in air: sources, distribution, exposure and associated illnesses in children, *Ann Glob Health*, 84 (2018) 225.
- [202] M. Li, Q. Li, M.H. Nantz, X.-A. Fu, Analysis of carbonyl compounds in ambient air by a microreactor approach, *ACS omega*, 3 (2018) 6764-6769.

- [203] Y. Saalberg, M. Wolff, VOC breath biomarkers in lung cancer, *Clinica Chimica Acta*, 459 (2016) 5-9.
- [204] C. Liaud, N. Nguyen, R. Nasreddine, S. Le Calvé, Experimental performances study of a transportable GC-PID and two thermo-desorption based methods coupled to FID and MS detection to assess BTEX exposure at sub-ppb level in air, *Talanta*, 127 (2014) 33-42.
- [205] A. Daifullah, B. Girgis, Impact of surface characteristics of activated carbon on adsorption of BTEX, *Colloids Surfaces A: Physicochemical Engineering Aspects*, 214 (2003) 181-193.
- [206] C. Lu, F. Su, S. Hu, Surface modification of carbon nanotubes for enhancing BTEX adsorption from aqueous solutions, *Applied Surface Science*, 254 (2008) 7035-7041.
- [207] I. Voiculescu, M. Zaghoul, N. Narasimhan, Microfabricated chemical preconcentrators for gas-phase microanalytical detection systems, *TrAC Trends in Analytical Chemistry*, 27 (2008) 327-343.
- [208] K. Elke, E. Jermann, J. Begerow, L. Dunemann, Determination of benzene, toluene, ethylbenzene and xylenes in indoor air at environmental levels using diffusive samplers in combination with headspace solid-phase microextraction and high-resolution gas chromatography–flame ionization detection, *J Chromatogr A*, 826 (1998) 191-200.
- [209] X. Pang, A.C. Lewis, M. Rodenas-Garcia, Microfluidic lab-on-a-chip derivatization for gaseous carbonyl analysis, *J Chromatogr A*, 1296 (2013) 93-103.

- [210] Y. Chen, Q. Li, Z. Xie, X.-a.J.J.o.C.B. Fu, Characterization of DNPH-coated microreactor chip for analysis of trace carbonyls with application for breath analysis, 1106 (2019) 58-63.
- [211] R. Spaulding, M. Charles, Comparison of methods for extraction, storage, and silylation of pentafluorobenzyl derivatives of carbonyl compounds and multi-functional carbonyl compounds, *Anal bioanal chem*, 372 (2002) 808-816.
- [212] V.Y. Seaman, M.J. Charles, T.M. Cahill, A sensitive method for the quantification of acrolein and other volatile carbonyls in ambient air, *Anal Chem*, 78 (2006) 2405-2412.
- [213] M. Serrano, M. Silva, M. Gallego, Development of an environment-friendly microextraction method for the determination of aliphatic and aromatic aldehydes in water, *Analytica Chimica Acta*, 784 (2013) 77-84.
- [214] M. Rodigast, A. Mutzel, Y. Iinuma, S. Haferkorn, H. Herrmann, Characterisation and optimisation of a sample preparation method for the detection and quantification of atmospherically relevant carbonyl compounds in aqueous medium, *Atmospheric Measurement Techniques*, 8 (2015) 2409-2416.
- [215] Y. Shen, S.S. Que Hee, Optimization of a solid sorbent dynamic personal air sampling method for aldehydes, *Applied Occupational Environmental Hygiene*, 15 (2000) 228-234.
- [216] H.S. Fogler, S.H. Fogler, *Elements of chemical reaction engineering*, Pearson Educacion, 1999.

- [217] X. Pang, A.C. Lewis, A microfluidic lab-on-chip derivatisation technique for the measurement of gas phase formaldehyde, *Analytical Methods*, 4 (2012) 2013-2020.
- [218] S.S.H. Ho, J.Z. Yu, Feasibility of collection and analysis of airborne carbonyls by on-sorbent derivatization and thermal desorption, *Anal Chem*, 74 (2002) 1232-1240.
- [219] J. Herrington, L. Zhang, D. Whitaker, L. Sheldon, J.J. Zhang, Optimizing a dansylhydrazine (DNSH) based method for measuring airborne acrolein and other unsaturated carbonyls, *Journal of Environmental Monitoring*, 7 (2005) 969-976.
- [220] S.S.H. Ho, J.Z. Yu, Determination of airborne carbonyls: Comparison of a thermal desorption/GC method with the standard DNPH/HPLC method, *Environ. Sci. Technol.*, 38 (2004) 862-870.
- [221] J.L. Falconer, J.A. Schwarz, Temperature-programmed desorption and reaction: applications to supported catalysts, *Catalysis Reviews Science Engineering*, 25 (1983) 141-227.
- [222] T. Lomonaco, A. Romani, S. Ghimenti, D. Biagini, F.G. Bellagambi, M. Onor, P. Salvo, R. Fuoco, F. Di Francesco, Determination of carbonyl compounds in exhaled breath by on-sorbent derivatization coupled with thermal desorption and gas chromatography-tandem mass spectrometry, *Journal of Breath Research*, 12 (2018) 046004.
- [223] D. Urupina, T. Leonardis, S. Crunaire, N.J.E.T. Locoge, Innovation, What are the limitations for the use of Carboxpack X as passive or active sampling adsorbent for determination of 1, 3-butadiene in ambient environment?, (2022) 102711.

- [224] E. Gallego, P. Teixidor, F.J. Roca, J.F. Perales, E. Gadea, Outdoor air 1, 3-butadiene monitoring: Comparison of performance of Radiello® passive samplers and active multi-sorbent bed tubes, *Atmospheric environment*, 182 (2018) 9-16.
- [225] G.L. Long, J.D. Winefordner, Limit of detection. A closer look at the IUPAC definition, *Anal Chem*, 55 (1983) 712A-724A.
- [226] A.Y. Goren, Y.K. Receptoğlu, A. Khataee, Language of response surface methodology as an experimental strategy for electrochemical wastewater treatment process optimization, in: *Artificial Intelligence and Data Science in Environmental Sensing*, Elsevier, 2022, pp. 57-92.
- [227] M.A. Bezerra, R.E. Santelli, E.P. Oliveira, L.S. Villar, L.A. Escaleira, Response surface methodology (RSM) as a tool for optimization in analytical chemistry, *Talanta*, 76 (2008) 965-977.
- [228] A. Mohammadi, Y. Ghassoun, M.-O. Löwner, M. Behmanesh, M. Faraji, S. Nemati, A. Toolabi, A. Abdolahnejad, H. Panahi, H. Heydari, Spatial analysis and risk assessment of urban BTEX compounds in Urmia, Iran, *Chemosphere*, 246 (2020) 125769.
- [229] Z. Jiang, B. Grosselin, V. Daële, A. Mellouki, Y. Mu, Seasonal and diurnal variations of BTEX compounds in the semi-urban environment of Orleans, France, *Science of the Total Environment*, 574 (2017) 1659-1664.

CURRICULUM VITAE

Sujoy Halder

216 Eastern Parkway, Louisville, KY 40208

+1 (502)-819-4717 || sujoy.halder@louisville.edu

HIGHLIGHTS

- 4+ years of research experience in chromatography, analytical method development, microfluidic device fabrication, and characterization.
- 4 years of industrial experience as a process engineer in the petrochemical industry.
- Knowledge in statistical process control (SPC) and design of experiments (DOE). Achieved six sigma green belt certification.
- 2 peer-reviewed articles published as a first author in scientific journals.

EDUCATION

University of Louisville	Louisville, KY
Ph.D. in Chemical Engineering	Aug 2018 – Apr 2023
Shahjalal University of Science & Technology	Sylhet, Bangladesh
B.S. (Engineering) in Chemical Engineering & Polymer Science	2009 – 2012

TECHNICAL SKILLS

Chromatography equipment: GC-MS, HPLC-MS, GC-PID

Microfabrication techniques: Photolithography, Wet etching, Deep reactive-ion etching, Plasma processing, Thermal processing, Anodic bonding

Instrumentation: Dektak 8M Profilometer, Filmetrics, VASE Ellipsometer

Software skills: MS Office, L-edit, AutoCAD, COMSOL Multiphysics

Data analysis: Origin, Excel, Minitab, JMP

RESEARCH & PROFESSIONAL EXPERIENCE

University of Louisville	Louisville, KY
Research Assistant	Aug 2018 – Present

- Developed gas sensor arrays on silicon substrate for sensing hazard gases.
- Developed a novel microfluidic device for detecting a wide range of airborne VOCs.
- Operation & troubleshooting chromatography equipment (GC-MS, HPLC, GC-PID).
- Developed analytical methods to detect molecules using SPME, microreactor, GCMS, and HPLC.

- Operated and supervised condensate fractionation unit, hydro desulfurization unit, catalytic reforming unit, BTX column, recycle gas compressor, and fired heaters.
- Studied the kinetics of catalysts and their performance using statistical process control.
- Commissioned condensate fractionation facility, boiler, and nitrogen generator.

PUBLICATIONS

1. P. K. Adhietty, **S. Halder**, J. B. Jasinski, X. Fu, and M. H. Nantz, "Harnessing the cation- π interactions of metalated gold monolayer-protected clusters to detect aromatic volatile organic compounds" *Talanta*, 253 (2023) 123915 (*Equal first author contribution with P. K. Adhietty*).
2. **S. Halder**, Z. Xie, M. H. Nantz, and X. Fu, "Integration of a micropreconcentrator with solid-phase microextraction for analysis of trace volatile organic compounds by gas chromatography-mass spectrometry" *Journal of Chromatography A* 1673 (2022) 463083.
3. **S. Halder**, E. Reed, M. H. Nantz, and X. Fu, "Analysis of toxic volatile organic compounds in environmental air with dual-compartment microproconcentrators" (in preparation).
4. P. K. Adhietty, **S. Halder**, U. O. Abu, X. Fu, and M. H. Nantz, "A MEMS sensor to selectively detect trichloroethylene (TCE) in the air" (in preparation).
5. **S. Halder**, Z. Xie, J. D. Morris, M. H. Nantz, and X. Fu, "Detection of COVID-19 from exhaled breath" (in preparation).

CONFERENCE PRESENTATIONS

1. **S. Halder**, P. K. Adhietty, M. H. Nantz, and X. Fu, "Development of a Gas Sensor Array for Detecting Toxic VOCs Using Metalated Gold Monolayer Protected Clusters", 2022 Superfund Research Program Annual Meeting, Raleigh, NC, Dec 14 – 16, 2022.
2. **S. Halder**, Z. Xie, M. H. Nantz, and X. Fu, "Detection of airborne VOCs using micropreconcentrator integrated with solid phase microextraction", 2022 Superfund Research Program Annual Meeting, Raleigh, NC, Dec 14 – 16, 2022.
3. **S. Halder**, P. K. Adhietty, M. H. Nantz, and X. Fu, "Gas Sensor Array for Detecting Aromatic VOCs Using Metalated Gold Monolayer Protected Clusters", 2022 NNCI Nano + Additive Manufacturing Summit, Louisville, KY, Aug 7 – 8, 2022.
4. **S. Halder**, Z. Xie, M. H. Nantz, and X. Fu, "Detection of Benzene, Toluene, Ethylbenzene and Xylene in Air Using Micro-Preconcentrator/Solid Phase Micro-Extraction/Gas Chromatography-Mass Spectrometry", 2021 AIChE Annual Meeting, Boston, MA, Nov 7 – 11, 2021.
5. **S. Halder**, P. K. Adhietty, Z. Xie, M. H. Nantz, and X. Fu, "Fabrication and characterization of a sensor array to detect volatile organic compounds in environmental air ", 2020 Superfund Research Program Annual Meeting, virtual, December 14 – 16, 2020.
6. **S. Halder**, P. K. Adhietty, Z. Xie, M. H. Nantz, and X. Fu, "A Sensor Array for Detection of Multiple Volatile Organic Compounds in Air", 2019 Superfund Research Program Annual Meeting, Seattle, WA, Nov 18 – 20, 2019.

7. **S. Halder**, Z. Xie, P. K. Adhihetty, M. H. Nantz, and X. Fu, "Gas sensor array for detecting acetone by using functionalized alkylurea thiol gold nanoparticle", 2019 KY Nanotechnology and Additive Manufacturing Symposium, Louisville, KY, July 31 – August 1, 2019.

TEACHING EXPERIENCE

1. **Teaching Assistant (TA)**: worked as a TA for multiple courses such as Chemical Engineering Thermodynamics II, Materials Science, Computer Applications in Chemical Engineering, Separation Operations, and the Strategy of Design in the department of chemical engineering at the University of Louisville.
2. **Mentoring**: Supervised several graduate and undergraduate students for their research projects by encouraging them to develop sound hypotheses and validate their findings.

AWARDS/ACHIEVEMENTS

1. **Second prize winner**, KY Nanotechnology and Additive Manufacturing Symposium 2019, Louisville, KY.
2. **Graduate School Travel Grant**, Graduate Student Council, UofL, 2021.
3. **Six Sigma Green Belt certification** (Institute of Industrial and Systems Engineers).

REFERENCES

Available upon request